Structural insight into photobleaching mechanisms of reversible photoswitchable fluorescent proteins

Chenxi Duan

UNIVERSITÉ DE GRENOBLE

THÈSE

Pour obtenir le grade de

DOCTEUR DE L'UNIVERSITÉ DE GRENOBLE

Spécialité : **Biologie Structurale et Nanobiologie**

Arrêté ministériel : 7 août 2006

Présentée par **Chenxi DUAN**

Thèse dirigée par **Martin BYRDIN**
codirigée par **Dominique BOURGEOIS**

préparée au sein de **l'Institut de Biologie Structurale**
École Doctorale Chimie et Science du vivant

Etude structurale des mécanismes de photoblanchiment des protéines fluorescentes photocommutables

Thèse soutenue publiquement le **5 Décembre 2014**,
devant le jury composé de :

Mme Marie ERARD
Enseignant-Chercheur, Laboratoire de Chimie Physique, Paris, Rapporteur
Mr Christian CAMBILLAU
Directeur de recherche, Laboratoire d'Architecture et Fonction des Molécules Biologiques, Marseille, Rapporteur
Mr Stefan JAKOBS
Professeur, Max-Planck-Institut, Göttingen, Germany, Examinateur
Mr Jacques DEROUARD
Professeur, Laboratoire interdisciplinaire de Physique, Grenoble, Président
Mr Martin BYRDIN
Ingénieur-Chercheur, Institut de Biologie Structurale, Grenoble, Directeur de thèse
Mr Dominique BOURGEOIS
Directeur de recherche, Institut de Biologie Structurale, Grenoble, Co-directeur de thèse

Remerciement / Acknowledgements

Je n'arrive pas à exprimer mes sentiments complexes maintenant. Le temps passe si vite, au moment de ma soutenance, ça fait déjà quatre ans dans l'équipe PIXEL. En revanche, mon souvenir de la première journée dans cette équipe est plus clair que celle d'hier.

Je voudrais bien remercier particulièrement mes directeurs de thèse : Martin BYRDIN et Dominique BOURGEOIS. Vous m'avez appris les connaissances en physique, optique et spectroscopie petit à petit. Etant un biologiste de base, ce n'est pas une tâche facile. Je vous remercie d'avoir une patience importante envers moi surtout quand j'ai fait des bêtises.

Je tiens à remercier à Virgile ADAM, chercheur dans l'équipe. Avec lui, j'ai acquis énormément de connaissances sur la cristallographie, les protéines fluorescentes et la microscopie, qui me permettent d'avancer mes projets en douceur.

Romain BERARDOZZI, doctorant en 2ème année. Grace à lui, je me suis familiarisé avec notre nouveau bâtiment IBS puisque j'étais en Allemagne lors qu'on déménageait vers ce nouveau bâtiment. Je te souhaite une bonne continuation et un bon avenir.

Un grand merci à Delphine ARCIZET, l'ancienne post-doc d'équipe qui était ma tutrice de stage. Une personne avec pleine de charme et gentillesse. Merci beaucoup de ton accompagnement au début de mes recherches.

Aline REGIS FARO, l'ancienne doctorante de l'équipe qui m'a passé le bâton. Elle donnait toujours un coup de main lorsque j'ai rencontré des difficultés.

Merci à tous nos collaborateurs : Cécile MORLOT, Thierry VERNET, Laure ROUX, Xavier Henry, Florence GERIN, Isabelle DEMACHY, Jacqueline RIDARD, Bernard LEVY, Mikolaj FELIKS, Martin FIELD, Sylvie KIEFFER-JAQUINOD, et David VON STETTEN, je ne pourrais pas avancer mes projets sans votre aide.

A cause de ma santé, j'ai subi une période difficile depuis le début 2014. Merci à tous les personnels administratifs qui m'ont supporté et m'ont aidé, avec votre immense gentillesse je suis capable de finir ma thèse.

Je souhaite remercier aussi les membres de mon comité de suivi de thèse : Frank FIESCHI, Marc JAMIN et Eve DE ROSNY. Nous avons une réunion par an pour discuter l'avancement de thèse. A chaque fois, j'ai pu recevoir des conseils importants.

Je voudrais exprimer ma reconnaissance envers tout le monde avec qui j'ai travaillé: Christophe GUERIN, Jérémie GAILLARD, Laurent GUILLON, Laurent BLANCHOIN, Martin WEIK, Virginia GUILLON, Mudalige S. GUNEWARDENE, Sergiy AVILOV,

Mariam EL KHATIB, Nicolas COQUELLE, Jaques-PHILLIPPE COLLETIER, Damien CLAVEL, Maxime JACQ, Christian FRANK et Markus SAUER et tout le monde à l'IBS.

Enfin et surtout, le plus grand merci à ma femme Lin WU, qui m'accompagne tout au long de ma thèse, me supporte et m'écoute. Sans toi, je ne pourrais pas finir ma thèse. Je t'aime !

Table of contents

CHAPTER 1

Introduction

1.1 Fluorescent proteins (FPs)

Around the 1970s, wtGFP was firstly studied by a Japanese scientist named Osamu Shimomura (Shimomura et al., 1962). The protein was purified from a marine Hydrozoa species: *Aequorea victoria*, a jelly fish found off the West coast of North America. However, wtGFP didn't attract attention of biologists until 1992, when Douglas Prasher cloned and sequenced its gene although at that time few amino acids were missing (Prasher et al., 1992). Two years after, Martin Chalfie expressed the gene in *E. coli* and *C. elegans* cells (Chalfie et al., 1994) and successfully observed green fluorescence upon illumination with UV light. However, wtGFP has some drawbacks such as its major excitation peak located in the UV region (395-397nm) (Chattoraj et al., 1996) (**Fig1. A**), and poor folding at 37 °C (Tsien, 1998). Roger Y. Tsien began to engineer wtGFP by mutagenesis to produce GFP derivatives. The first important improvement was a single point mutation (GFP-S65T) (Heim et al., 1995). This mutation largely improved the spectral characteristics of GFP by shifting the major excitation peak to 488 nm (**Fig1. B**), and increased fluorescence brightness and photostability (Cubitt et al., 1995). Although organic dyes are reported to be more stable against photobleaching, FPs are still largely used as fluorescent markers thanks to their advantages such as labeling specificity, non-invasive labeling and one-to-one labeling that facilitates quantitative counting.

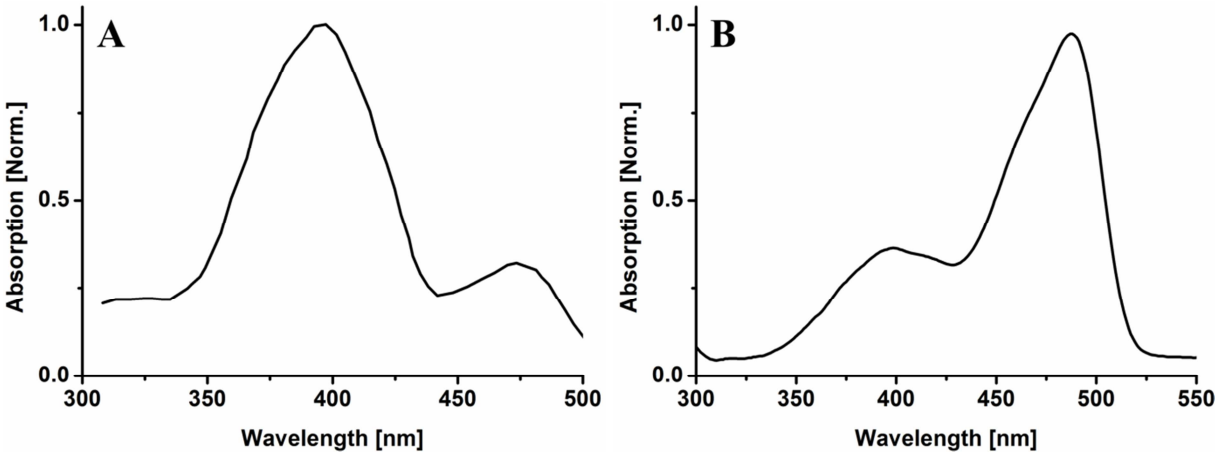

Fig1. *Absorption spectra of GFP (A) (Tsien, 1998), and EGFP (B).*

Tsien and collaborators continued to make various GFP mutants aiming at designing proteins with better brightness and different colors, such as yellow, cyan, blue and red, which cover almost the whole range of visible colors (**Fig2.**). Another important mutant of GFP,

Enhanced GFP (EGFP) developed by Thastrup and Falkow's lab has two mutations compared to wtGFP: F64L and S65T (Cormack et al., 1996). The F64L mutation increased largely the folding efficiency at 37 °C, which, combined with the improvements of S65T, makes EGFP more practical to use as compared to wtGFP.

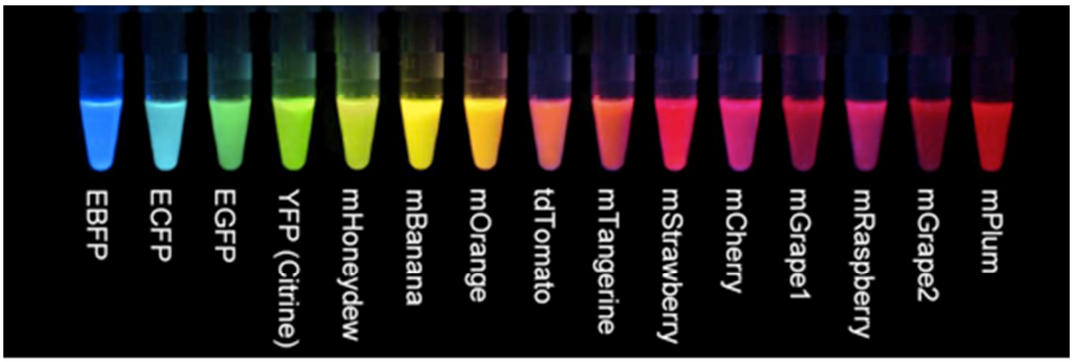

Fig2. *FP variants that emit from blue fluorescence to red fluorescence. (Image from internet)*

The Remington group firstly published the crystal structure of GFP-S65T (Ormö et al., 1996) and subsequently the wtGFP crystal structure was published by the Phillips group (Yang et al., 1996). GFP has a beta barrel structure with a length of 42 Å and a diameter of 24 Å. It is composed of 230 amino acids that form eleven beta strands connected by short polypeptide turns. There is one alpha helix going through the beta barrel with a chromophore 4-(p-hydroxybenzylidene)-5-imidazolinone (p-HBI) formed by the three central amino acids of this helix and situated in the center of the beta barrel. It is believed that this structure, fully conserved within all FPs, largely protects the chromophore from solvent interactions. However, within this thesis, our studies show that this strong protection might be overestimated. In wtGFP, the chromophore is formed by the three amino acids Ser65–Tyr66–Gly67. After protein folding, these three amino acids undergo a complex maturation reaction following a multi-step process including cyclization, oxidation and dehydration (Zhang et al., 2006) (Fig3.). In the first step, cyclization of Tyr and Gly initializes the maturation of the chromophore, and then with the presence of molecular oxygen a hydrogen peroxide is produced by the oxidation reaction. A hydroxylated cyclic imine is formed in this step. At last the final product, a double bonded imidazolinone ring, is formed and a matured chromophore that is fully conjugated is ready to fluoresce (Zhang et al., 2006). The maturation of the chromophore is an autocatalytic process and it doesn't need any external factor except molecular oxygen.

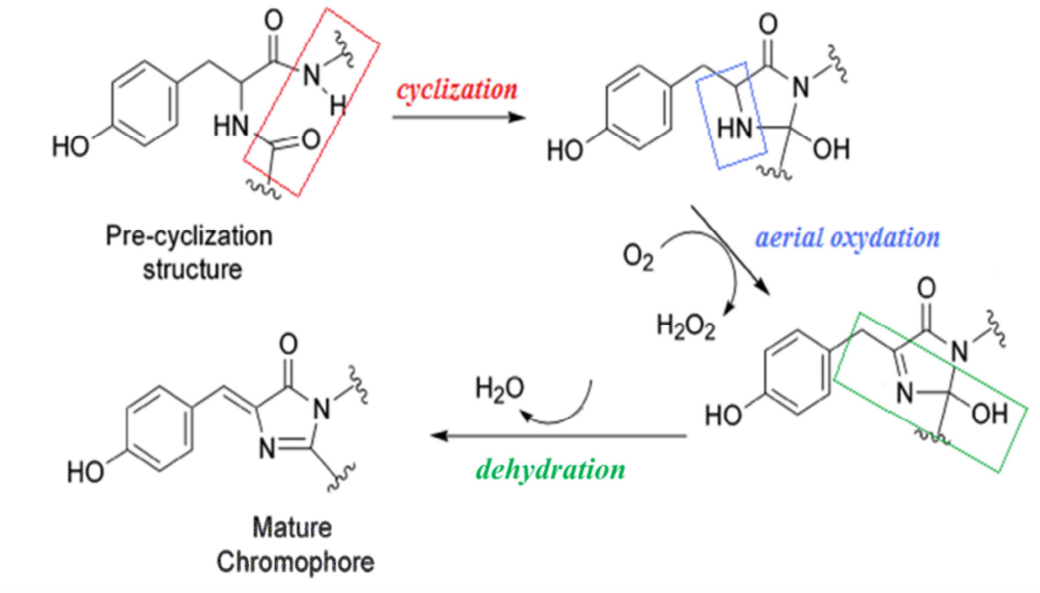

Fig3. *Maturation of the chromophore. (Zhang et al., 2006)*

The resolved structures allowed researchers to visualize the chromophore that is responsible for fluorescence as well as its environment and interactions with neighboring residues. With the help of these crystal structures, engineering of new GFP variants by directed mutagenesis was accelerated and rationalized.

We are far from completely understanding all residues' roles in the FPs, rational engineering of FPs is usually very difficult and brings unexpected consequences. Thus, random mutagenesis is a standard method used in developing FP mutants as well.

Martin Chalfie, Osamu Shimomura and Roger Y. Tsien were honored the 2008 Nobel Prize in Chemistry for their discovery and development of the green fluorescent protein (**Fig4.**).

Fig4. *The Nobel Prize in Chemistry 2008: Osamu Shimomura, Martin Chalfie, Roger Y Tsien (image from internet)*

1.2 PhotoTransformable Fluorescent Proteins (PTFPs)

A subfamily of fluorescent proteins called PhotoTransformable FPs (PTFPs) has the unique optical property that their fluorescent state can be quantitatively modified by actinic illumination. Most of the PTFPs were found in Anthozoan corals unlike wtGFP that is found in Hydrozoan Jellyfish. However, engineering of Hydrozoan FPs can also result in phototransformability. Thanks to their subtle manipulation by light, PTFPs are more and more in the focus of research and in fact, they revolutionized the field of fluorescent microscopy. PTFPs can be classified in three groups: PhotoActivatable Fluorescent Proteins (PAFPs) that can be activated from a non-fluorescent state to a fluorescent state irreversibly by proper light; PhotoConvertible Fluorescent Proteins (PCFPs) that exhibit a nonreversible photoconversion from one fluorescent emission state to another, normally from green to red; and finally, Reversibly Switchable Fluorescent Proteins (RSFPs) that are able to be reversibly switched between nonfluorescent state (*off*-state) and fluorescent state (*on*-state) many times.

1.2.1 PhotoActivatable Fluorescent Proteins (PAFPs)

A single site mutation T203H of wtGFP (Patterson and Lippincott-Schwartz, 2002) generated PhotoActivatable Green Fluorescent Protein (PA-GFP). Its chromophore is initially found in its protonated, non-fluorescent state. The T203H substitution made the side chain of Glu222 (GFP numbering) rotate away from His203. Thus it occupies a slightly different position than that in wtGFP and stabilizes the protonated chromophore that hence cannot fluoresce under 488-nm illumination (Henderson et al., 2009). By illumination with high energy violet light, the highly conserved Glu222 undergoes an oxidative decarboxylation (Kolbe mechanism) followed by a reorganization of the H-bond network, stabilizing the deprotonated chromophore. The fluorescence brightness under excitation by 488-nm light is thus increased 100 times after photoactivation (Patterson and Lippincott-Schwartz, 2002) (**Fig5.**). Other PAFPs such as PA-mRFP1 (Gurskaya et al., 2006), PA-mCherry1 (York et al., 2011), PA-TagRFP (Subach et al., 2010a) can also be activated by UV light to emit red fluorescence.

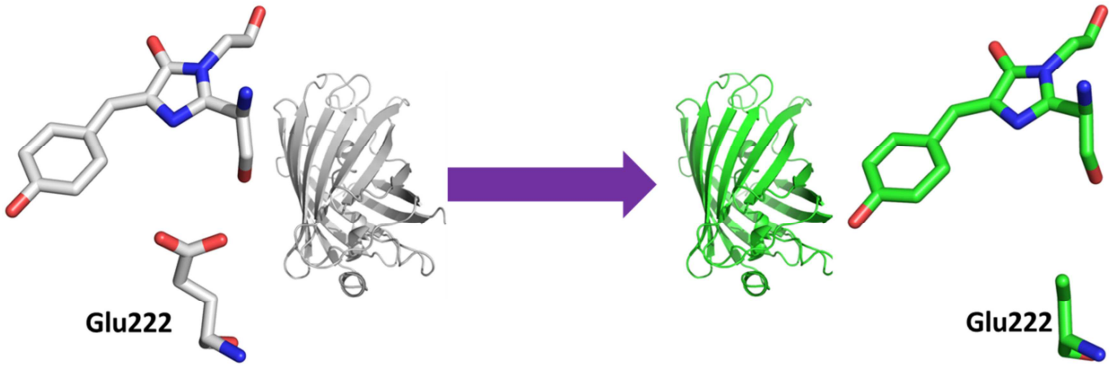

Fig5. *Photoactivation of PA-GFP.*

1.2.2 PhotoConvertible Fluorescent Proteins (PCFPs)

Green-to-Red photoconvertible fluorescent proteins were discovered by chance. Once, Ando *et al* left a sample of Kaede protein on the lab bench without any protection from sunlight. The next day, they noticed that the exposed sample emitted red fluorescence instead of green fluorescence (Ando et al., 2002). Further studies revealed that this green to red conversion mechanism is due to the cleavage of the protein backbone, between the amide nitrogen and Cα atoms of His62 (Mizuno et al., 2003) (**Fig6.**). This cleavage resulted from the absorption of UV light in the protonated state of the chromophore and produced an extension of the electron conjugated system of the chromophore, which induced a red-shifted fluorescence emission. Other proteins such as EosFP (Wiedenmann et al., 2004), mEosFP (Wiedenmann et al., 2004), mEosFP2 (McKinney et al., 2009), Dendra (Gurskaya et al., 2006), Dendra2 (Evrogen) all belong to this protein type. PCFPs are mostly used in PALM (PhotoActivated Localization Microscopy) technique thanks to their good brightness in the green form that is observed at the ensemble level and in the red form that is observed at the single molecule level.

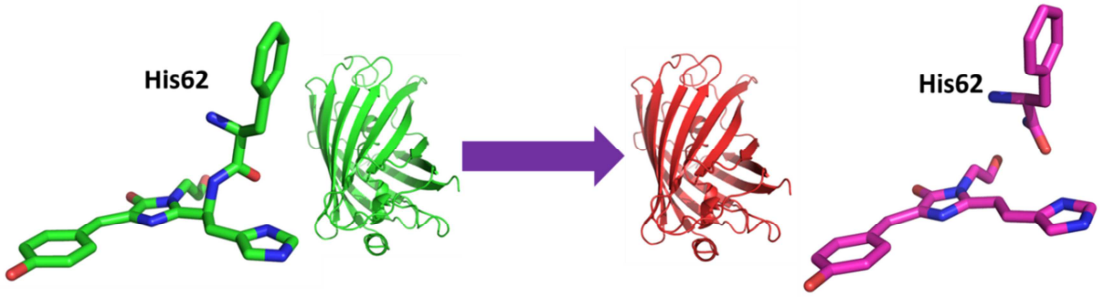

Fig6. *Photoconversion of Kaede.*

1.2.3 Reversibly Switchable Fluorescent Proteins (RSFPs)

The phenomenon of reversible photoswitching was first observed in wtGFP and its yellow variants (Dickson et al., 1997). However, their switching contrast (ratio of emitted fluorescence in the *on* and *off* states) was limited. The first well studied RSFP was Dronpa (Mizuno et al., 2008) due to its good photoswitching behavior. Thanks to the unique ability of repetitive switching, RSFPs open up a number of new possibilities including photochromic FRET (Giordano et al., 2002), and super-resolution microscopy such as two-color PALM (Shroff et al., 2007), RESOLFT (REversible Saturable OpticaL Fluorescence Transitions) (Hofmann et al., 2005) and SSIM (Saturated Structured Illumination Microscopy) (Rego et al., 2012) approaches. With years of development, by using site-directed mutagenesis or random mutagenesis, the RSFP family has largely expanded. In particular, Anthozoan RSFPs and their variants are widely used such as mGOS family (Chang et al., 2012), rsTagRFP (Subach et al., 2010b) and the Dronpa family: Dronpa(Ando et al., 2004), Dronpa2 (Ando et al., 2007), Dronpa3 (Ando et al., 2007), bsDronpa (Andresen et al., 2008), rsFastLime (Stiel et al., 2007) and Padron (Andresen et al., 2008). In recent years, by protein engineering of Hydrozoan EGFP, Mut2Q, EYQ1, EYQ2 (Bizzarri et al., 2010), Dreiklang (Brakemann et al., 2011) , modBFP (Jablonski et al., 2013), rsEGFP (Grotjohann et al., 2011) and rsEGFP2 (Grotjohann et al., 2012) were introduced and reported to have a very good performance in photoswitching.

RSFPs can be subdivided in three types: negative RSFPs, positive RSFPs, and decoupled RSFP.

Crystallographic structures suggested that in negative and positive RSFPs, photoswitching is the consequence of *cis-trans* isomerization of the chromophore, whereas spectroscopic studies showed that light induced protonation/deprotonation were also involved in the photoswitching.

In negative RSFPs such as Dronpa and its variants, in the native state of the proteins, the chromophores are in their *on* state. The excitation light makes the proteins fluoresce and in the meantime, *on*-to-*off* photoswitching competes with the fluorescence. Generally, the chromophore is changed from the *cis* conformation to the *trans* conformation and the protein absorption peak switches from blue to UV, which means *off* switched proteins are protonated. Fluorescence emission can decrease to a very low level. However, the fluorescence emission level can be brought back when the protein is illuminated by UV light (**Fig7.**).

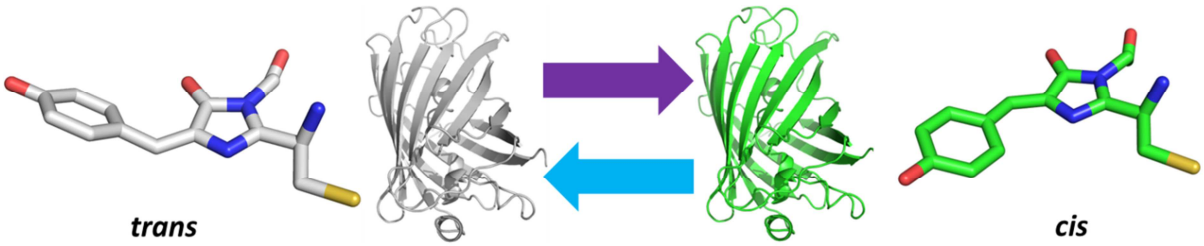

Fig7. *Photoswitching of Dronpa.*

On the contrary to the negative RSFPs, positive RSFPs are typically non-fluorescent in their native state. Chromophores are in their *off* state and upon excitation, they are switched from the *off* state to the *on* state and fluorescence emission level keeps increasing. Padron and asFP595 belong to this group (**Fig8.**).

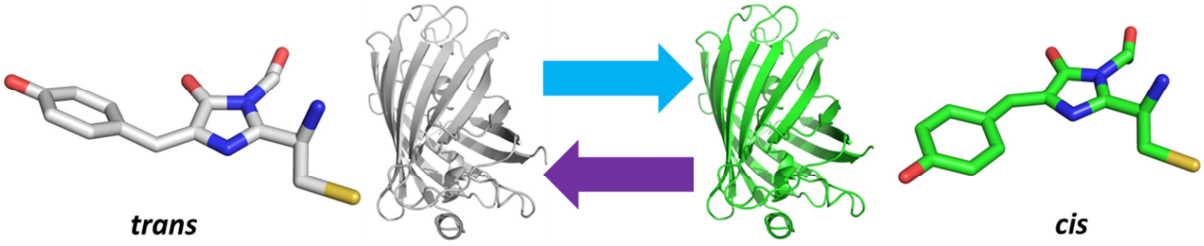

Fig8. *Photoswitching of Padron.*

In 2011, the Jakobs group reported a RSFP with a different photoswitching mechanism: Dreiklang. Dreiklang is neither a negative nor a positive RSFP. Based on crystallography studies, it is proposed that a water molecule close to the imidazolinone ring can be covalently attached or detached, upon photoswitching. This hydration and dehydration is triggered by light that is not absorbed by the *on* or *off* states, hence decoupled from excitation (**Fig9.**).

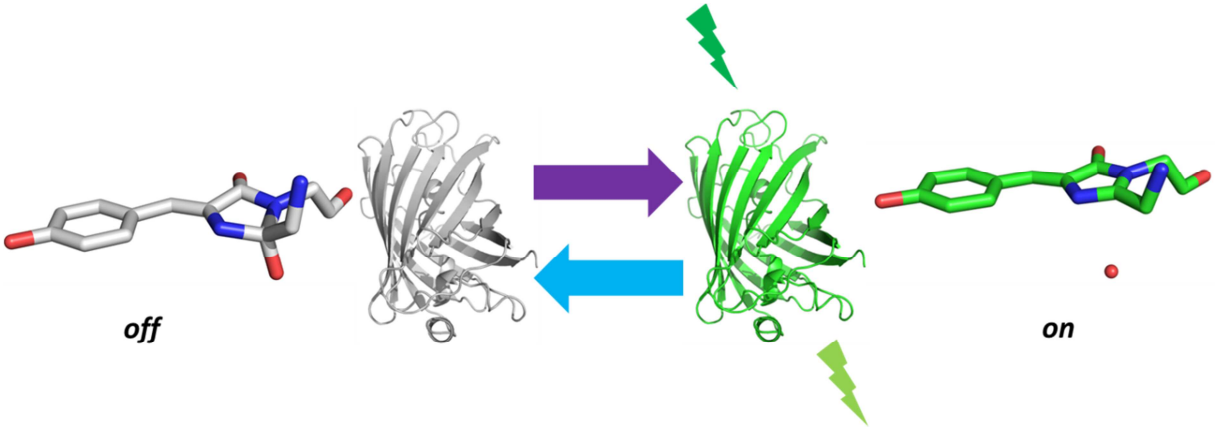

Fig9. *Photoswitching of Dreiklang.*

In recent years, researchers aimed to develop switching speed and contrast of RSFPs to adapt them to advanced imaging technics. For example, rsEGFP2 is a fast switcher with high switching contrast, which allows it to be a good fluorescent marker for RESOLFT. Thanks to its fast switching speed, it significantly accelerates the scanning speed of RESOLFT.

1.3 IrisFP : A combination of RSFP and PCFP

IrisFP is derived from EosFP, a PCFP that is able to be converted from green to red emission by 405 nm light. Mutation of F173S together with a silent mutation F191L generated IrisFP, the first FP reported to combine the properties of RSFPs and PCFPs at the same time. IrisFP is able to photoswitch efficiently in its green state. Upon UV illumination, it can be converted into a red form in which it is also able to switch (**Fig10.**).

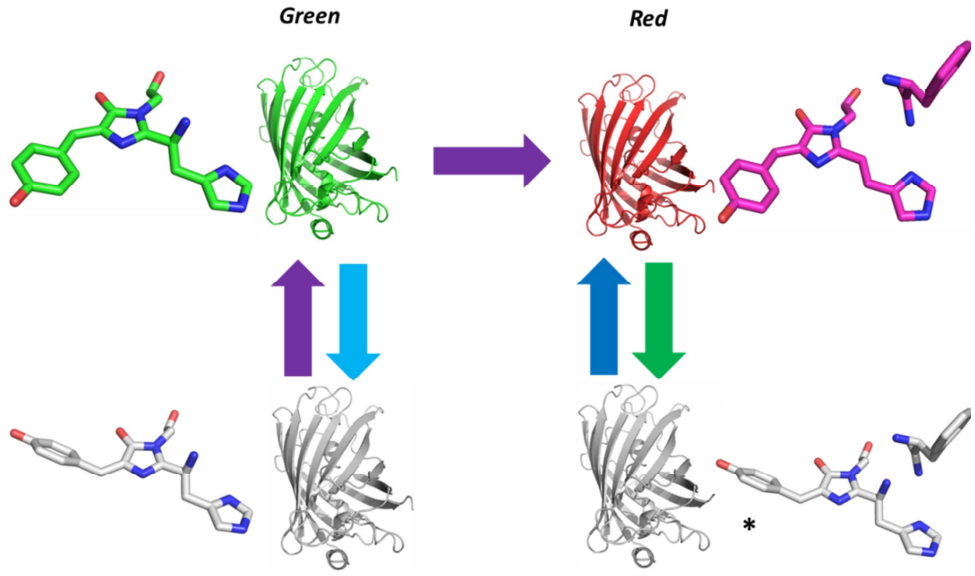

Fig10. *Photoswitching and photoconversion of IrisFP. *Red-trans structure is not available*

Based on the crystallographic structures of IrisFP-green-*on* (PDB entry 2VVH), IrisFP-green-*off* (PDB entry 2VVI) and IrisFP-red-*on* (PDB entry 2VVJ), we can see that this protein undergoes a *cis-trans* isomerization of the chromophore during photoswitching in green form. Like in EosFP, absorption of UV light can lead to protein backbone cleavage and convert IrisFP to its red form. Although the structure of IrisFP in its red-*off* state could not be obtained, it is reasonable to think that in the red state the chromophore isomerizes as well.

The reason why the F173S mutation can turn EosFP into a photoswitchable protein is that Phe173 in EosFP occupies a large space. Upon substitution by the smaller serine residue, a considerable space is freed, which becomes occupied by a labile water molecule w2166 that makes an H-bond to both Ser173 and Thr59. Moreover, Met159 is rotated towards Ser173, which results in another new water molecule w2188 filling the cavity. This water molecule is H-bonded to Ser142, lowering the bond energy of this residue to the chromophore (Moeyaert, 2010).

When illuminated by 488nm light (absorption peak in green-*on* form corresponding to deprotonated chromophore) we can see the decrease of both fluorescence at 512 nm and absorption at 488 nm, meanwhile the absorption peak at 390 nm corresponding to the protonated chromophore increases. When the *off* switched protein is illuminated by UV light (405 nm), the absorption of the protonated chromophore decreases and that of the deprotonated chromophore increases together with fluorescence emission. In the red form, the situation is similar, except that red fluorescence emission is at 580 nm and that 551 nm light is responsible for *on*-to-*off* switching and 450 nm light is responsible for *off*-to-*on* switching (**Fig11.**). Monomeric variants exist that combine properties of RSFPs and PCFPs such as Denra2-M159A, Dendra2-F173S (Adam et al., 2011), mIrisFP (Adam et al., 2011), pcDronpa2 (Moeyaert et al., 2014) and NijiFP (Adam et al., 2011).

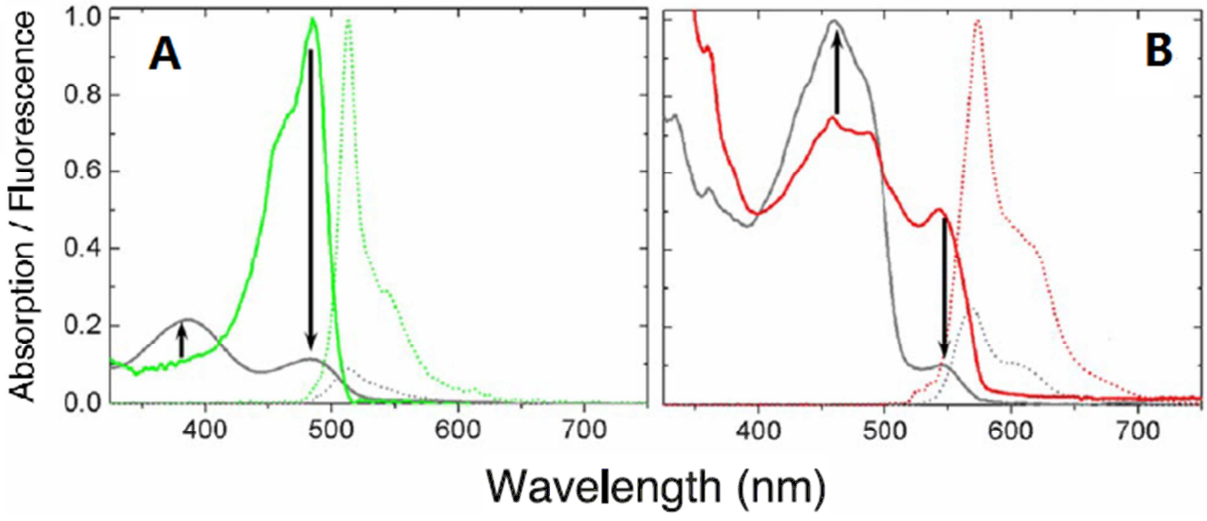

Fig11. *Absorption and emission spectra of IrisFP displayed by solide line and dashed lines, respectively. (A) Irradiation by 488 nm light, decreases absorption at 488 nm as well as fluorescence at 516 nm and increases absorption at 390 nm. (B) Irradiation by 532 nm light, decreases absorption at 551 nm and fluorescence at 580 nm and increases absorption at 440 nm. Image from (Adam et al., 2008)*

1.4 Photobleaching and photofatigue

Photobleaching (**Fig12.**) is the permanent loss of fluorescence emission capacity, in contrast to photoblinking that is reversible and photophysically more complex. We don't discuss the photoblinking in this thesis.

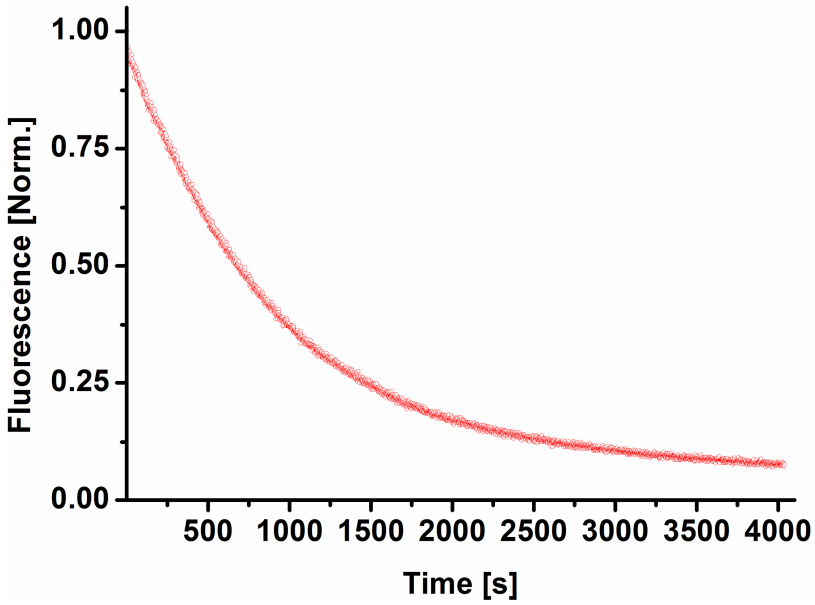

Fig12. *Photobleaching of EGFP. Fluorescence decays upon excitation of 473 nm light (~100W/cm²).*

In fluorescence microscopy, photobleaching is always a problematic issue since it can introduce difficulties for data accuracy and analysis. For example, in time-lapse fluorescence microscopy, a series of images are recorded as a function of time. Photobleaching of fluorescent markers makes the time of observation of live cells limited. Most published studies about photobleaching deal with organic dyes (Zheng et al., 2014). Oxygen is generally considered as the main factor that is responsible for photobleaching of these fluorophores (Christ et al., 2001; Song et al., 1995; Zondervan et al., 2004). It is reported that fluorophores in their singlet excited state can hardly react with oxygen due to the short lifetime (several ns) of these states (Gollnick et al., 1992). Because of the considerably longer lifetime of the triplet state, it is usually considered to be the departure point of the harmful reactions that can induce photobleaching (Song et al., 1996). Typically, electron transfer or energy transfer from a fluorophore in the triplet state to molecular oxygen (whose ground state is triplet state), can return the chromophore to its ground state and generate superoxide radical or singlet oxygen that are very reactive (Zheng et al., 2014). The reactive oxygen species (ROS) can easily

attack and destroy the fluorophore by introducing irreversible chemical modifications, typically oxidation. The generated ROS also have the possibility to diffuse and react with closeby molecules, which causes phototoxicity. Thus people often add antifading reagents (acting thanks to their reducing property), or oxygen scavenging enzyme (Cordes et al., 2009; Penttilä et al., 1996), or both of them (Rasnik et al., 2006) to the cell culture medium to reduce photobleaching effects. Some studies showed that the photobleaching rate non-linearly increases as a function of excitation power intensity, indicating multi-photon absorption by the chromophore (Hoogenboom et al., 2005).

However, in case of FPs, the photobleaching mechanism is more complicated. Unlike in the organic dyes that are fully exposed to the solvent environment, the chromophore of FPs is buried in the center of the beta barrel and has close interactions with the surrounding residues. The beta barrel limits the access of oxygen molecules. A study demonstrated that EGFP can generate singlet oxygen but with lower efficiency than that of the isolated HBDI chromophore exposed to the solvent, suggesting that the beta barrel provides shielding of the chromophore (Jimenez-Banzo et al., 2008). Therefore, less oxygen could produce less phototoxicity. However, photobleaching in FPs is facilitated due to the complex interaction of the chromophore with its surrounding residues. The generated ROS are not only able to attack the chromophore itself but also other residues inside the FP molecule. Another study showed that, for example, in RFP, photobleaching is caused by chromophore photoreduction (Vegh et al., 2014). Photobleaching also depends on the cell environment (Malkani and Schmid, 2011).

Photobleaching can be used at advantage in biological applications as well. The most widely used technics are FRAP (Fluorescence Recovery After Photobleaching) (White and Stelzer, 1999), FLIP (Fluorescence Loss In Photobleaching) (Wustner et al., 2012) that allow investigators to measure molecule mobility *in vivo*. Photobleaching can also be applied in counting protein molecules by stepwise photobleaching, which allows researchers to quantify molecule number in a cluster or determine the protein oligomerization sate (Groulx et al., 2011; Zijlstra et al., 2012). PALM is based on the principle of repeated single molecules activation, localization and photobleaching.

Different FPs display diverse photobleaching kinetics that result from different chromophore photostability and environments. Usually the fluorescence curve doesn't show a mono-exponential decay suggesting that multiple photophysical processes may occur.

Within RSFPs, upon excitation, fluorescence emission competes with other photophysical processes, in particular, *on*- or *off*–switching and photobleaching. For example, under illumination, negative RSFPs quickly lose their fluorescence due to a combination of

off-switching and photobleaching. In one photoswitching cycle, due to the much lower photobleaching quantum yield (typically 10^{-5}) than photoswitching quantum yield (10^{-2}-10^{-3}), most of the chromophores are switched to their *off* state and are still capable to fluoresce when switched *on* again. However, upon a large number of photoswitching cycles, the photobleached chromophores accumulate. Overall, at the ensemble level, the amplitude of fluorescence of each cycle decreases and the achievable number of photoswitching cycles is thus limited, a process known as photofatigue (**Fig13.**).

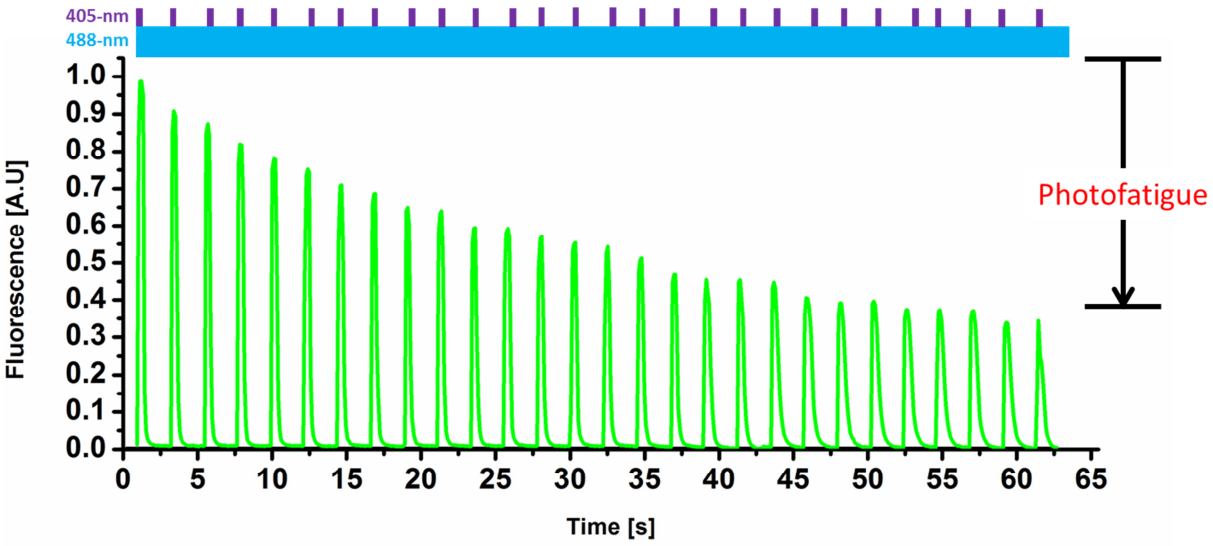

Fig13. *Photofatigue of IrisFP. The maximum of fluorescence intensity at each cycle decreases because of photobleaching.*

1.5 Goal of thesis

Due to their unique property of reversible switchability, RSFPs have become a very powerful tool in the field of bio-imaging, reversible data storage, viscosity measurement, optogenetics (**Fig14.**)

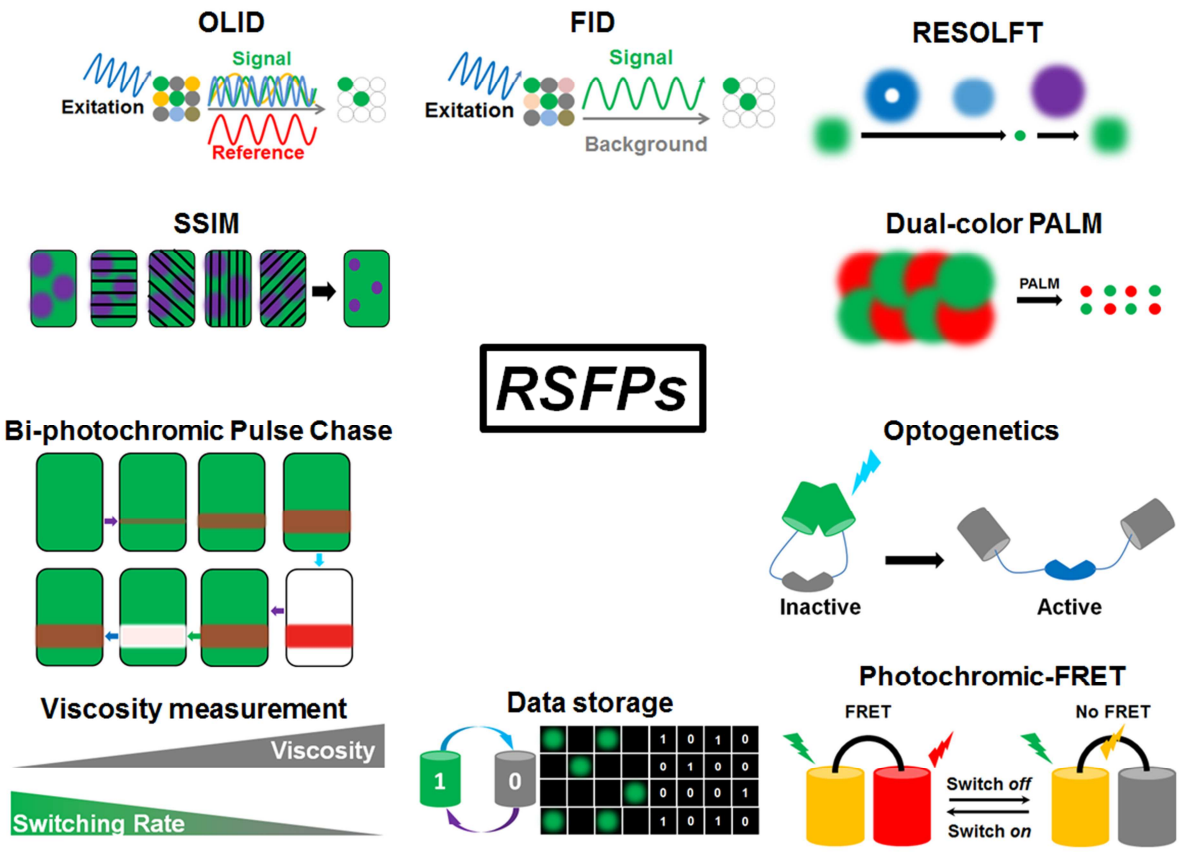

Fig14. *Applications of RSFPs (Duan et al., 2014).*

Amongst these technics, super-resolution imaging such as RESOLFT, Photochromic SOFI (pcSOFI) (Dedecker et al., 2012), Nonlinear Structured Illumination Microscopy (NSIM) (Gustafsson, 2005) essentially depend on a large number of switching cycles of RSFP molecules. Thus a high resistance against photofatigue is required. For instance, in RESOLFT, a confocal system is employed. At each position of the scanner, a donut shaped dump light is applied to switch off all the molecules in the peripheral area leaving only molecules in the beam center active. A readout beam is then applied to detect the active labeled molecules and their signals are recorded. At the end, a reset beam is employed to restore molecules back to their *on* state, then the detector head moves to the next point. To obtain a high spatial resolution, the scanning step is required to be very small. Thus, a given molecule should be able to undergo several dozens of switching cycles (typically ~100 to achieve a spatial resolution of 1/10 of the PSF width in both X and Y dimensions).

As mentioned before, the photobleaching mechanism of FPs is not clearly understood. And this also applies to the photobleaching mechanisms within RSFPs. Random mutagenesis and large scale screening are usually used to generate better RSFPs mutants in terms of brightness, fluorescence quantum yield, photoswitching speed, photoswitching contrast.

However, screening of mutants with enhanced photoresistance would be more delicate because it is notably time consuming. Thus, it would be strongly desirable to design better performing mutants in a rational manner. Although our understanding of brightness or fluorescence quantum yield is increasing, we still have very limited knowledge about photobleaching. Therefore, the understanding of the photobleaching mechanisms of RSFPs is very important. However, there was no previous study of photobleaching of RSFPs before this thesis. Thanks to our experience in combined kinetic X-ray crystallography and optical spectroscopy (absorption, fluorescence and Raman spectroscopy) and good knowledge of PTFPs, and in collaborating with researchers specialized in QM/MM and molecular dynamics modeling, we have acquired the tools to explore the photobleaching mechanisms of RSFPs. We have chosen IrisFP as our model FP to investigate the photobleaching mechanism in Anthozoan RSFPs since its photophysical properties have been extensively studied in our team, including its crystallographic structures in green-*cis*, green-*trans*, red-*cis* (Adam et al., 2008) and blinked states (Adam et al., 2009). Based on our understanding of the photobleaching mechanism of IrisFP from these studies, we rationally designed an IrisFP mutant with increased photostability that could be more suitable to the above-mentioned techniques.

CHAPTER 2

Articles

Article 1: **Duan, C., Adam, V., Byrdin, M., Ridard, J., Kieffer-Jaquinod, S., Morlot, C., Arcizet, D., Demachy, I., Bourgeois, D., 2013. Structural evidence for a two-regime photobleaching mechanism in a reversibly switchable fluorescent protein. J Am Chem Soc 135, 15841-15850.**

Article 2: **Duan, C., Byrdin, M., El Khatib, M., Henry, X., Adam, V., Bourgeois, D., 2014b. Rational Design of Enhanced Photoresistance in a Photoswitchable Fluorescent Protein. Methods and Applications in Fluorescence, In press.**

Article 3: **Duan, C., Adam, V., Byrdin, M., Bourgeois, D., 2014a. Structural basis of photoswitching in fluorescent proteins. Methods Mol Biol 1148, 177-202.**

Abstract of article 1

The first photobleached structure of IrisFP that we observed was from a crystal irradiated by X-rays at cryotemperature (100K). It displayed a decarboxylation of Glu212 and a distorted chromophore. However, this condition is far from the condition that is found in a microscopy experiment. We were interested to know if these structural changes also happen under real experimental conditions. Thus, we tried to carry out experiments at room temperature using the PALM microscope that was set up in our lab. Using the PALM setup, we were able to photobleach protein crystals under PALM conditions. X-ray crystallography then showed that an oxygen-independent photobleaching occurred where dramatic structural changes happened (characterized by light-induced decarboxylation of the strictly conserved Glutamate 212 coupled with chromophore conformational changes and H-bond network rearrangement, which destroy the π conjugated system of the chromophore). To try to figure out the chemical nature of the photobleached chromophore, molecular dynamics simulations were performed by our collaborators at Physical Chemistry Laboratory at University of Paris 11. Suggested by the simulation, under high-intensity illumination, photobleaching is a redox-based process, where the methylene bridge of the chromophore was reduced resulting in the destruction of the π conjugated system. Due to the high laser intensity, the crystals were often damaged. In order to preserve crystal quality, we largely decreased the laser intensity. To our surprise, although crystals survived photobleaching, they had even worse diffraction quality. We found that, in contrast to the high-intensity illumination, under low-intensity illumination, an oxygen-dependent photobleaching occurred, which introduces only few structural changes. The photobleached structure shows an intact chromophore and surrounding H-bond network. The decarboxylation of Glu212 doesn't take place. Crystallographic data showed positive electron densities close to Met159 and Cys171. To interpret this data, we collaborated with Sylvie Kieffer-Jaquinod at Laboratoire de Biologie à Grande Echelle at CEA. Confirmed by mass spectrometry, Met159 and Cys171 are found sulfoxided. The neighboring Met159 is supposed to be responsible for the photobleaching, because when sulfoxided, it forms a strong H-bond with the chromophore, trapping it in a protonated state that is non-fluorescent.

JACS
JOURNAL OF THE AMERICAN CHEMICAL SOCIETY

Article

pubs.acs.org/JACS

Structural Evidence for a Two-Regime Photobleaching Mechanism in a Reversibly Switchable Fluorescent Protein

Chenxi Duan,[†,‡,§,∥] Virgile Adam,[†,‡,§,∥] Martin Byrdin,[†,‡,§,∥] Jacqueline Ridard,[⊥] Sylvie Kieffer-Jaquinod,[#,$] Cécile Morlot,[†,‡,§] Delphine Arcizet,[†,‡,§,∥] Isabelle Demachy,[⊥] and Dominique Bourgeois*[,†,‡,§,∥]

[†]Université Grenoble Alpes, Institut de Biologie Structurale (IBS), F-38027 Grenoble, France
[‡]CNRS, IBS, F-38027 Grenoble, France
[§]CEA, DSV, IBS, F-38027 Grenoble, France
[∥]Laboratoire de Physiologie Cellulaire et Végétale, IRTSV, CNRS/CEA/INRA/Université Grenoble Alpes, Grenoble, 38054, France
[⊥]Laboratoire de Chimie Physique, UMR 8000, CNRS, Université Paris Sud 11, 91405 Orsay, France
[#]Biologie à Grande Echelle, IRTSV, CEA, Grenoble, France
[$]INSERM, U1038, Grenoble, France

Supporting Information

ABSTRACT: Photobleaching, the irreversible photodestruction of a chromophore, severely limits the use of fluorescent proteins (FPs) in optical microscopy. Yet, the mechanisms that govern photobleaching remain poorly understood. In Reversibly Switchable Fluorescent Proteins (RSFPs), a class of FPs that can be repeatedly photoswitched between nonfluorescent and fluorescent states, photobleaching limits the achievable number of switching cycles, a process known as photofatigue. We investigated the photofatigue mechanisms in the protein IrisFP using combined X-ray crystallography, optical *in crystallo* spectroscopy, mass spectrometry and modeling approaches. At laser-light intensities typical of conventional wide-field fluorescence microscopy, an oxygen-dependent photobleaching pathway was evidenced. Structural modifications induced by singlet-oxygen production within the chromophore pocket revealed the oxidation of two sulfur-containing residues, Met159 and Cys171, locking the chromophore in a nonfluorescent protonated state. At laser-light intensities typical of localization-based nanoscopy (>0.1 kW/cm^2), a completely different, oxygen-independent photobleaching pathway was found to take place. The conserved Glu212 underwent decarboxylation concomitantly with an extensive rearrangement of the H-bond network around the chromophore, and an sp^2-to-sp^3 hybridization change of the carbon atom bridging the chromophore cyclic moieties was observed. This two-regime photobleaching mechanism is likely to be a common feature in RSFPs from Anthozoan species, which typically share high structural and sequence identity with IrisFP. In addition, our results suggest that, when such FPs are used, the illumination conditions employed in localization-based super-resolution microscopy might generate less cytotoxicity than those of standard wide-field microscopy at constant absorbed light-dose. Finally, our data will facilitate the rational design of FPs displaying enhanced photoresistance.

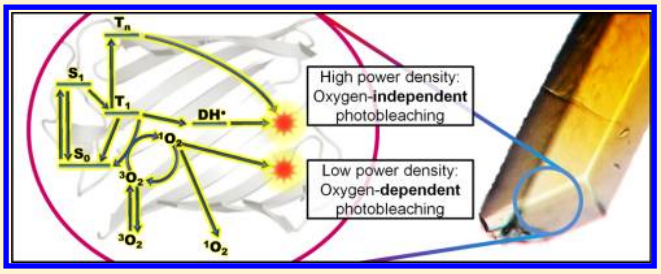

INTRODUCTION

Recent progresses in fluorescence bioimaging techniques have benefited from the rapid development of a large palette of fluorescent proteins (FPs).[1] However, the limited photostability of FPs has remained a major impediment to their successful use in many approaches including single-molecule, FRET, time-lapse or super-resolution microscopies. FPs typically can only emit ∼10^5 photons before their chromophores fall victim to irreversible photodestruction.[2] The detailed photophysical mechanisms leading to photobleaching in FPs remain largely unknown, although some structural insight has been obtained in the case of KillerRed, a highly phototoxic FP.[3−5] Successful efforts to obtain more photostable variants have mainly relied on directed evolution approaches.[2,6−8]

In reversibly switchable fluorescent proteins (RSFPs),[9] photobleaching manifests itself in a process referred to as "photofatigue". RSFPs can be repeatedly photoswitched between a fluorescent (on) and a nonfluorescent (off) state by illumination with visible light of appropriate wavelengths. Photoswitching capabilities are central to a growing number of advanced techniques including a variety of super-resolution modalities,[10−14] photochromic FRET,[15] optical lock-in detection,[16] frequency-domain imaging,[17] optogenetic manipula-

Received: July 5, 2013
Published: September 23, 2013

   dx.doi.org/10.1021/ja406860e | J. Am. Chem. Soc. 2013, 135, 15841−15850

tion[18] and bio data-storage.[19,20] However, because photobleaching competes with photoswitching, a progressive decrease in fluorescence intensity at each on−off cycle (that is, photofatigue) is observed in ensemble experiments, and at the single molecule level, the number of achievable on−off cycles is limited. Thus, photofatigue fundamentally limits the achievable resolution in nanoscopy approaches such as optically linear fluorescence transition microscopy (RESOLFT)[10] and nonlinear structured illumination microscopy (NSIM),[14] or the contrast enhancement capability in frequency-domain based microscopy schemes.[16,17] Efforts to develop fatigue-resistant RSFPs have been made recently, again essentially based on directed-evolution approaches.[20−22]

Several parameters exert an influence on the photostability of fluorescent proteins. Although the compact FP β-barrel partially shields the chromophore against molecular oxygen, a number of experimental,[23−25] and theoretical[26,27] investigations concluded that O_2 plays an important role in photobleaching of FPs. However, the exact mechanism by which oxygen-dependent chromophore photodestruction occurs has not been directly visualized. Light-induced redox chemistry has also been described to cause a variety of chromophore phototransformations[28] and the photostability of GFP and some derivatives has been shown to depend on the presence of redox-active components in the environment.[29,30] Decarboxylation of the strictly conserved Glu212 (IrisFP numbering, corresponding to Glu222 in GFP) has been described in several cases and is notably involved in photoactivation[31−33] or the formation of super-red species.[34] Such decarboxylation was also observed in experimental conditions not routinely used in fluorescence microscopy, such as at cryogenic temperature[5,35] or under X-ray irradiation.[36,37] The possible involvement of Glu212 decarboxylation in photobleaching under commonly used fluorescence microscopy schemes, nevertheless, has not been documented. In general, it has been repeatedly reported that the photostability of fluorescent proteins may strongly depend on illumination conditions.[2,38−41]

Here, we set out to study the photofatigue mechanism of the biphotochromic RSFP named IrisFP,[42] under experimental conditions typical of wide-field diffraction-limited and super-resolution microscopy. Our previous investigations had revealed the structural and spectroscopic signature of IrisFP in its green and red on-states (chromophore in *cis* conformation), in the corresponding off-states (chromophore in *trans* conformation), and in a reversible dark state (displaying a transiently distorted chromophore geometry consistent with a radical species protonated at atom Cα of the methylene bridge[37,43]). In the present work, employing a combination of kinetic X-ray crystallography, *in crystallo* UV−vis absorbance, fluorescence and Raman spectroscopies, mass spectrometry, and molecular dynamics simulations, we discovered two distinct photobleaching mechanisms in IrisFP. The first mechanism is oxygen-independent, whereas the second is oxygen-dependent. A switch from the first to the second mechanism was observed as the illumination power density was decreased from levels typical of localization-based nanoscopy to those of standard wide-field microscopy.

EXPERIMENTAL PROCEDURES

Experimental procedures are described in details in the Supporting Information.

RESULTS

Photofatigue at High Illumination Intensity. In green IrisFP, illumination by 488-nm (cyan) light isomerizes the fluorescent *cis* anionic chromophore to a *trans* nonfluorescent neutral configuration (quantum yield = 3.2×10^{-3}). Back-switching to the fluorescent *cis* state is efficiently achieved with 405-nm (violet) light (quantum yield =0.15).[42] We thought of studying the photofatigue of green IrisFP in crystallo under experimental conditions typical of super-resolution PALM microscopy, that is, under relatively high excitation laser power density (~0.1 kW/cm^2 at 488 nm, see the Supporting Information, Figure S1A). After 10 min of alternating illumination at 488 and 405 nm, corresponding to about 260 switching cycles, the fluorescence intensity was largely reduced (Figure 1). The decay of the fluorescence envelope appears

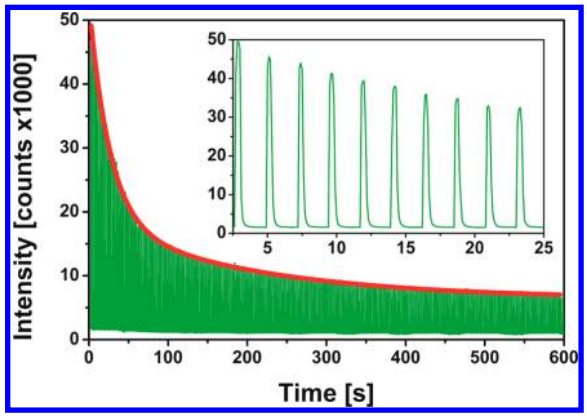

Figure 1. Photofatigue fluorescence decay of crystalline IrisFP under high-intensity illumination by 488-nm (~100 W/cm^2, continuous) and 405-nm (~1 W/cm^2, on for 0.3 s every 2.3 s) laser light. Fluorescence was recorded at 512 nm. The crystal was submitted to 260 switching cycles during 10 min of illumination, which resulted in the loss of ~75% of its initial fluorescence emission. The inset shows an enlarged view of the decay over the first 10 cycles. The fluorescence envelope can be fitted with a biexponential decay model (red trace).

biphasic and can be fitted with a biexponential model in which ~75% of the molecules undergo rapid bleaching and ~25% undergo ~10 times slower bleaching (see discussion in the Supporting Information). Absorbance by the anionic chromophores largely decreased without any increase of the neutral species, suggesting that most molecules were irreversibly bleached (Figure 2A). Similar behavior was observed in solution (Figure S2, Supporting Information).

Experimental difference electron density maps between fatigued and nonfatigued parts of a single crystal (Figure 2C and Table S1, Supporting Information) revealed a complex set of structural modifications confined in the chromophore pocket (Figure S5A, Supporting Information). Strong negative electron density at Glu212 suggested decarboxylation of this residue, as unambiguously confirmed by mass spectrometry analysis (Table S2, Supporting Information). The hydrogen-bond network around the chromophore was largely perturbed, with three water molecules being dislocated and Arg66 and His194 adopting a conformation similar to that found in the *trans* state of the chromophore. The phenolate group of the chromophore appeared largely disordered, together with the hydroxyl group of Ser142 normally H-bonded to the chromophore phenolate. The imidazolinone ring, however, remained planar. These crystallographic data suggest that the chromophore is no longer

dx.doi.org/10.1021/ja406860e | J. Am. Chem. Soc. 2013, 135, 15841−15850

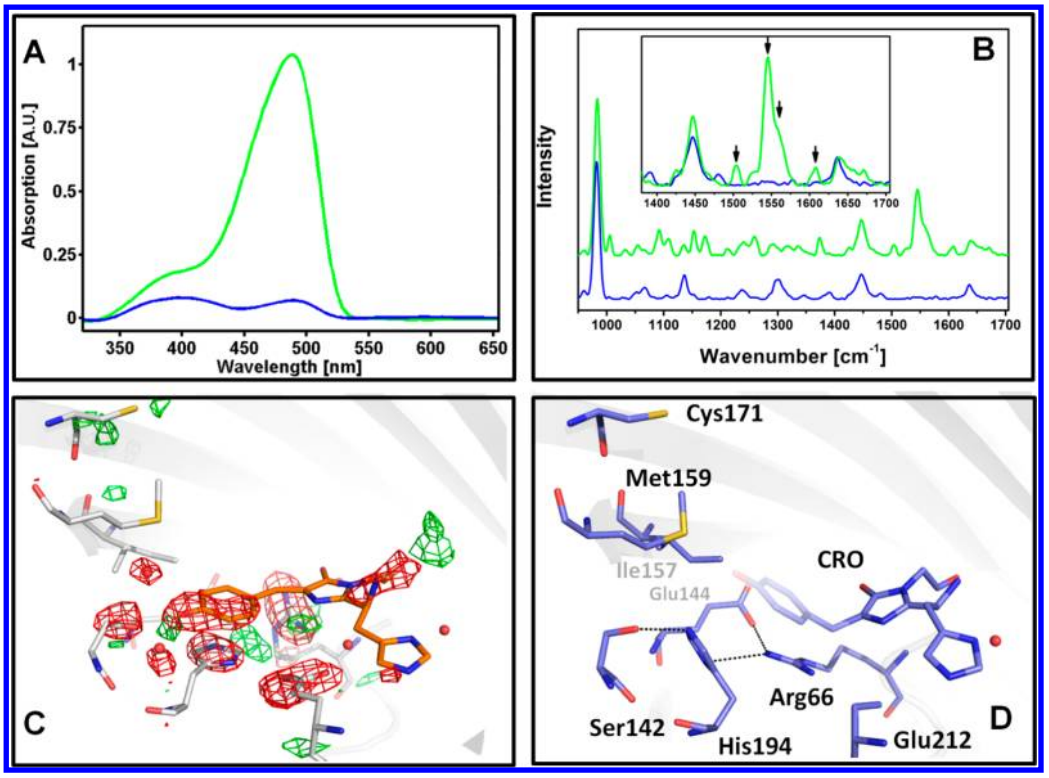

Figure 2. (A) Absorption spectra of crystalline IrisFP before (green) and after (blue) high-intensity photobleaching. Both anionic and neutral bands are largely decreased. (B) Raman spectra of crystalline IrisFP before (green) and after (blue) high-intensity photobleaching. The complete disappearance of the 1503, 1545, 1604, and 1564 cm^{-1} bands (inset, arrows) suggests the breakage of the chromophore methylene bridge π-conjugation (C) NCS-averaged experimental difference electron density map $F_{obs,bleached} - F_{obs,native}$ upon high-intensity photobleaching, overlaid on the crystallographic structure of intact IrisFP (PDB model 2VVH). The chromophore (orange) and the important surrounding residues (gray) in the chromophore pocket are shown. Positive electron density is shown in green (+5 σ) and negative electron density is shown in red (−5 σ). (D) Refined model of high-intensity photobleached IrisFP. The chromophore phenolate moiety is represented in dim color to highlight the disorder observed in the electron difference density map. H-bonds are represented with dashed lines, and water molecules as red balls.

properly held in place by the protein matrix and may have lost its electron conjugation.

To gain further insight into the chemical modifications of the chromophore, we performed *in crystallo* Raman spectroscopy of IrisFP crystals illuminated in the same manner. Upon photobleaching, the spectra (Figure 2B) showed considerable modifications (see discussion in the Supporting Information), notably a complete disappearance of the bands at 1503 cm^{-1} and 1545 cm^{-1} (anionic chromophore) and 1564 cm^{-1} and 1604 cm^{-1} (neutral chromophore). The strongly resonance-enhanced band at 1545 cm^{-1} has been assigned to a mode that combines stretching of the Cα═C5 exocyclic double bond and deformation of the imidazolinone moiety of the chromophore[44] (for chromophore atoms nomenclature, see Scheme S1 in the Supporting Information). In the neutral state of the chromophore, this band is shifted to 1564 cm^{-1}, consistent with a more localized electron density in this state. The loss of these bands, together with the vanished UV−vis absorbance, strongly suggests that the Cα carbon atom of the chromophore methylene bridge converts from an sp^2-hybridized to an sp^3-hybridized configuration, possibly as a result of intramolecular electron and proton transfer.[43] Based on these findings, as well as on further molecular dynamics simulations (see below) a model of photodamaged IrisFP was refined (Figure 2D).

Overall, these data suggest that under high-intensity illumination IrisFP suffers from a redox-based photofatigue mechanism, which is associated to decarboxylation of Glu212.

Photofatigue at Low Illumination Intensity. Submitting IrisFP crystals to repeated high-intensity laser illumination is a harsh procedure that often compromises their diffraction quality. In an attempt to better preserve the samples, we photofatigued IrisFP crystals at ∼10 times lower power density (∼10 W/cm^2 at 488 nm, see the Supporting Information, Figure S1B). After 100 min of alternating cyan and violet illumination (460 switching cycles), fluorescence emission was again largely reduced (Figure 3). However, the fluorescence photofatigue decay profile (Figure 3, red curve) significantly differed from that under high illumination, although a biexponential model was still required to achieve a satisfactory fit (see discussion in the Supporting Information).

To our surprise, the diffraction quality of the crystals was not improved. Instead, it was generally even more degraded. Furthermore, crystallographic analysis revealed neither any substantial structural changes of Glu212 nor any significant distortion or disorder of the chromophore (Figure 4C and Table S1, Supporting Information). Instead, additional positive electron density close to the sulfur atoms of both Met159 and Cys171 was noticed in the difference electron density maps (Figure 4C and Figure S5B, Supporting Information). Absorption spectra of crystals fatigued in this way showed a decreased anionic band but an increased neutral band (Figure 4A). A titration experiment revealed that the pK_a of the photofatigued chromophore increased to ∼12 (Figure S8, Supporting Information) instead of 5.7 under native conditions,[45] suggesting that the chromophore has been trapped in

dx.doi.org/10.1021/ja406860e | J. Am. Chem. Soc. 2013, 135, 15841−15850

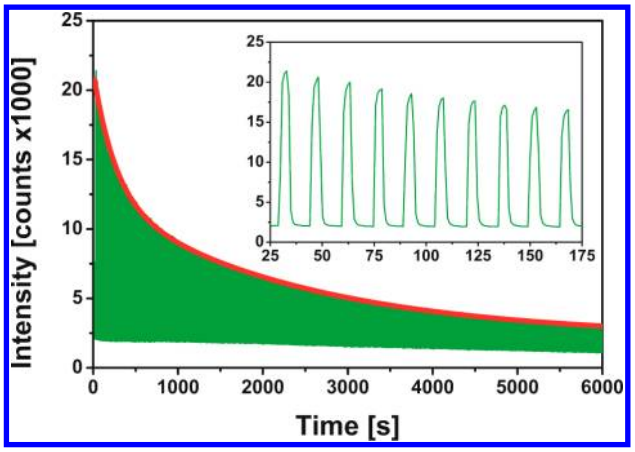

Figure 3. Photofatigue fluorescence decay of crystalline IrisFP under low-intensity illumination by 488-nm (~10 W/cm^2, continuous) and 405-nm (~0.01 W/cm^2, on for 4 s every 12 s) laser light. Fluorescence was recorded at 512 nm. The crystal was submitted to 460 switching cycles during 100 min of illumination, which resulted in the loss of ~90% of its initial fluorescence emission. The inset shows an enlarged view of the decay over the first 10 cycles. The fluorescence envelope can be fitted with a biexponential decay model (red trace).

a nonfluorescent protonated state. Raman spectrometry of a partially fatigued crystal confirmed this finding, displaying an increase of the vibrational bands associated with the neutral chromophore (1564 cm^{-1}, 1604 cm^{-1}) at the expense of those associated with the anionic chromophore (1503 cm^{-1}, 1545 cm^{-1}) (Figure 4B), but without signs of a ruptured π-system. Finally, peptide analysis of a photofatigued sample by mass spectrometry revealed a substantial increase in the level of oxidation of a number of fragments containing methionine, cysteine, and tryptophan residues (Figure S9, Supporting Information). In particular, fragments that contained Met159 had ~320% higher mono-oxidation levels than those of intact IrisFP. Oxidation levels of fragments containing Cys171 were also raised significantly (see Figure S9 caption in the Supporting Information). Conversely, the decarboxylation level of Glu212 remained unaltered as compared to nonbleached IrisFP (Table S2, Supporting Information). These data suggest that, under low-intensity illumination, photofatigue of IrisFP results in sulfoxidation of Met159 and Cys171, followed by oxidation of other residues more remote from the chromophore pocket. Comforted by the mass spectrometry results, we modeled the two positive features near Met159 and Cys171 in the difference electron density map as oxygen atoms covalently bonded to the sulfur atoms of these residues, respectively (Figure 4D). A new water molecule was also modeled next to Met159, above the chromophore hydroxybenzylidene ring. The sulfoxidized Met159 was found to form a tight H-bond (2.8 Å) between the newly added oxygen atom and the presumably protonated chromophore phenol moiety. This tight H-bond is consistent with the extremely high pK_a measured for the fatigued chromophore. Interestingly, the level of Met159 and Cys171 sulfoxidation

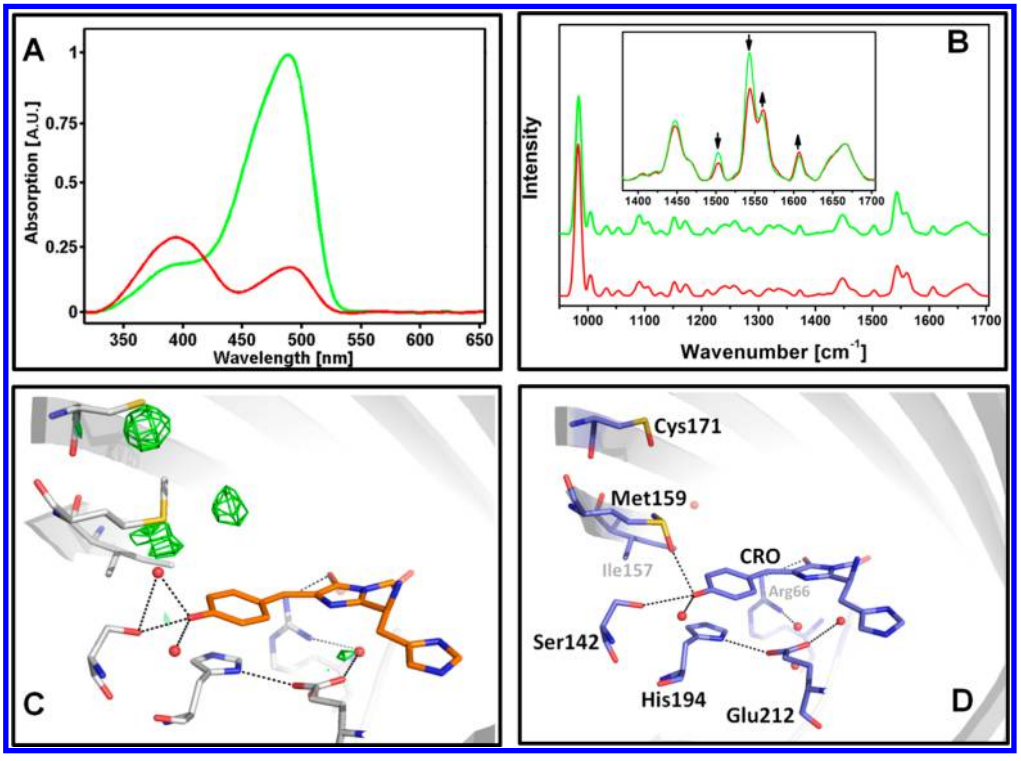

Figure 4. (A) Absorption spectra of crystalline IrisFP before (green) and after (red) low-intensity photobleaching. The intensity of the anionic band at 488 nm decreased while that of the neutral band at 390 nm increased. (B) Raman spectra of crystalline IrisFP before (green) and after (red) partial low-intensity photobleaching. The decrease of the 1503 cm^{-1} and 1545 cm^{-1} bands and the increase of the 1604 cm^{-1} and 1564 cm^{-1} bands (inset, arrows) is consistent with a conversion from the anionic to a neutral state of the chromophore without the loss of π-conjugation (C) NCS-averaged electron difference density map $F_{obs} - F_{calc}$ upon low-intensity photobleaching, overlaid on the crystallographic structure of intact IrisFP (PDB model 2VVH), as in Figure 2C. Positive electron density is shown in green (+5.3 σ) and negative electron density is shown in red (−5.3 σ, no feature visible). (D) Refined model of low-intensity photobleaching IrisFP. H-bonds are represented with dashed lines, and water molecules as red balls.

dx.doi.org/10.1021/ja406860e | J. Am. Chem. Soc. 2013, 135, 15841−15850

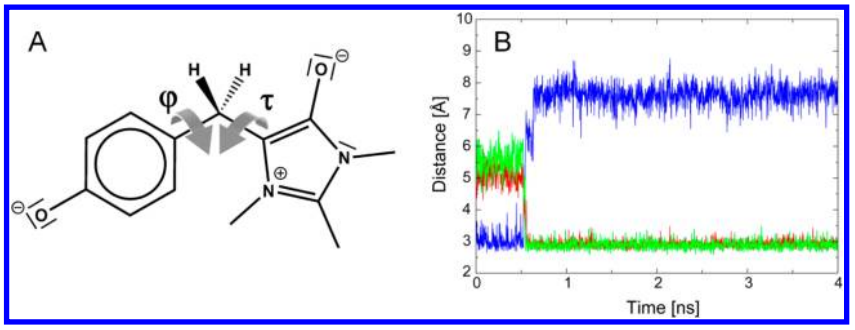

Figure 5. (A) Lewis representation of the proposed doubly reduced/protonated chromophore CαN photobleached under high-intensity illumination conditions. This structure was used to model the bleached pBl_{red} and Bl_{red} states. (B) MD simulations: time-evolution of characteristic distances between atoms involved in the H-bond network around the IrisFP chromophore pocket, from the pBl_{red} to the Bl_{red} states. Blue: His194(NE2)-Glu144. Red: His194(ND1)-Arg66. Green: His194(NE2)-Ser142.

observed in the electron density maps strongly varied between the four IrisFP monomers. Whereas significant electron densities were observed in monomers A, B, and D, no sign of sulfoxidation could be detected in monomer C (Figure S6A–D, Supporting Information). This difference could be explained by a variable diffusion capacity of oxygen molecules into the chromophore pocket via pores in the IrisFP β-barrel, probably due to crystal packing effects. In monomers A, B, and D, inspection of the IrisFP static structure showed a pore between the residues Glu140 and Ile196, in the close vicinity of the chromophore phenolate (Figure S6E–H, Supporting Information) at a location previously identified in other FPs such as His148Asp-YFP[46] or the Arthropoda TurboGFP.[47] This pore is occluded in monomer C.

Overall, the data suggest that under low-intensity illumination IrisFP suffers from an oxidation-based photofatigue mechanism, which is initiated by the production of singlet-oxygen within the chromophore pocket.

Further Insight into IrisFP Photobleaching under High-Intensity Illumination. The novelty of the decarboxylation-based photofatigue mechanism of IrisFP, its complex structural signature and its potential relevance for high-resolution microscopy prompted us to investigate this mechanism in more details. Notably, we asked the four following questions: (i) Which wavelength (488 or 405 nm) is primarily responsible for photodestruction? (ii) What is the temporal order of the structural events leading to the observed photofatigued structure? (iii) What is the chemical nature of the photobleached chromophore? (iv) Is a two-consecutive-photon absorption process involved?

Question i can be readily answered in the case of low-intensity photobleaching, as the chromophore clearly adopts a *cis* configuration in this bleached state, strongly suggesting that photobleaching results from the absorption of a 488-nm photon. The question is more delicate to answer in the case of high-intensity photobleaching, as two arguments could favor the hypothesis that photodestruction originates from violet light illumination. First, it has been reported that decarboxylation reactions occurring via a Photo-Kolbe mechanism are favored in the UV range.[48] Second, the conformational switch of the His194-Arg66 pair observed in our structure (Figure 2C and 2D) seems at first glance consistent with the chromophore being photobleached in its *trans* configuration by violet light. However, close inspection of the difference electron density map of Figure 2C shows that residue Ile157 maintains a conformation typical of the *cis* chromophoric state.[42] This suggests that the His194-Arg66 switch could be a consequence of photobleaching by cyan light in the *cis* configuration of the chromophore. To test this hypothesis, crystals of green IrisFP were illuminated at 100 K at 488 nm for a prolonged time. At this temperature, chromophore isomerization is prevented, likely due to the lack of sufficient conformational flexibility of the IrisFP chromophore pocket, and thus no switching by *cis–trans* isomerization can occur. Despite a deterioration of the crystalline order resulting from this harsh sample treatment, difference electron density maps clearly showed that 488 nm light is able to induce extensive Glu212 decarboxylation, similarly to 405 nm light (Figure S4, Supporting Information). The conformational switch of the His194-Arg66 pair subsequent to Glu212 decarboxylation in the *cis* chromophoric state was then confirmed by molecular dynamics simulations (see below). These arguments, together with the fact that the sample was exposed to ~600 times more cyan than violet photons, favor the hypothesis that photodestruction upon repeated switching in IrisFP predominantly results from light absorption at 488 nm by the *cis* chromophore.

We next attempted to disentangle the order of the structural events leading to chromophore destruction (question ii) by collecting a high-quality structure of IrisFP en-route to photobleaching. Knowing that X-rays efficiently induce IrisFP photobleaching through Glu212 decarboxylation,[37] we reasoned that collecting a pair of high-resolution crystallographic structures at 100K at different X-ray doses might uncover structural differences representative of early events along the photobleaching pathway. The results, presented in Figure S7 (Supporting Information) (see also Tables S1 and S3, Supporting Information), reveal decarboxylation of Glu212 as well as the disappearance of several water molecules participating in the hydrogen bond network surrounding the chromophore. However, instead of the disorder of the phenolate moiety observed in the photofatigued structure, the chromophore exhibits a clear distortion with an upward tilt of the chromophore phenolate and a downward bend of the methylene bridge. This distortion is also consistent with sp^3-hybridization of the C_α carbon atom (Figure 2D). Furthermore, His194 and Arg66 are not significantly displaced as compared to their native conformation. If we admit that photobleaching pathways induced by high-intensity visible and X-ray light are both initiated by redox processes leading to Glu212 decarboxylation, it is reasonable to associate these structural changes with an early intermediate state along the high-intensity photofatigue pathway.

To further investigate whether the X-ray bleached cryo-structure is a plausible intermediate state along the high-

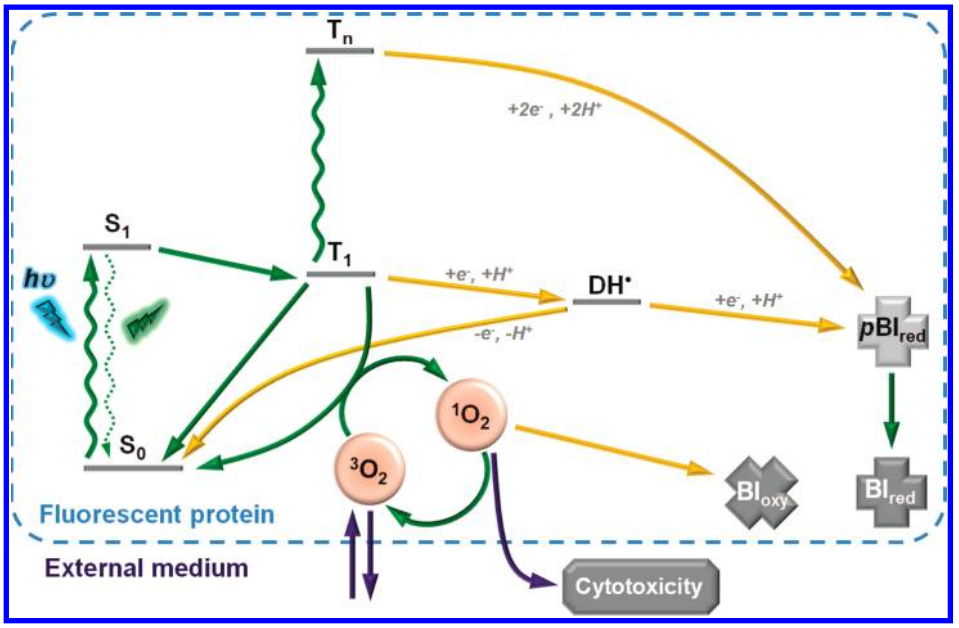

Figure 6. Proposed photophysical scheme for a two-regime photobleaching in IrisFP. Yellow arrows represent chemical steps involving electron/proton transfer or oxidation reactions. Blue arrows represent entry/exit of oxygen species.

intensity photofatigue pathway, we conducted molecular dynamics simulations using software specifically tailored for fluorescent proteins simulations.[49] These simulations also allowed us to examine the chemical nature of the fatigued chromophore (question iii). Starting from the putative intermediate state with the chromophore adopting various chemical structures, we analyzed whether or not the IrisFP conformation evolved toward the experimentally observed fatigued structure. In order to ensure the sp^3-character of the Cα atom revealed by Raman spectroscopy while excluding an unstable radical state of the fatigued chromophore, the latter must be considered as formally reduced by two hydrogen atoms. Among all available choices tested (Figure S10, Table S4, Supporting Information), the reduced structure protonated at positions Cα and N4 (referred to as CαN) was found to be the only one compatible with our experimental data (Figure 5A). Protonation at other positions either altered the planar character of the imidazolinone ring or weakened the hydrogen bond between that ring and Arg91 (see further discussion in the Supporting Information). Using structure CαN in our MD simulations, we noticed that the conformational switch of His194 and Arg66 to their positions observed in the fatigued structure occurred within a nanosecond (Figure 5B and Figure S14, Supporting Information). Furthermore, large fluctuations of the chromophore torsions around the Cα atom were observed afterward (the 80% confidence interval of the dihedral τ angle ranged from $-5°$ to $55°$), reflecting the interplay between the intramolecular energy landscape of the reduced chromophore CαN (Figure S11, Supporting Information) and the decreased constraints due to the protein environment. These fluctuations are consistent with the phenolate disorder observed experimentally.

Finally, in order to investigate whether the high-intensity bleaching mechanism involves a two-consecutive-photon absorption process (question iv), we measured the initial photofatigue rate as a function of the illumination power density in the absence of oxygen (Figure S3, Supporting Information). The results confirm that O_2 is indeed not required in this mechanism. The best linear fit to a double-logarithmic plot of the data showed a slope of 1.8 ± 0.3 (Figure S3, Supporting Information), indicating a mechanism mainly involving two photons with a possible weak residual from a one-photon contribution.

DISCUSSION

Our study of the photofatigue mechanism of the reversibly switchable protein IrisFP reveals a two-regime photodestruction pathway. At illumination intensities of ~100 W/cm^2, photobleaching of IrisFP involves decarboxylation of Glu212 probably via electron transfer to the chromophore in a photo-Kolbe reaction.[31,48] We propose that this leads to a prebleached dark state, represented by the cryo-trapped structure of Figure S7 (Supporting Information), in which the chromophore is already reduced and protonated at the Cα atom and at the N4 nitrogen atom. In this state, denoted pBI_{red}, the chromophore has lost its electron conjugation and adopts a tilted geometry. (Note that pBI_{red} differs from the blinked radical state $DH^{\bullet}$ described earlier by us.[43]) Subsequently, while the chemical structure of the chromophore does not evolve further, the hydrogen bond network surrounding it collapses, and the His194-Arg66 pair flips to a conformation resembling that of IrisFP in its switched-off state. The phenolate moiety of the chromophore loses its anchoring to the protein matrix, resulting in large fluctuations of the τ and φ dihedral angles. A complete loss of absorbance and fluorescence is thus observed in this bleached state, referred to as BI_{red}, and the presence of oxygen is not required.

At illumination intensities ten times lower (~10 W/cm^2), a completely different scenario takes place. The chromophore reacts in its triplet state T_1 with molecular oxygen to produce singlet oxygen $^1O_2$. We propose that singlet oxygen then rapidly reacts with the nearby Met159 and a water molecule to produce sulfoxidized-Met159 and hydrogen peroxide H_2O_2.[50] H_2O_2 in turn attacks Cys171 to give sulfoxidized Cys171 and a hydroxyl molecule.[50] Because the S−O bond in a sulfoxidized methionine is highly polarized, with partial negative charge on

dx.doi.org/10.1021/ja406860e | J. Am. Chem. Soc. 2013, 135, 15841−15850

the oxygen atom, the chromophore is trapped in a protonated state due to the establishment of a strong H-bond interaction. Loss of fluorescence is observed, but partial absorption by the neutral chromophore is maintained. Alternatively to oxidizing Met159 and Cys171, singlet oxygen may also diffuse further throughout the IrisFP matrix and attack more remote amino acids, as revealed by mass spectrometry. We refer to either of these oxygen dependent bleached states as Bl_{oxy}. Singlet oxygen may also undergo a different fate: it can escape into the solvent and generate cytotoxicity. This is consistent with the estimated $^1O_2$ lifetime and diffusion length in cells of 250 ns and 45 nm, respectively.[51] Diffusion out of the IrisFP β-barrel could occur via the pore identified in this work, or through other pores opening transiently that will necessitate future investigations by molecular dynamics simulations.[26,27]

Sulfur-containing residues are major targets of reactive oxygen species (ROS) and are most susceptible to oxidation.[52] Notably, methionine oxidation by singlet oxygen has been described in the context of chromophore assisted light inactivation (CALI), typically resulting in enzyme inactivation.[53] Here, low-intensity photobleaching of IrisFP can be viewed as a special case of intramolecular CALI. We note that it is unlikely that methionine sulfoxide reductases, which are enzymes known to revert methionine sulfoxidation[54] would salvage IrisFP fluorescence, because Met159 is buried into the β-barrel. Further oxidation of remote sensitive residues could also be associated with a loss of fluorescence possibly linked to partial unfolding of the IrisFP β-barrel, in turn corroborating the loss of diffraction observed in crystals treated with prolonged low-intensity light. This observation is reminiscent of the loss of enzymatic activity observed in enzymes submitted to a high-level of oxidation by ROS,[50,55] and it is consistent with the loss of fluorescence observed in other FPs submitted to ROS by pulse radiolysis.[56]

The photophysical scheme of Figure 6 recapitulates the proposed photobleaching pathways. Upon excitation, the ground-state singlet chromophore S_0 reaches the first electronically excited state S_1, from which it can either fluoresce, deactivate nonradiatively (through isomerization, giving rise to off-switching), or undergo intersystem crossing to the long-lived triplet state T_1. From T_1, a number of possible pathways can be envisaged. T_1 can relax to S_0 either spontaneously or, more efficiently, by triplet−triplet quenching if molecular oxygen is present near the chromophore. This results in the production of $^1O_2$ which may, as described above, attack the fluorescent protein or escape into the medium. The photofatigued state Bl_{oxy} is produced. Alternatively, the high oxidation potential of the excited chromophore may drive electron transfer from Glu212 without the need for oxygen, leading to the nonfluorescent prebleached state pBl_{red} from which the photofatigued state Bl_{red} occurs.

It is interesting to determine which factors control the switch from one photobleaching regime to the other. Two hypotheses can be proposed. First, the entry rate of molecular oxygen into the IrisFP β-barrel could play a role. A slow O_2 entry rate relative to the rate of photon absorption would disfavor the reaction of the excited IrisFP chromophore with oxygen, leaving redox chemistry as the dominant route to photobleaching. Second, as strongly suggested by our data (Figure S3, Supporting Information), the onset of redox photobleaching at high intensity could result from a mechanism relying on the consecutive absorption of two photons. The increase of the T_1 lifetime while oxygen is absent from the chromophore pocket would further boost such mechanism. In order to test these hypotheses, the complete kinetic model illustrated in Figure S15 (Supporting Information) was challenged by simulations predicting the relative fraction of the two photofatigued species Bl_{red} and Bl_{oxy} as a function of the applied laser intensity, assuming realistic rates for entry/exit of oxygen in/from the chromophore pocket (see discussion in the Supporting Information and Figure S16). The model consistently predicts dominant oxygen-dependent and oxygen-independent photobleaching pathways under the experimental low- and high-intensity illumination conditions, respectively. We propose that the photobleached state Bl_{red} can be reached via one- or two-consecutive-photon excitation. In the first case, the radical state $DH^{\bullet}$ could be involved, as suggested by our previous simulations using QM/MM approaches.[43] In the second case, absorption of the second photon could take place in T_1 or another state of the chromophore with micro- to millisecond lifetime, thus accelerating formation of Bl_{red} at high excitation rates. The existence of a two-consecutive-photon absorption route leading to Glu222 decarboxylation has been noticed in GFP[57] and is consistent with the high laser intensities observed to build-up the super-red species in DsRed.[34] Furthermore, by analogy to the results found in GFP,[57] it may be speculated that conventional two-photon-excitation schemes, in view of the high laser power-densities used, could favor the oxygen-independent bleaching pathway.

In the crystalline state, assuming a typical concentration of oxygen of 200 μM, there is a large excess of IrisFP monomers (>100). Assuming a bulk diffusion coefficient of 2×10^{-5} cm^2/s, a single molecule of O_2 is able to explore only ~20 unit cells in a microsecond. Thus, it is likely that the rate at which oxygen molecules penetrate into a given crystalline IrisFP monomer is lower than the excitation rate of the chromophore, at least under our high-intensity illumination conditions (5×10^4 s^{-1}). In solution samples or in biological cells this situation might differ, with more molecular oxygen available per fluorophore. This may possibly shift upward the intensity threshold between the two photobleaching pathways. More generally, we expect this threshold to depend not only on the fluorescent protein and molecular oxygen concentrations but also on the redox environment, as well as on other parameters such as pH, viscosity of the medium, or even the nature of fusion constructs.

Photo-Kolbe reactions in fluorescent proteins have been described several times.[31−33,48,58] The invoked mechanism, however, always leaves the chromophore intact. Indeed, it is generally proposed that following electron transfer from Glu212 to the chromophore, an electron (and proton) is transferred back from the chromophore to the $CH_2^{\bullet}$ radical of the decarboxylated Glu212. By contrast, the chromophore of IrisFP is chemically altered, with the methylene bridge ending up in an sp^3-hybridized state as demonstrated by Raman spectroscopy. The photobleached chromophore is thus likely to be photochemically reduced, which implies the net transfer of two electrons and two protons. Our MD simulations favor such a process, suggesting the formation of a zwitterionic imidazolinone ring in which the oxygen atom is negatively charged and stabilized by two H-bonds to the guanidinium groups of Arg66 and Arg91 while the N4 nitrogen atom is protonated and positively charged. Whereas the proton ending up on the Cα carbon could originate from Arg66,[43] we speculate that the second electron and proton could be

dx.doi.org/10.1021/ja406860e | J. Am. Chem. Soc. 2013, 135, 15841−15850

provided by a reducing molecule in the surrounding medium.[29] Further studies will be needed, however, to precisely unravel the redox mechanism allowing these transfers.

Studying the photobleaching mechanisms of RSFPs is important because these markers play an increasing role in several advanced fluorescence microscopy applications. It could be argued, however, that the photoswitching capabilities of RSFPs complicate the investigation of irreversible photodestruction processes. On the contrary, and consistently with previous work,[41] we propose that the investigation of photobleaching pathways through repeated photoswitching provides the advantage that uncontrolled accumulation of reversible dark states ("shelving")[2] is largely reduced: the overall slow photofatigue of RSFPs facilitates the recovery of thermally unstable dark states, and repeated illumination by 405 nm light often promotes fast recovery of light-sensitive dark states, as is the case for the main *trans*-isomeric off state. Overall, studying photobleaching of RSFPs facilitates the decoupling of irreversible and reversible photophysical processes.

The photobleaching mechanisms described here for IrisFP might be conserved in other photoconvertible and photoswitchable fluorescent proteins derived from Anthozoan species such as Dronpa, mTFP0.7, Kaede, EosFP, Dendra2, and their variants.[39] Indeed, all these proteins display very similar structural organizations of their chromophore pocket, with nearly identical hydrogen bond networks involving Glu212, His194, Arg66, and Glu144. Their sequence identity and global structural similarity is also high, suggesting the possibility of a common pathway for oxygen diffusion toward the chromophore and/or common redox mechanisms. Moreover, all these proteins, except mTFP0.7, contain a methionine at position 159. The observation of a trapped neutral chromophore upon Met159 sulfoxidation might therefore be a general feature of this family of proteins. We note that, in the context of the present study, the presence of this residue at this position can be considered as a fortunate feature that allowed us to provide the first structural evidence of singlet oxygen production within a FP chromophore pocket. Interestingly, during the directed evolution of mCherry from mRFP1, it was reported that the mutation Met163Gln was entirely responsible for the 10-fold enhanced photostability of mCherry.[2] This finding could relate to our observations in IrisFP, although recent molecular dynamics simulations proposed that this mutation essentially served to block the entry of molecular oxygen within the barrel.[27]

In general, the photobleaching mechanisms observed in IrisFP are unlikely to apply to Hydrozoan RSFPs such as rsEGFP.[20,21] While oxygen diffusion pathways probably differ, Glu212 decarboxylation in Hydrozoan FPs typically induces photoactivation rather than photobleaching. Nevertheless, competing photobleaching routes probably also exist in Hydrozoan RSFPs and would deserve investigations similar to those described in this work. Likewise, non-RSFPs of Anthozoan origin are likely to exhibit yet different photobleaching mechanisms. In the red fluorescent protein KillerRed, for which structures of photobleached states under low intensity illumination have been published,[3,4] the chromophore was found either disordered[3] or distorted,[4] possibly consistent with sp^3-hybridization of the methylene bridge, and no substantial modifications of the chromophore environment was noticed. These differences with our low-intensity IrisFP bleached structure might arise from a type I photosensitization mechanism in KillerRed[3] versus a type II mechanism in IrisFP and be a consequence of the different chromophore structures and environments in the two proteins.

Our results provide some of the molecular basis required for the rational design of more photoresistant Anthozoan RSFPs. For example, in IrisFP, mutations Met159Ala[45] or Glu212Gln[59] could be carried out and their effect on photobleaching investigated, with the potential caveat that mutations enhancing photoresistance may also modify important properties such as photoswitching yields or maturation efficiency. Further directed-evolution based engineering of electron transfer pathways and oxygen entry routes will probably be required to obtain optimal photoresistant variants.

■ CONCLUSION

Despite considerable advances in fluorescent proteins research in the recent past, the high susceptibility of FPs to irreversible photobleaching still remains a major bottleneck to their use in advanced microscopy applications. Here, we have explored the photobleaching mechanisms in IrisFP, a representative of the important class of reversibly switchable fluorescent proteins. Under low-intensity illumination (~0.01 kW/cm^2) typical of standard wide-field fluorescence microscopy, an oxygen-dependent mechanism dominates, that damages the IrisFP chromophore environment mainly through sulfoxidation reactions and releases singlet oxygen in the medium. Under high-intensity illumination (~0.1 kW/cm^2) approaching laser-light levels used in localization-based super-resolution microscopy, an oxygen-independent mechanism takes over, that damages the chromophore itself via decarboxylation of the strictly conserved Glu212.

As a consequence of this work we speculate that high-intensity illumination of Anthozoan phototransformable FPs might generate less cytotoxicity than low-intensity illumination at constant integrated dose. This prediction is consistent with previous findings that light-induced damage of cellular samples labeled with fluorescent proteins mostly originates from ROS released by the fluorescent markers under typical widefield illumination regimes.[60,61] However, at high-intensity, additional effects due to, e.g., singlet oxygen release by endogenous chromophores (such as flavins) and rapid depletion of ROS scavenging cellular components (such as glutathione) may play an adverse role. Overall, our results might be related to the observation that prolonged PALM illumination of Anthozoan FPs generally induces tolerable phototoxicity in live cells,[62−65] but call for further quantitative investigations of the light-intensity dependence of cytotoxic effects in biological samples. The two-regime photobleaching mechanism characterized in this work may also play a role in the frequently observed discrepancy between bleaching kinetics measured under a variety of conditions, typically low versus high intensity wide-field or wide-field versus confocal. In the latter case, however, the short illumination dwell-times and typically much higher instantaneous power densities (>10 kW/cm^2) probably call for yet other photobleaching mechanisms to be explored in the future.

■ ASSOCIATED CONTENT

Supporting Information

Materials and methods for crystal growth, X-ray data collection and structure determination, photobleaching procedures, optical spectroscopy and mass spectrometry, quantum mechanics and molecular dynamics simulations. Discussions

of laser beam heterogeneity, QM/MD simulations, modeling of kinetic scheme, Raman spectra from photobleached crystals. This material is available free of charge via the Internet at http://pubs.acs.org.

AUTHOR INFORMATION

Corresponding Author

dominique.bourgeois@ibs.fr

Notes

The authors declare no competing financial interest

ACKNOWLEDGMENTS

The ESRF and SLS synchrotron facilities are acknowledged for providing beamtime. We thank Martin Fuchs, Guillaume Pompidor, and Florian Dworkowski for help in X-ray data collection at the SLS, Aline Faro for scientific discussions, and David von Stetten for support in using the Cryobench laboratory of the ESRF. We acknowledge technical help by Laure Roux, Jérémie Gaillard and Christophe Guerin. We thank Gabriella Jonasson and Bernard Lévy for fruitful discussions and invaluable help. D.B. acknowledges financial support by the ANR (ANR-2011-BSV5-012-01 NOBLEACH). This work used the platforms of the Grenoble Instruct center (ISBG; UMS 3518 CNRS-CEA-UJF-EMBL) with support from FRISBI (ANR-10-INSB-05-02) and GRAL (ANR-10-LABX-49-01) within the Grenoble Partnership for Structural Biology (PSB). This work was granted access to the HPC resources of CINES under the allocation 2012-c2012086318 made by GENCI (Grand Equipement National de Calcul Intensif).

REFERENCES

(1) Dedecker, P.; De Schryver, F. C.; Hofkens, J. *J. Am. Chem. Soc.* **2013**, *135*, 2387.

(2) Shaner, N. C.; Lin, M. Z.; McKeown, M. R.; Steinbach, P. A.; Hazelwood, K. L.; Davidson, M. W.; Tsien, R. Y. *Nat. Methods* **2008**, *5*, 545.

(3) Pletnev, S.; Gurskaya, N. G.; Pletneva, N. V.; Lukyanov, K. A.; Chudakov, D. M.; Martynov, V. I.; Popov, V. O.; Kovalchuk, M. V.; Wlodawer, A.; Dauter, Z.; Pletnev, V. *J. Biol. Chem.* **2009**, *284*, 32028.

(4) Carpentier, P.; Violot, S.; Blanchoin, L.; Bourgeois, D. *FEBS Lett.* **2009**, *583*, 2839.

(5) de Rosny, E.; Carpentier, P. *J. Am. Chem. Soc.* **2012**, *134*, 18015.

(6) Ai, H. W.; Henderson, J. N.; Remington, S. J.; Campbell, R. E. *Biochem. J.* **2006**, *400*, 531.

(7) Subach, O. M.; Cranfill, P. J.; Davidson, M. W.; Verkhusha, V. V. *PLoS One* **2011**, *6*, e28674.

(8) Christie, J. M.; Hitomi, K.; Arvai, A. S.; Hartfield, K. A.; Mettlen, M.; Pratt, A. J.; Tainer, J. A.; Getzoff, E. D. *J. Biol. Chem.* **2012**, *287*, 22295.

(9) Bourgeois, D.; Adam, V. *IUBMB Life* **2012**, *64*, 482.

(10) Hofmann, M.; Eggeling, C.; Jakobs, S.; Hell, S. W. *Proc. Natl. Acad. Sci. U.S.A.* **2005**, *102*, 17565.

(11) Dedecker, P.; Hotta, J.; Flors, C.; Sliwa, M.; Uji-i, H.; Roeffaers, M. B.; Ando, R.; Mizuno, H.; Miyawaki, A.; Hofkens, J. *J. Am. Chem. Soc.* **2007**, *129*, 16132.

(12) Bock, H.; Geisler, C.; Wurm, C. A.; Von Middendorff, C.; Jakobs, S.; Schonle, A.; Egner, A.; Hell, S. W.; Eggeling, C. *Appl. Phys. B-Lasers Opt.* **2007**, *88*, 161.

(13) Shroff, H.; Galbraith, C. G.; Galbraith, J. A.; White, H.; Gillette, J.; Olenych, S.; Davidson, M. W.; Betzig, E. *Proc. Natl. Acad. Sci. U.S.A.* **2007**, *104*, 20308.

(14) Rego, E. H.; Shao, L.; Macklin, J. J.; Winoto, L.; Johansson, G. A.; Kamps-Hughes, N.; Davidson, M. W.; Gustafsson, M. G. *Proc. Natl. Acad. Sci. U.S.A.* **2011**, *109*, E135.

(15) Subach, F. V.; Zhang, L. J.; Gadella, T. W. J.; Gurskaya, N. G.; Lukyanov, K. A.; Verkhusha, V. V. *Chem. Biol.* **2010**, *17*, 745.

(16) Marriott, G.; Mao, S.; Sakata, T.; Ran, J.; Jackson, D. K.; Petchprayoon, C.; Gomez, T. J.; Warp, E.; Tulyathan, O.; Aaron, H. L.; Isacoff, E. Y.; Yan, Y. L. *Proc. Natl. Acad. Sci. U. S. A.* **2008**, *105*, 17789.

(17) Tian, Z.; Li, A. D. *Acc. Chem. Res.* **2013**, *46*, 269.

(18) Zhou, X. X.; Chung, H. K.; Lam, A. J.; Lin, M. Z. *Science* **2012**, *338*, 810.

(19) Adam, V.; Mizuno, H.; Grichine, A.; Hotta, J. I.; Yamagata, Y.; Moeyaert, B.; Nienhaus, G. U.; Miyawaki, A.; Bourgeois, D.; Hofkens, J. *J. Biotechnol.* **2010**, *149*, 289.

(20) Grotjohann, T.; Testa, I.; Leutenegger, M.; Bock, H.; Urban, N. T.; Lavoie-Cardinal, F.; Willig, K. I.; Eggeling, C.; Jakobs, S.; Hell, S. W. *Nature* **2011**, *478*, 204.

(21) Grotjohann, T.; Testa, I.; Reuss, M.; Brakemann, T.; Eggeling, C.; Hell, S. W.; Jakobs, S. *Elife* **2012**, *1*, e00248.

(22) Chang, H.; Zhang, M.; Ji, W.; Chen, J.; Zhang, Y.; Liu, B.; Lu, J.; Zhang, J.; Xu, P.; Xu, T. *Proc. Natl. Acad. Sci. U.S.A.* **2012**, *109*, 4455.

(23) Greenbaum, L.; Rothmann, C.; Lavie, R.; Malik, Z. *Biol. Chem.* **2000**, *381*, 1251.

(24) Jimenez-Banzo, A.; Nonell, S.; Hofkens, J.; Flors, C. *Biophys. J.* **2008**, *94*, 168.

(25) Jimenez-Banzo, A.; Ragas, X.; Abbruzzetti, S.; Viappiani, C.; Campanini, B.; Flors, C.; Nonell, S. *Photochem. Photobiol. Sci.* **2010**, *9*, 1336.

(26) Roy, A.; Carpentier, P.; Bourgeois, D.; Field, M. *Photochem. Photobiol. Sci.* **2010**, *9*, 1342.

(27) Regmi, C. K.; Bhandari, Y. R.; Gerstman, B. S.; Chapagain, P. P. *J. Phys. Chem. B* **2013**, *117*, 2247.

(28) Subach, F. V.; Verkhusha, V. V. *Chem. Rev.* **2012**, *112*, 4308.

(29) Bogdanov, A. M.; Bogdanova, E. A.; Chudakov, D. M.; Gorodnicheva, T. V.; Lukyanov, S.; Lukyanov, K. A. *Nat. Methods* **2009**, *6*, 859.

(30) Malkani, N.; Schmid, J. A. *PLoS One* **2011**, *6*.

(31) van Thor, J. J.; Gensch, T.; Hellingwerf, K. J.; Johnson, L. N. *Nat. Struct. Biol.* **2002**, *9*, 37.

(32) Henderson, J. N.; Gepshtein, R.; Heenan, J. R.; Kallio, K.; Huppert, D.; Remington, S. J. *J. Am. Chem. Soc.* **2009**, *131*, 4176.

(33) Subach, F. V.; Malashkevich, V. N.; Zencheck, W. D.; Xiao, H.; Filonov, G. S.; Almo, S. C.; Verkhusha, V. V. *Proc. Natl. Acad. Sci. U.S.A.* **2009**, *106*, 21097.

(34) Habuchi, S.; Cotlet, M.; Gensch, T.; Bednarz, T.; Haber-Pohlmeier, S.; Rozenski, J.; Dirix, G.; Michiels, J.; Vanderleyden, J.; Heberle, J.; De Schryver, F. C.; Hofkens, J. *J. Am. Chem. Soc.* **2005**, *127*, 8977.

(35) van Thor, J. J.; Georgiev, G. Y.; Towrie, M.; Sage, J. T. *J. Biol. Chem.* **2005**, *280*, 33652.

(36) Royant, A.; Noirclerc-Savoye, M. *J. Struct. Biol.* **2011**, *174*, 385.

(37) Adam, V.; Carpentier, P.; Violot, S.; Lelimousin, M.; Darnault, C.; Nienhaus, G. U.; Bourgeois, D. *J. Am. Chem. Soc.* **2009**, *131*, 18063.

(38) Shcherbo, D.; Murphy, C. S.; Ermakova, G. V.; Solovieva, E. A.; Chepurnykh, T. V.; Shcheglov, A. S.; Verkhusha, V. V.; Pletnev, V. Z.; Hazelwood, K. L.; Roche, P. M.; Lukyanov, S.; Zaraisky, A. G.; Davidson, M. W.; Chudakov, D. M. *Biochem. J.* **2009**, *418*, 567.

(39) Chudakov, D. M.; Matz, M. V.; Lukyanov, S.; Lukyanov, K. A. *Physiol. Rev.* **2010**, *90*, 1103.

(40) Carlton, P. M.; Boulanger, J.; Kervrann, C.; Sibarita, J. B.; Salamero, J.; Gordon-Messer, S.; Bressan, D.; Haber, J. E.; Haase, S.; Shao, L.; Winoto, L.; Matsuda, A.; Kner, P.; Uzawa, S.; Gustafsson, M.; Kam, Z.; Agard, D. A.; Sedat, J. W. *Proc. Natl. Acad. Sci. U.S.A.* **2010**, *107*, 16016.

(41) Dean, K. M.; Lubbeck, J. L.; Binder, J. K.; Schwall, L. R.; Jimenez, R.; Palmer, A. E. *Biophys. J.* **2011**, *101*, 961.

(42) Adam, V.; Lelimousin, M.; Boehme, S.; Desfonds, G.; Nienhaus, K.; Field, M. J.; Wiedenmann, J.; McSweeney, S.; Nienhaus, G. U.; Bourgeois, D. *Proc. Natl. Acad. Sci. U.S.A.* **2008**, *105*, 18343.

(43) Roy, A.; Field, M. J.; Adam, V.; Bourgeois, D. *J. Am. Chem. Soc.* **2011**, *133*, 18586.

(44) He, X.; Bell, A. F.; Tonge, P. J. *J. Phys. Chem. B* **2002**, *106*, 6056.

(45) Adam, V.; Moeyaert, B.; David, C. C.; Mizuno, H.; Lelimousin, M.; Dedecker, P.; Ando, R.; Miyawaki, A.; Michiels, J.; Engelborghs, Y.; Hofkens, J. *Chem. Biol.* **2011**, *18*, 1241.
(46) Wachter, R. M.; Elsliger, M. A.; Kallio, K.; Hanson, G. T.; Remington, S. J. *Struct. Fold. Des.* **1998**, *6*, 1267.
(47) Evdokimov, A. G.; Pokross, M. E.; Egorov, N. S.; Zaraisky, A. G.; Yampolsky, I. V.; Merzlyak, E. M.; Shkoporov, A. N.; Sander, I.; Lukyanov, K. A.; Chudakov, D. M. *EMBO Rep.* **2006**, *7*, 1006.
(48) Bell, A. F.; Stoner-Ma, D.; Wachter, R. M.; Tonge, P. J. *J. Am. Chem. Soc.* **2003**, *125*, 6919.
(49) Jonasson, G.; Teuler, J. M.; Vallverdu, G.; Merola, F.; Ridard, J.; Levy, B.; Demachy, I. *J. Chem. Theor. Comput.* **2011**, *7*, 1990.
(50) Pattison, D. I.; Rahmanto, A. S.; Davies, M. J. *Photochem. Photobiol. Sci.* **2012**, *11*, 38.
(51) Ochsner, M. *J. Photochem. Photobiol. B* **1997**, *39*, 1.
(52) Vogt, W. *Free Radic. Biol. Med.* **1995**, *18*, 93.
(53) Yan, P.; Xiong, Y. J.; Chen, B. W.; Negash, S.; Squier, T. C.; Mayer, M. U. *Biochemistry* **2006**, *45*, 4736.
(54) Schoneich, C. *Biochim. Biophys. Acta* **2005**, *1703*, 111.
(55) Kim, Y. H.; Berry, A. H.; Spencer, D. S.; Stites, W. E. *Protein Eng.* **2001**, *14*, 343.
(56) Alvarez, L.; Levin, C. H.; Merola, F.; Bizouarn, T.; Pasquier, H.; Baciou, L.; Rusconi, F.; Erard, M. *Photochem. Photobiol.* **2010**, *86*, 55.
(57) Langhojer, F.; Dimler, F.; Jung, G.; Brixner, T. *Biophys. J.* **2009**, *96*, 2763.
(58) Ding, L. N.; Chung, L. W.; Morokuma, K. *J. Phys. Chem. B* **2013**, *117*, 1075.
(59) Gayda, S.; Nienhaus, K.; Nienhaus, G. U. *Biophys. J.* **2012**, *103*, 2521.
(60) Dixit, R.; Cyr, R. *Plant J.* **2003**, *36*, 280.
(61) Hoebe, R. A.; Van Oven, C. H.; Gadella, T. W., Jr.; Dhonukshe, P. B.; Van Noorden, C. J.; Manders, E. M. *Nat. Biotechnol.* **2007**, *25*, 249.
(62) Shroff, H.; Galbraith, C. G.; Galbraith, J. A.; Betzig, E. *Nat. Methods* **2008**, *5*, 417.
(63) Manley, S.; Gillette, J. M.; Patterson, G. H.; Shroff, H.; Hess, H. F.; Betzig, E.; Lippincott-Schwartz, J. *Nat. Methods* **2008**, *5*, 155.
(64) Gudheti, M. V.; Curthoys, N. M.; Gould, T. J.; Kim, D.; Gunewardene, M. S.; Gabor, K. A.; Gosse, J. A.; Kim, C. H.; Zimmerberg, J.; Hess, S. T. *Biophys. J.* **2013**, *104*, 2182.
(65) Henriques, R.; Griffiths, C.; Rego, E. H.; Mhlanga, M. M. *Biopolymers* **2011**, *95*, 322.

Supporting Information

Structural evidence for a two-regime photobleaching mechanism in a reversibly switchable fluorescent protein.

Chenxi Duan, Virgile Adam, Martin Byrdin, Jacqueline Ridard, Sylvie Kieffer-Jaquinod, Cécile Morlot, Delphine Arcizet, Isabelle Demachy and Dominique Bourgeois

Materials and Methods

Expression and purification

IrisFP was expressed in *Escherichia coli* BL21 (DE3), using a pQE32 plasmid encoding the full-length IrisFP as described previously.[1] The bacterial culture was grown at 37°C to $OD_{600\ nm}$ = 0.6. Overexpression was induced by adding 0.1 mM IPTG and the culture was incubated 7 days at 4°C. After centrifugation, the cell pellet was resuspended in a solution containing 50 mM HEPES pH 7.5 and 150 mM NaCl, and then lysed by sonication. The His-tagged recombinant protein was purified in two steps, using a pre-packed Talon metal affinity column (Clontech Laboratories, California, USA) and then a Hiload 16/60 Superdex 75 gel-filtration column (GE healthcare, Pennsylvania, USA). Fractions suitable for spectroscopic characterization and crystallization trials were concentrated to 20 mg/ml and dialyzed against a 50 mM sodium phosphate buffer (pH 7) containing 300 mM NaCl.

Crystallization

Crystals were grown at 293 K using the hanging drop method, using 2.1 M $(NH_4)_2SO_4$ and 100 mM Bicine pH 8.0 as crystallization buffer. Rod-shaped yellowish crystals appeared within 24 h and reached their final size (typically $50 \times 100 \times 1000\ \mu m^3$) within a few days.

Cryoprotection

For X-ray diffraction and UV-visible microspectrophotometry, photofatigued crystals were rapidly transferred to a cryoprotectant solution (10% glycerol/ 2.1 M $(NH_4)_2SO_4$ /100 mM Bicine pH 8.0) before being flash-frozen in gaseous nitrogen at 100 K. Glycerol was not used for Raman spectroscopy to avoid spectral contamination by this molecule.

Photobleaching procedures

Photobleaching at room temperature

To photofatigue IrisFP crystals under high-intensity conditions, we used our super-resolution PALM microscope. Crystallization drops were deposited on a glass slide, and were surrounded by several drops of crystallization medium to prevent drying. The drops were covered with a coverslip and sealed with grease. The samples were then placed on the stage of an inverted microscope (IX-81, Olympus) equipped with a ×20 objective. 488-nm and 405-nm lasers (Gaussian beam FWHMs: ~100 and ~200 µm) were then focused onto the part of the crystal to be treated (Figure S1A). Continuous illumination at 488 nm (73 W/cm²) was applied at room temperature for 10 minutes while the 405-nm laser (1 W/cm²) was turned on for 0.3 s every 2 s to restore the *cis* conformation of the chromophore. Only few crystals withstood this harsh treatment, which often resulted in significant unit-cell expansion in the bleached region, preventing the computation of accurate difference electron density maps. Higher laser power-densities resulted in crystal cracking and could not be used. To monitor photofatigue decays, the EMCCD camera of the microscope was replaced by a CCD-based spectrometer (AvaSpec-ULS2048, Avantes, Eerbeek, The Netherlands).

Solution samples were treated similarly, except that the crystallization drops were replaced by films of polyvinyl alcohol (PVA) containing purified IrisFP at a concentration of 0.74 mM (Figure S2 and S3).

To photofatigue IrisFP crystals under the low-intensity conditions, the same inverted-geometry setup turned out to be inappropriate, as the much longer experiment time required to achieve extensive photofatigue typically resulted in crystal drying. Thus, we designed an alternative setup based on an upright microscope which allowed photobleaching crystals directly in their crystallization trays (Figure S1B). Laser light was brought to the samples with a 200 µm diameter optical fiber, the tip of which was positioned above the crystal of interest with the aid of the microscope eyepieces. The measured FWHMs of the 488-nm and 405-nm laser beams obtained in these conditions at the sample position were ~220 µm (a smaller value than anticipated, possibly due to a lens effect of the crystallization drops). Crystals were continuously illuminated by the 488-nm laser (9 W/cm²) for 2 hours while the 405-nm laser (10 mW/cm²) was turned on for 4 s every 12 s to restore the *cis* conformation of the chromophore. The same optical fiber was used to detect fluorescence emission, which was redirected with a dichroic mirror to a CCD-based spectrometer.

In all cases, the switching cycles were terminated by a final exposure to 405-nm light to avoid the presence of residual non-fluorescing IrisFP molecules in their switched-off state.

Photobleaching at cryogenic temperature

Photofatigue of crystalline IrisFP at cryogenic temperature (Figure S4) was performed using a microspectrophotometer on which samples were mounted with standard cryoloops. Crystals were flash-cooled to 100 K by a nitrogen gas cryo-stream (Oxford cryostream, Series 600, Oxford, UK). For photobleaching of the *cis*-state, crystals were mounted and illuminated by laser light (51 W/cm²) for 1 hour. For photobleaching of the *trans*-state, crystals were first illuminated in their crystallization drops by unfocused 488-nm light in order to isomerize the chromophore to the *trans* conformation. They were then mounted onto the spectrometer and illuminated by 405-nm laser light (40 W/cm²) for 1 hour.

X-Ray data collection

X-ray diffraction data sets were collected at 100 K at the European Synchrotron Radiation Facility (ESRF) on beamlines ID14-2 and ID29, with an ADSC Q210 and a PILATUS 6M detector, respectively, and at the Swiss Light Source (SLS) on beamline PXII, with a PILATUS 6M detector. Diffraction experiments on ID14-2 and PXII were combined with online microspectrophotometry in order to properly locate photobleached areas on the crystals, based on absorption spectra.

The structure of photofatigued IrisFP under high-intensity illumination conditions (Figures 2C, 2D) was obtained at beamline ID14-2 of the ESRF. Two data sets were collected on the same crystal, one centered on the photobleached zone and the other on an intact zone. The X-ray beam size was $100 \times 100\ \mu m^2$, somewhat larger than the photobleached zone. Many crystals showed a reduced diffraction quality in the photobleached area, usually coupled to a substantial increase in the unit-cell dimensions.

The structure of photofatigued IrisFP under low-intensity illumination conditions (Figures 4C, 4D) was obtained at beamline PXII of the SLS. Two data sets were collected on the same crystal, one centered on the photobleached zone and the other on an intact zone. The X-ray beam size was $50 \times 50\ \mu m^2$. Many crystals showed poor diffraction quality in the

photobleached area. Only a few moderately photofatigued crystals conserved acceptable diffraction quality, and the unit-cell dimensions always increased in the fatigued zone.

The structure of X-ray bleached IrisFP (Figure S7) was collected at beamline ID29 of the ESRF. Two data sets were helically collected along the rod-shaped crystal in order to minimize the spread of X-ray damage within each data set.

X-Ray data processing

All crystallographic data sets were reduced with the XDS package.[2] Data collection statistics are compiled in Table S1. Experimental difference electron density maps ($F_{obs,\ bleached} - F_{obs,\ green}$) were calculated with CCP4[3] after Bayesian q-weighting of the difference structure factor amplitudes[4] performed with IDL (ITT, Boulder, Colorado, USA) and using phases from the green structure of IrisFP (PDB entry 2VVH). Such maps are able to reveal subtle conformational changes by a small fraction of the molecules in the crystal, but only in the absence of significant changes in the unit-cell dimensions. Under high-intensity illumination conditions, one crystal showed no such change and provided the data presented in Figure 2C. Due to the larger X-ray beam size relative to the bleached crystal volume, the fraction of bleached molecules observed crystallographically was estimated to be ≤ 20%. Under low-intensity illumination conditions, unit-cell expansion in the bleached area was always too large to compute reliable experimental difference electron density maps. Instead, standard difference Fourier maps ($F_{obs,\ bleached} - F_{calc,\ green}$) were generated (Figure 4C).

NCS-averaged maps were calculated with Coot.[5] Figures presenting crystallographic data were prepared with Pymol (Schrödinger, LLC., New York, USA).

Model refinement

In order to obtain refined models of pBl_{red} and Bl_{red}, we employed the difference refinement method[6] after a molecular replacement step using the program MOLREP[7] with PDB entry 2VVH as a search model. We used extrapolated structure factors:

$$F_{Bred} = F_{Green} + \frac{1}{\alpha} \times \frac{q}{\langle q \rangle} \times \frac{m}{\langle m \rangle} \times (F_{Bleached} - F_{Green})$$

where α is a scaling factor corresponding to the fraction of photobleached chromophores, *q* is the weight calculated from the ''q-weighting'' procedure[4] and *m* is Read's figure of merit.[8] Stereo-chemical restraints for the chromophore were taken as published in Roy et al.[9] in order to properly describe the methylene bridge C_α carbon in a sp^3-configuration and a planar imidazolinone ring. The structures were refined with PHENIX[10] along with manual inspection and corrections in Coot.[5]

In order to obtain a refined model of Bl_{oxy}, a standard refinement procedure using PHENIX[10] and Coot[5] was employed.

Refinement statistics can be found in Table S1. The relatively poor R_{cryst} and R_{free} factors obtained for the structure of photobleached IrisFP under high-intensity illumination conditions is explained by the low occupancy of the photobleached state in the crystal volume probed by X-rays ($\alpha \approx 0.2$), resulting in rather high sigma values for the extrapolated structure factor amplitudes. However, the refined structure was found to correctly match the experimental difference electron density features of Figure 2C, providing credit to its significance.

Atomic coordinates and structure factors amplitudes of IrisFP in states $Bl_{red,}$ pBl_{red} and Bl_{oxy} have been deposited in the Protein Data Bank (www.pdb.org) under the PDB accession codes 4LJB, 4LJC and 4LJD, respectively.

Optical microspectrophotometry

Absorption spectra from IrisFP crystals (Figures 2 and 4) or PVA-embedded samples (Figure S2) were recorded at 100 K and at room temperature, respectively, using a microspectrophotometer setup described previously[11]. Solution spectra (Figure S2) were measured at RT using a 3-window quartz-cell (50 µL, optical path 3 mm). The cell was connected to the lamp and spectrometer of our microspectrophotometer setup through 100-µm optical fibers. Actinic light was delivered at right angle via a third fiber of 200-µm diameter, so that the laser beams covered completely the third window. For anaerobic measurements, the quartz-cell was nitrogen-bubbled beforehand and sealed (Figure S2 and S8).

Spectroscopic data were processed using homemade routines based on the MATLAB software (The MathWorks Inc., Natick, Massachusetts, USA). Absorption spectra were corrected for background using a polynomial baseline subtraction. Model fitting of the photofatigue decays was performed with Origin (OriginLab, Northampton, Massachusetts, USA). Fluorescence emission spectra were corrected for background using an offset baseline subtraction at 450 nm.

Raman spectroscopy

In crystallo Raman spectroscopy was performed at the Cryobench laboratory (ID29-1, ESRF). Off-resonance Raman spectra were recorded at 100 K from IrisFP crystals mounted in standard cryoloops, using a 785-nm laser. Samples were photofatigued using the same protocols as described above, except that, for the low-intensity illumination condition, crystals were prepared using the inverted PALM microscope, which allowed achieving only partial photobleaching before crystal drying occurred. As for X-ray data, Raman spectra were recorded on both bleached and non-bleached parts of the same crystal. Spectra were recorded in 10 min over the spectral window (200 – 2000 cm^{-1}). Baseline subtraction was carried out with an automated baseline-flattening routine.[12] Spectra were scaled with MATLAB (The MathWorks Inc., Natick, Massachusetts, USA), after normalization at the amide I band (1665 cm^{-1}).

Mass spectrometry

Mass spectrometry was used to confirm Glu212 decarboxylation and amino acids oxidation levels under high- and low-intensity illumination conditions, respectively. Crystals were prepared following the same protocol as described above, except that the entire crystal volume was treated. The crystals were then dissolved in 20 µl Tris buffer (50 mM, pH 8.0); Solution samples were directly prepared either in PVA films (to prevent molecular diffusion, high-intensity conditions, 1 µl, 740 µM) or in a quartz cuvette (low-intensity conditions, 30 µl, 10 µM). Samples in 50 mM Tris were diluted to have a final concentration of 10% of acetonitrile; heated at 90°C during 5 min then cooled with an ice bath to unfold the FP structure. A 1/20 ratio of trypsin was added to the mixture and the digestion was extended overnight. ~ 100 ng of each trypsin digested sample was analyzed in triplicate by nano-liquid chromatography coupled to tandem mass spectrometry (Ultimate3000, Dionex and LTQ-Orbitrap XL, Thermo Fischer, Waltham, Massachussets, USA). Fragments were identified using the Mascot software (version 2.4, Matrix Science) against a custom database containing the target protein.[13] We specified Met/Trp/His/Tyr oxidations, Cys di- and tri-oxidation and Glu decarboxylation as possible variable modifications (Figure S9, Table S2). ESI-TRAP was selected as the analytical instrument, semi-Trypsin as the enzyme and 3 missed cleavage were allowed. Precursor and fragment mass error tolerances were set respectively at 10 ppm and 0.6 Da. For the evaluations of the ratio between oxidized and non-oxidized forms, the 6 raw files were deconvoluted and aligned using the Decon-2ls and MultiAlign software suite.

(PNNL, Richland, WA). The intensities of the Mascot identified peptides corresponding to reduced and oxidized Met, Cys or Trp were compared in the two conditions. Averages and standard deviations of the percentages of oxidized forms were calculated from the triplicate experiments. (Figure S9).

The Decon-2LS and Multi-Align softwares used for MS data processing were provided by the W. R. Wiley Environmental Molecular Science Laboratory, a national scientific user facility sponsored by the US Department of Energy's Office of Biological and Environmental Research, located at PNNL. (OMICS.PNL.GOV).

Quantum mechanical and molecular dynamics simulations

To assess the chemical structure of the chromophore in both the pBl_{red} (X-ray bleached) and Bl_{red} photobleached structures (a prerequisite to perform the molecular dynamics simulations), quantum mechanical (QM) calculations at the B3LYP/6-31G* level using Gaussian[14] were performed. In the absence of experimental evidence concerning the charge state of the chromophore in these bleached structures, the anionic form, with a deprotonated phenolate ring, was assumed. The only simple way to account for the observed chromophore tilted geometry is that an H atom is added on the bridge carbon atom Cα, as previously described.[9] In such conditions, however, the chromophore becomes a free radical and something else necessarily happens. We examined if a second H atom may be accommodated by the imidazolinone ring. The requirement of the observed planar geometry of that ring excludes all sites except the oxygen atom O and the nitrogen atom N4 (see Figure S10). Three chemical structures were thus explored : two structures with an hydrogen atom on O, that differ from each other by the orientation of the hydroxyl group, either towards the phenolate ring (structure referred to as CαOI) or in the opposite direction (CαOII), and the one with an hydrogen atom on N4 (CαN) (Figure S10).

The QM calculations showed that the three structures are stable with respect to the addition of the second hydrogen atom, by an energy amount of 40-60 kcal/mol depending of the structure.

Molecular dynamics (MD) simulations were performed in order to examine whether the X-ray bleached structure (Figure S7 and Table S3) might spontaneously transform into the Bl_{red} photobleached structure at room temperature. The chromophore force field, apart from the dihedral potential, was obtained as described previously.[15] The missing carboxylate of Glu212 was replaced by a hydrogen atom. For all standard amino-acids the AMBER force field "ff99"

was used.[16] MD simulations were run with the parallel module PMEMD of the AMBER suite[16] modified by Jonasson et al.[15] that allows using coupled dihedral potentials. The MD protocol consists of minimization and equilibration phases, where constraints on the protein are progressively removed, followed by 4-ns free runs at constant temperature (300 K) and pressure (1 atm). In the case of the CαN chemical structure, four free runs were carried out, starting with different snapshots of the last equilibrium phase. For each of the two structures CαOI and CαOII three free runs were carried out in the same way. A run with the chromophore in its fluorescent *cis* form (see Jonasson et al.[15] for the force field) was also performed in order to get some information about the influence of Glu212 decarboxylation and of chromophore denaturation.

An essential point in the molecular dynamics simulations is the torsional behavior of the chromophore around Cα. It is expected to significantly differ from a free rotation profile, due to the two rings. We used coupled dihedral potentials V(τ,φ) (see Figure S10 for the definition of τ and φ) determined as in Jonasson et al.[15] For each of the three reduced chemical structures, a specific potential was obtained by fitting an *ab initio* two dimensional potential energy surface (PES) calculated at the B3LYP/6-31G* level using Gaussian.[14] The three PES are shown in Figure S11. The iso-energy curves around the minima are ellipses with axes largely tilted by respect to the τ and φ axes, showing that the usual additive form V(τ)+V(φ) would have been inappropriate to fit the dihedral profile.

Laser beam heterogeneity

In all cases, photofatigue experiments were carried out using laser beams adopting a near-Gaussian two-dimensional profile rather than a top-hat profile. Therefore, the beam power-densities were not homogeneous throughout the samples. Notably, under our “high-intensity” illumination conditions, a fraction of the IrisFP molecules at the periphery of the illuminated profile rather experienced “low-intensity” illumination conditions. For a monophasic photobleaching process, it has been shown that the observed fluorescence emission decay of a sample bathed in a Gaussian-shaped laser beam can be expressed as:[17]

$$F(t) = ka^2 \frac{1-\exp(-t/\tau_0)}{t/\tau_0}$$

where a is the radius of the laser beam and τ_0 is the inverse of the bleaching rate at the beam center. Attempts to fit our photofatigue decays (Figures 1 and 3) using such a model did not

provide satisfactory results, suggesting that in both cases the photobleaching processes are multiphasic. The most satisfactory fit with a biphasic model under both low- and high-intensity illumination conditions is likely to incorporate both the effects of the beam heterogeneity and the various bleaching mechanisms that may be present. The different decay profiles observed in the two illumination conditions, however, strongly suggest that a distinct distribution of bleaching mechanisms are involved in the two cases. The more pronounced biphasic shape of the photofatigue decay under high-intensity illumination is consistent with a large fraction of the molecules experiencing oxygen-independent bleaching while a smaller fraction, remote from the beam center, experiences slower, oxygen-dependent bleaching.

It should be noted that the various techniques used in this work to probe photobleaching mechanisms typically interrogate volumes of the treated crystals that differ in size: mass spectrometry used the entire crystal volume (photofatigued on multiple spots), crystallography typically employed a 100 µm diameter X-ray beam of approximately the same size as the photofatigued region (but possibly slightly offset), fluorescence spectroscopy used exactly the same size (with no offset), optical absorption microspectrophotometry used a 50-µm white-light beam slightly smaller (with little offset), and Raman spectroscopy used a ~10-µm near-IR-laser beam much smaller than the photofatigued region (with little offset).

We also note that, on the PALM microscope, the size of the 405 nm beam was larger than that of the 488 nm beam. As a result, for samples treated on this microscope, volume peripheral to the photofatigued region underwent green-to-red photoconversion (Figure S12A). Residual difference electron density map corresponding to this photoconversion is visible in figure 2C around the Phe61-His62 backbone linkage. A calculated difference density map between the models of green and red photoconverted IrisFP (Figure S12B) confirmed that no other density features observed in Figure 2C may originate from unwanted photoconversion.

Detailed results on QM and MD simulations

The three torsional landscapes of the chromophore corresponding to the three putative chemical structures of the bleached pBl_{red} and Bl_{red} states largely differ from each other (Figure S11). In the case of the CαN structure it presents a deep energy minimum around the geometry τ=0°, φ=±90°. In the case of CαOI a deep minimum is also observed, centered on τ=180°, φ=±90°. Concerning CαOII, the energy profile is very flat compared to the preceding

ones, allowing very large torsional movements away from the minimum energy point centered at τ=120°, φ=-75°.

The main results of the MD simulations are summarized in Table S4.

CαOI structure: No switch of Arg66 and His194 is observed in any of the three runs. The internal forces of the chromophore drive it to conformations with τ and φ average values equal to respectively 169° and -74°, near the equilibrium geometry of the isolated chromophore. Inspection of the chromophore environment in the MD trajectories shows that in these conformations the phenolate ring hinders the movement of the Arg66 sidechain that would drive this residue to its conformation in Bl_{red} (Figure S13A).

CαOII structure: No switch happens in the first two runs. Average values of τ and φ are 146° and -60°, values located in the large basin of the potential energy surface, close to the minimum energy point. Inspection of the trajectories lead to the same analysis as above: the movement of Arg66 is prevented by the phenolate. In the third run the switch is observed at the very beginning of the run, when the phenolate ring does not yet block the Arg66 displacement.

An interesting feature of the CαOI and CαOII MD simulations is the significant weakening of the usually strong hydrogen bond between the imidazolinone oxygen O with Arg91, clearly due to the addition of the hydrogen atom on O.

CαN structure: With this chemical structure, the mean values of the dihedral angles τ and φ are 25° and -85°. In such geometries the phenolate ring lets the Arg66 sidechain free to move (Figure S13B), and the switch is observed in all four runs. This results in the loss of the H-bond between His194 and Glu144, and in the formation of two new H-bonds: a strong one between His194 and Arg66, and a non-permanent one between His194 and Ser142. Figure S14 shows that these H-bond modifications are simultaneous. In addition a first movement of Arg66 was observed in the last part of the equibration phase, leading to the formation of a H-bond with Glu144.

The mean value of τ (25°) is in good agreement with the experimental values in the Bl_{red} photobleached structure. The large fluctuations observed (standard deviation of 16°, much larger than the 6° deviation observed for the fluorescent chromophore) are consistent with the disorder of the phenolate in the crystallographic structure. The mean value of φ is -85°, far from the crystallographic values. However this comparison is not pertinent due to the observed disorder of the phenolate.

It is worth noting that the rearrangement of the switch of Arg66 and His194 is observed with the fluorescent planar *cis* chromophore as well, as long as Glu212 is decarboxylated. Thus, Glu212 decarboxylation, resulting in an H-bond missing for His194, appears to be sufficient to induce this rearrangement, provided that the phenolate does not hinder the displacement of Arg66.

These results show that IrisFP structural dynamics at 300 K is indeed able to drive His194 and Arg66 from their conformations in the cryo-X-ray-bleached structure towards those in the Bl_{red} photobleached one, adding value to the notion that the former structure may be viewed as an intermediate along the Bl_{red} bleaching pathway. More generally, they strongly suggest that the decarboxylation of Glu212 is sufficient to induce the large displacement of His194 and Arg66. The results also provide an answer to question (iii) of the main text, concerning the chemical structure of the chromophore : the most probable structure is the zwitterionic CαN.

Modeling of kinetic scheme

In order to simulate the observed two-regime bleaching behavior, we consider the kinetic scheme S15.

The chromophore in its singlet ground state S_0 absorbs photons with rate k_{ex}, exciting it to the first singlet excited state S_1 from where it can return to S_0 by fluorescence or non-radiative decay (both processes described by rate k_F). Alternatively, the singlet excited chromophore can undergo intersystem crossing to the triplet excited state T_1 with rate k_{IS}. T_1 may then engage into a number of pathways.

First, it can spontaneously convert to the ground state (rate constant $k_{T1,1}$), or be quenched by triplet oxygen (rate constant $k_{T1,2}$), creating highly reactive singlet oxygen. $^1O_2$ may in turn face three different fates : intersystem crossing to restore triplet oxygen (k_1), exit from the protein to the solvent (k_2) or reactive attack on the FP itself, thus leading to permanent oxygenic bleaching of the chromophore fluorescence (state Bl_{oxy} formed with k_3).

Second, T_1 may experience electron/proton transfer with rate constant k_4, leading to a doublet radical state $DH^{\bullet}$. This « blinked » dark state may either recombine with rate constant k_5 to the intact singlet ground state or further react with rate constant k_6 to a permanently (« redox ») bleached state Bl_{red}.[9]

Third, T_1 may undergo a second excitation to a higher excited triplet state T_n that may rapidly return to the ground state or go through electron/proton transfer to the permanently bleached state Bl_{red} (we assume that this bleached state is close or identical to that reached

through $DH^{\bullet}$). The overall rate for this latter process is unknown but is likely to be limited by the preceding second excitation; therefore the whole process is described by the rate constant $k_{T1,ex}$.

Within the framework of this simplified kinetic scheme, there exist two possible mechanisms that can introduce a dependence of the prevailing bleaching pathway on the excitation rate k_{ex}.

A) The T_1 state is populated by k_{ex} via k_{IS} and depopulated essentially by $k_{T1,2}$, fuelling the k_3 oxygen dependent bleaching pathway. If, in the high-energy case, oxygen replenishment by $k_{O2,in}$ and k_1 is too slow to compete with k_{ex}, the lack of available oxygen within the FP barrel will be limiting the Bl_{oxy} pathway. The entry and exit rates of oxygen in and out of the barrel are poorly known and therefore, we introduce $k_{O2,in}$ as well as $k_{O2,out}$ as adjustable parameters.

B) The weight of the T_n pathway will increase with k_{ex}, as the chance of the absorption of the second photon necessary for this pathway is directly proportional to the excitation power density, ie $k_{T1,ex}.\alpha\ k_{ex}$. However, currently the absorption cross section of T_1 is not known, and we use $k_{T1,ex}$ as an adjustable parameter for the probability of this pathway.

Fixing the rate constants to the values given in the legend of Figure S16 and varying the excitation power density from 10 to 100 $W.cm^{-2}$, we can actually observe the gradual change from prevailing oxidative damage to more and more redox and second photon induced decarboxylation with increasing energy (Figure S16).

Raman spectra from photobleached crystals

Modifications of the Raman spectra of IrisFP crystals induced by photobleaching at high illumination intensity are drastic throughout the whole investigated wavenumber range (Figure 2B), indicative of the chemical transformation of the chromophore. In addition to the complete disappearance of the bands at 1503 cm^{-1}, 1545 cm^{-1}, 1564 cm^{-1} and 1604 cm^{-1} described in the main manuscript, many bands in the range 1000 to 1500 cm^{-1} are also strongly decreased, while a few others appear or are increased. A precise assignment of these vibrational bands has not been performed, but some indications can be given based on

previous work on the HBDI chromophore.[18] The decreased band at 1037 cm^{-1} can be assigned to a coupled imidazolinone C-C stretching mode and C=O mode. The decreased bands at 1093 cm^{-1} and 1111 cm^{-1}, and the increased band at 1069 $cm^{-1}$are unassigned. The strongly increased band at 1137 cm^{-1} is possibly assigned to an imidazolinone mode, while the vanished bands at 1154 and 1172 cm^{-1} could be assigned to a phenol C-H deformation band. Decreased bands at 1217 and 1260 cm^{-1} are unassigned. The increased band at 1304 cm^{-1}, and the decreased bands at 1321 and 1338 cm^{-1} are possibly assigned to phenol modes. The decreased band at 1375 cm^{-1} and the increased band at 1395 cm^{-1} are unassigned. The slightly decreased strong band at 1448 cm^{-1} could possibly be assigned to a phenol C-H deformation mode, and the slightly increased band at 1484 cm^{-1} remains unassigned. The disappearance of the ill-defined band around 1665 cm^{-1} could correspond to an imidazolinone C=O stretching mode. Although the exact interpretation of all these changes remains out of the scope of this paper, they strongly suggest that the chemical structure of the chromophore is not only altered at the methylene bridge, but also at the phenol and imidazolinone cyclic moieties, consistent with our proposal of a reduced chromophore.

Modifications of the Raman spectra induced by photobleaching at low illumination intensity appear much less pronounced throughout the entire wavenumber range (Figure 4B), although in this case an incompletely bleached crystal was interrogated, which limits the accuracy with which spectral modifications can be detected. The reason for partial bleaching was to probe the Raman signature of the Met159 sulfoxidation reaction, while avoiding the overall barrel destabilization due to oxidation of residues more remote from the chromophore that was found to occur upon long illumination. Apart from the protonation of the chromophore, as described in the main manuscript, these Raman spectra suggest that the chemical structure of the chromophore remains chemically unaltered under these conditions.

References

(1) Adam, V.; Lelimousin, M.; Boehme, S.; Desfonds, G.; Nienhaus, K.; Field, M. J.; Wiedenmann, J.; McSweeney, S.; Nienhaus, G. U.; Bourgeois, D. *Proc. Natl. Acad. Sci. U S A* **2008**, *105*, 18343.

(2) Kabsch, W. *Acta Crystallogr. D Biol. Crystallogr.* **2010**, *66*, 125.

(3) Winn, M. D.; Ballard, C. C.; Cowtan, K. D.; Dodson, E. J.; Emsley, P.; Evans, P. R.; Keegan, R. M.; Krissinel, E. B.; Leslie, A. G.; McCoy, A.; McNicholas, S. J.; Murshudov, G. N.; Pannu, N. S.; Potterton, E. A.; Powell, H. R.; Read, R. J.; Vagin, A.; Wilson, K. S. *Acta Crystallogr. D Biol. Crystallogr.* **2011**, *67*, 235.

(4) Ursby, T.; Bourgeois, D. *Acta Crystallogr. A* **1997**, *53*, 564.

(5) Emsley, P.; Cowtan, K. *Acta Crystallogr. D Biol. Crystallogr.* **2004**, *60*, 2126.

(6) Terwilliger, T. C.; Berendzen, J. *Acta Crystallogr. D Biol. Crystallogr.* **1995**, *51*, 609.

(7) Vagin, A.; Teplyakov, A. *Acta Crystallogr. D Biol. Crystallogr.* **2010**, *66*, 22.

(8) Read, R. J. *Acta Crystallogr. A* **1986**, *42*, 140.

(9) Roy, A.; Field, M. J.; Adam, V.; Bourgeois, D. *J. Am. Chem. Soc.* **2011**, *133*, 18586.

(10) Adams, P. D.; Afonine, P. V.; Bunkoczi, G.; Chen, V. B.; Davis, I. W.; Echols, N.; Headd, J. J.; Hung, L. W.; Kapral, G. J.; Grosse-Kunstleve, R. W.; McCoy, A. J.; Moriarty, N. W.; Oeffner, R.; Read, R. J.; Richardson, D. C.; Richardson, J. S.; Terwilliger, T. C.; Zwart, P. H. *Acta Crystallogr. D Biol. Crystallogr.* **2010**, *66*, 213.

(11) Faro, A. R.; Adam, V.; Carpentier, P.; Darnault, C.; Bourgeois, D.; de Rosny, E. *Photochem. Photobiol. Sci.* **2010**, *9*, 254.

(12) Schulze, H. G.; Foist, R. B.; Okuda, K.; Ivanov, A.; Turner, R. F. *Appl. Spectrosc.* **2011**, *65*, 75.

(13) Perkins, D. N.; Pappin, D. J.; Creasy, D. M.; Cottrell, J. S. *Electrophoresis* **1999**, *20*, 3551.

(14) Frisch, M. J.; Trucks, G. W.; Schlegel, H. B.; Scuseria, G. E.; Robb, M. A.; Cheeseman, J. R.; Montgomery, J., J. A.; Vreven, T.; Kudin, K. N.; Burant, J. C.; Millam, J. M.; Iyengar, S. S.; Tomasi, J.; Barone, V.; Mennucci, B.; Cossi, M.; Scalmani, G.; Rega, N.; Petersson, G. A.; Nakatsuji, H.; Hada, M.; Ehara, M.; Toyota, K.; Fukuda, R.; Hasegawa, J.; Ishida, M.; Nakajima, T.; Honda, Y.; Kitao, O.; Nakai, H.; Klene, M.; Li, X.; Knox, J. E.; Hratchian, H. P.; Cross, J. B.; Bakken, V.; Adamo, C.; Jaramillo, J.; Gomperts, R.; Stratmann, R. E.; Yazyev, O.; Austin, A. J.; Cammi, R.; Pomelli, C.; Ochterski, J. W.; Ayala, P. Y.; Morokuma, K.; Voth, G. A.; Salvador, P.; Dannenberg, J. J.; Zakrzewski, V. G.; Dapprich, S.; Daniels, A. D.; Strain, M. C.; Farkas, O.; Malick, D. K.; Rabuck, A. D.; Raghavachari, K.; Foresman, J. B.; Ortiz, J. V.; Cui, Q.; Baboul, A. G.; Clifford, S.; Cioslowski, J.; Stefanov, B. B.; Liu, G.; Liashenko, A.; Piskorz, P.; Komaromi, I.; Martin, R. L.; Fox, D. J.; Keith, T.; Al-Laham, M. A.; Peng, C. Y.; Nanayakkara, A.; Challacombe, M.; Gill, P. M. W.; Johnson, B.; Chen, W.; Wong, M. W.; Gonzalez, C.; Pople, J. A. *Gaussian 03, Revision C.02* **Gaussian, Inc., Wallingford CT, 2004**.

(15) Jonasson, G.; Teuler, J. M.; Vallverdu, G.; Merola, F.; Ridard, J.; Levy, B.; Demachy, I. *J. Chem. Theory Comput.* **2011**, *7*, 1990.

(16) Case, D. A.; Darden, T. A.; Cheatham, I., T. E.; Simmerling, C. L.; Wang, J.; Duke, R. E.; Luo, R.; Crowley, M.; Walker, R. C.; Zhang, W.; Merz, K. M.; Wang, B.; Hayik, S.; Roitberg, A.; Seabra, G.; Kolossváry, I.; Wong, K. F.; Paesani, F.; Vanicek, J.; Wu, X.; Brozell, S. R.; Steinbrecher, T.; Gohlke, H.; Yang, L.; Tan, C.; Mongan, J.; Hornak, V.; Cui,

G.; Mathews, D. H.; Seetin, M. G.; Sagui, C.; Babin, V.; Kollman, P. A. *AMBER 10* **University of California, San Francisco, 2008**.

(17) Gavrilyuk, S.; Polyutov, S.; Jha, P. C.; Rinkevicius, Z.; Agren, H.; Gel'mukhanov, F. *J. Phys. Chem. A* **2007**, *111*, 11961.

(18) He, X.; Bell, A. F.; Tonge, P. J. *J. Phys. Chem. B* **2002**, *106*, 6056.

(19) Froelich, J. M.; Reid, G. E. *Proteomics* **2008**, *8*, 1334.

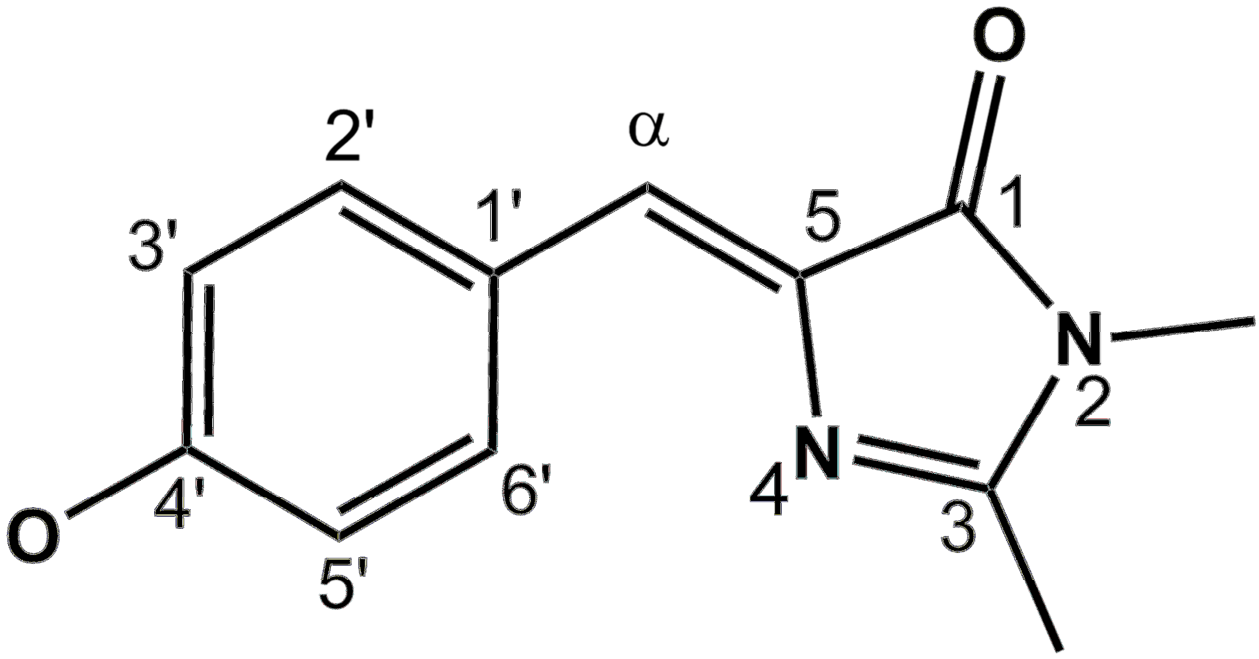

Scheme S1. Structural formula of the 4-(p-hydroxybenzylidene)-5-imidazolinone chromophore with atom labeling.

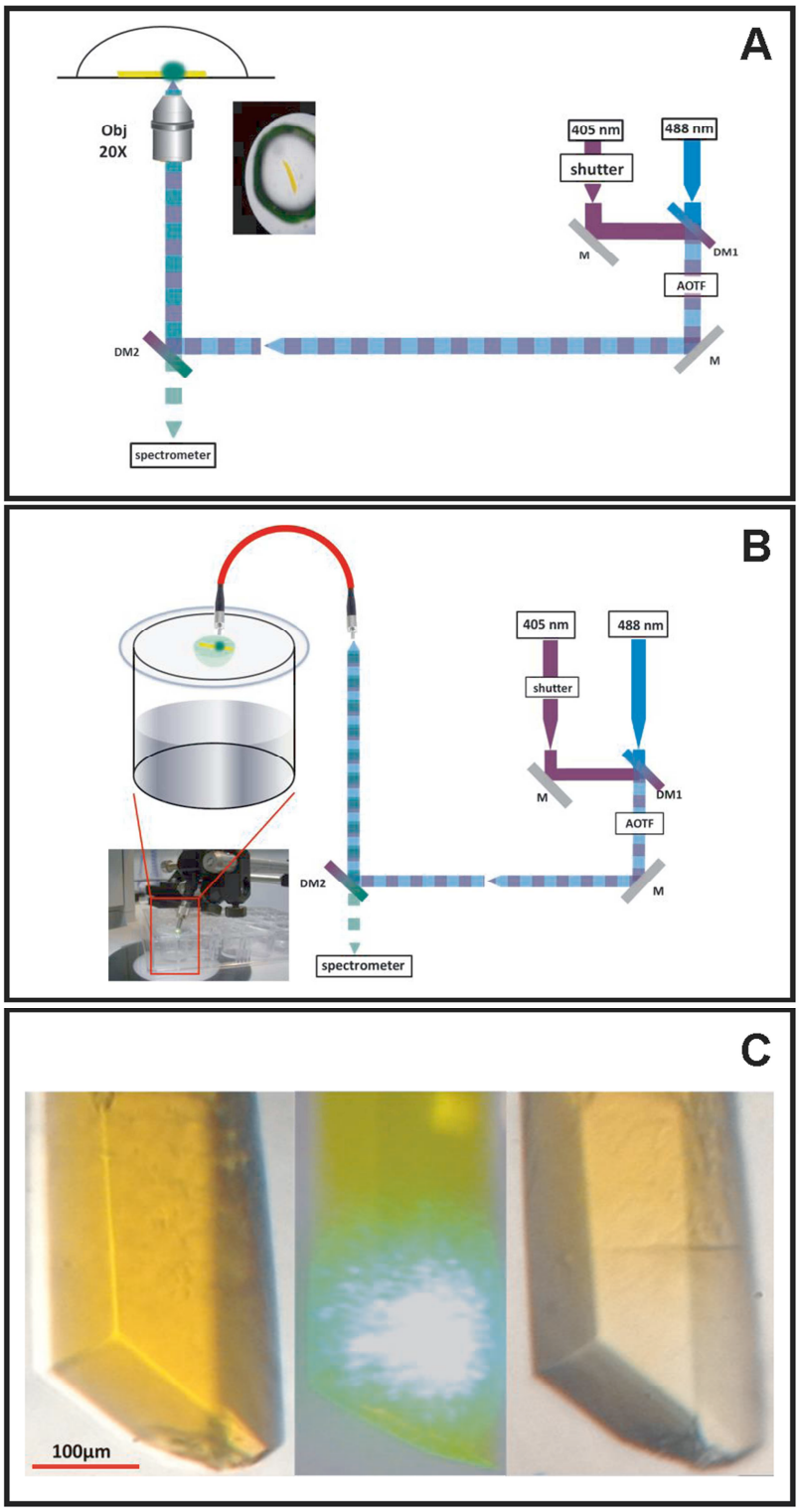

Figure S1. Optical setups for photofatigue of IrisFP crystals under conditions of high (A) and low (B) power density. M, mirror; DM, dichroic mirror; AOTF, acousto-optic tunable filter. (C) From left to right, photographs of an IrisFP crystal before, during and after experiment.

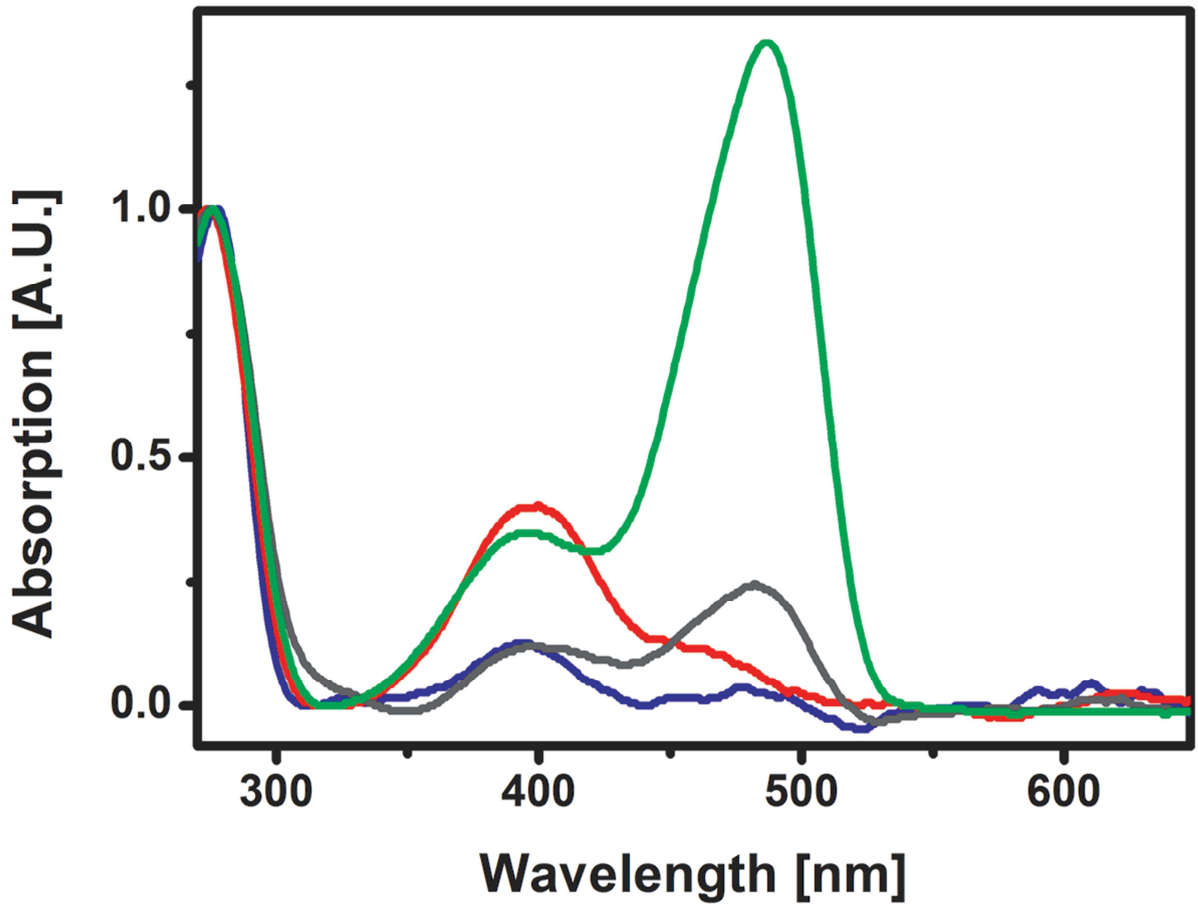

Figure S2. Absorption spectra of IrisFP in the solution state, normalized at 280 nm: Prior to illumination (green); Under aerobic illumination: after 570 switching cycles at low-intensity (red), after 184 cycles at high-intensity in PVA gel (blue); Under anaerobic illumination: after 744 switching cycles at low-intensity (dark gray).

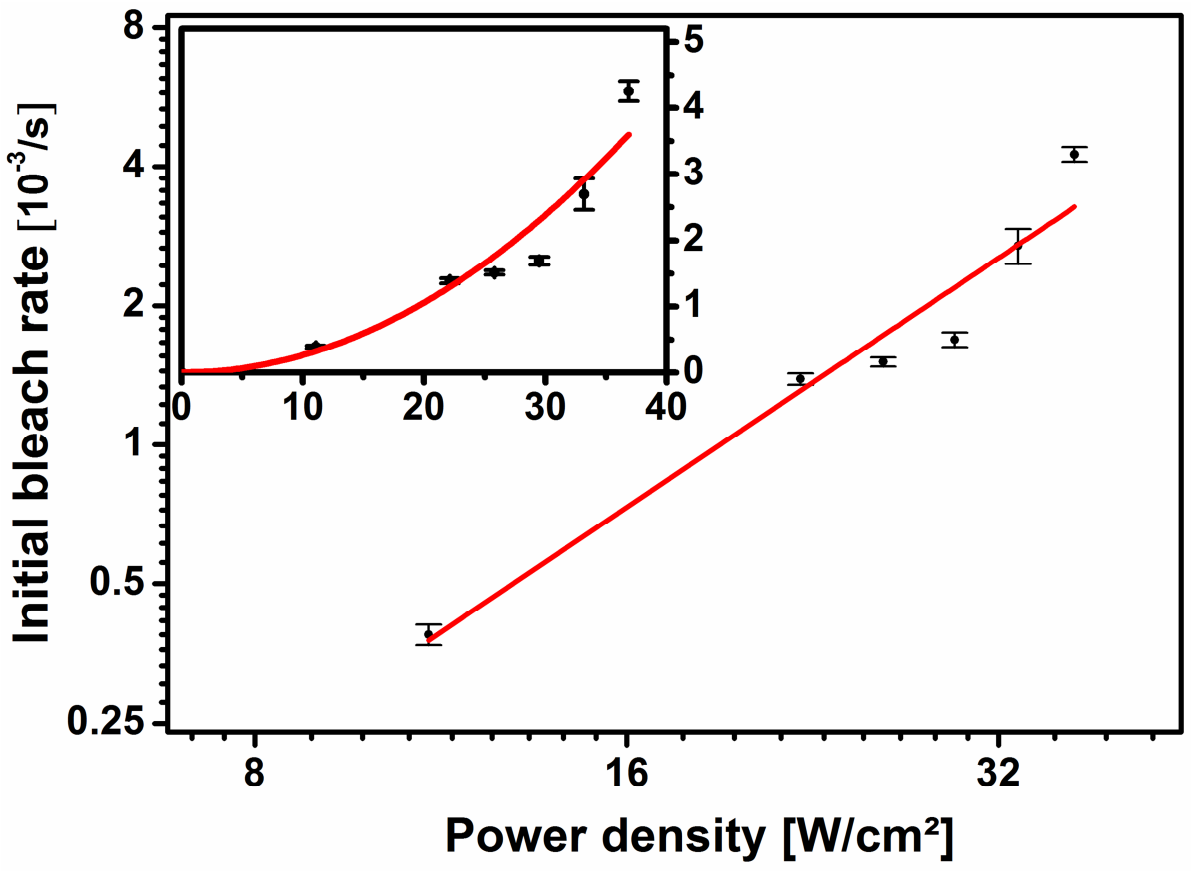

Figure S3. Photobleaching of IrisFP in the absence of oxygen mainly proceeds via a two-subsequent-photon absorption process. The fast component of a bi-exponential fit of the photo-fatigue envelope kinetics was used as the photo-fatigue rate. In this doubly logarithmic presentation, a linear fit (red line) of this rate as a function of the incident power density of the 488 nm beam gives a slope of 1.8 ± 0.3. The inset shows the same data with a linear presentation. The error bars represent the confidence interval of the fitted time-constant to the photofatigue curves. Actual errors are expected to be larger due to additional experimental imperfections.

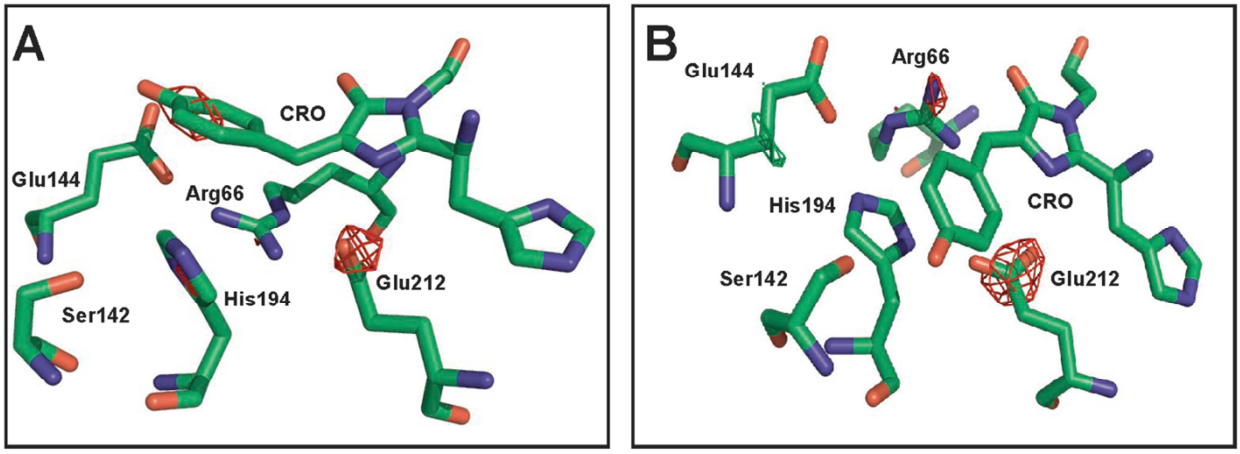

Figure S4. Visible-light-induced photobleaching at cryogenic temperature (100 K) shows a clear decarboxylation of Glu212 both in *cis* and *trans* conformations. (A) Photobleaching in *trans* conformation by 405-nm laser. NCS-averaged F_{obs}-F_{calc} difference electron densities are displayed in green (+6.5 σ) and red (-6.5 σ), respectively. (B) Photobleaching in *cis* conformation by 488-nm laser. NCS-averaged F_{obs}-F_{calc} difference electron densities are displayed in green (+4.5 σ) and red (-4.5 σ), respectively.

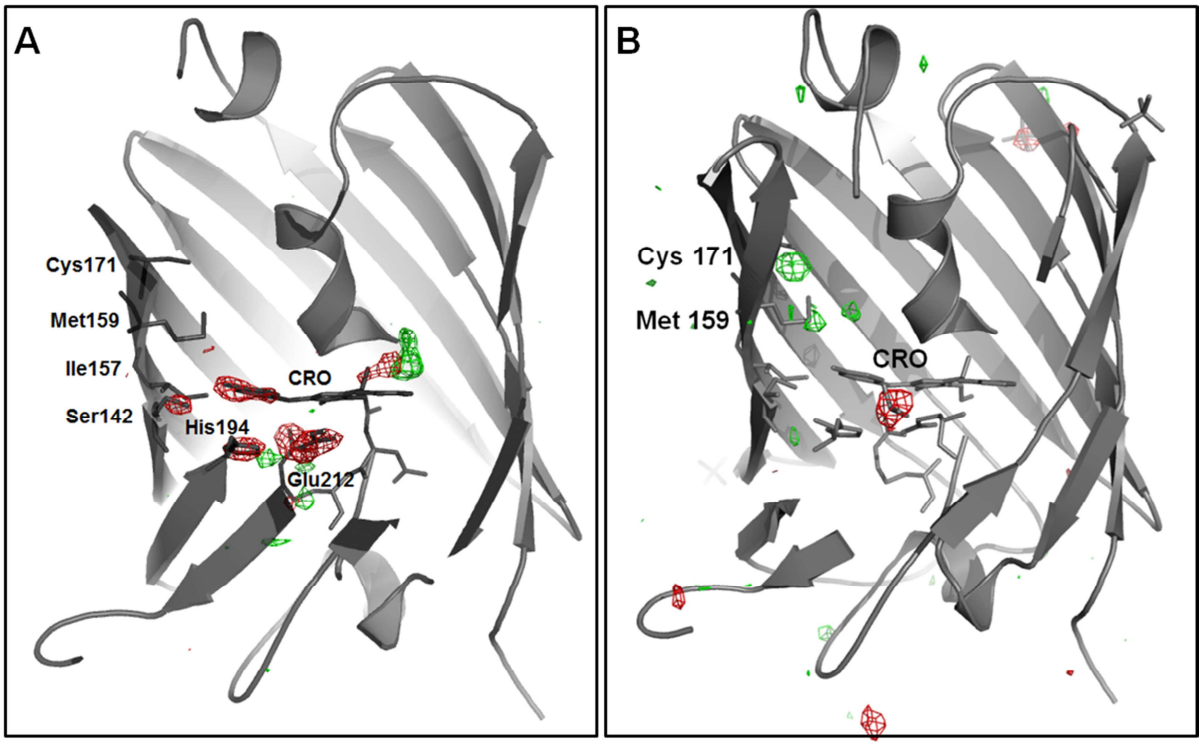

Figure S5. (A) Overall view of structural changes upon high-intensity-photobleaching of IrisFP. The structural modifications depicted by NCS-averaged electron density difference maps (± 6 σ) are all located around the chromophore. (B) Overall view of structural changes upon low-intensity-photobleaching of IrisFP. The major structural modifications depicted by NCS-averaged electron density difference maps (± 5.3 σ) are all located around the chromophore, near Met159 and Cys171. The negative densities in the back and in the front of the chromophore are due to disordered sulfate molecules.

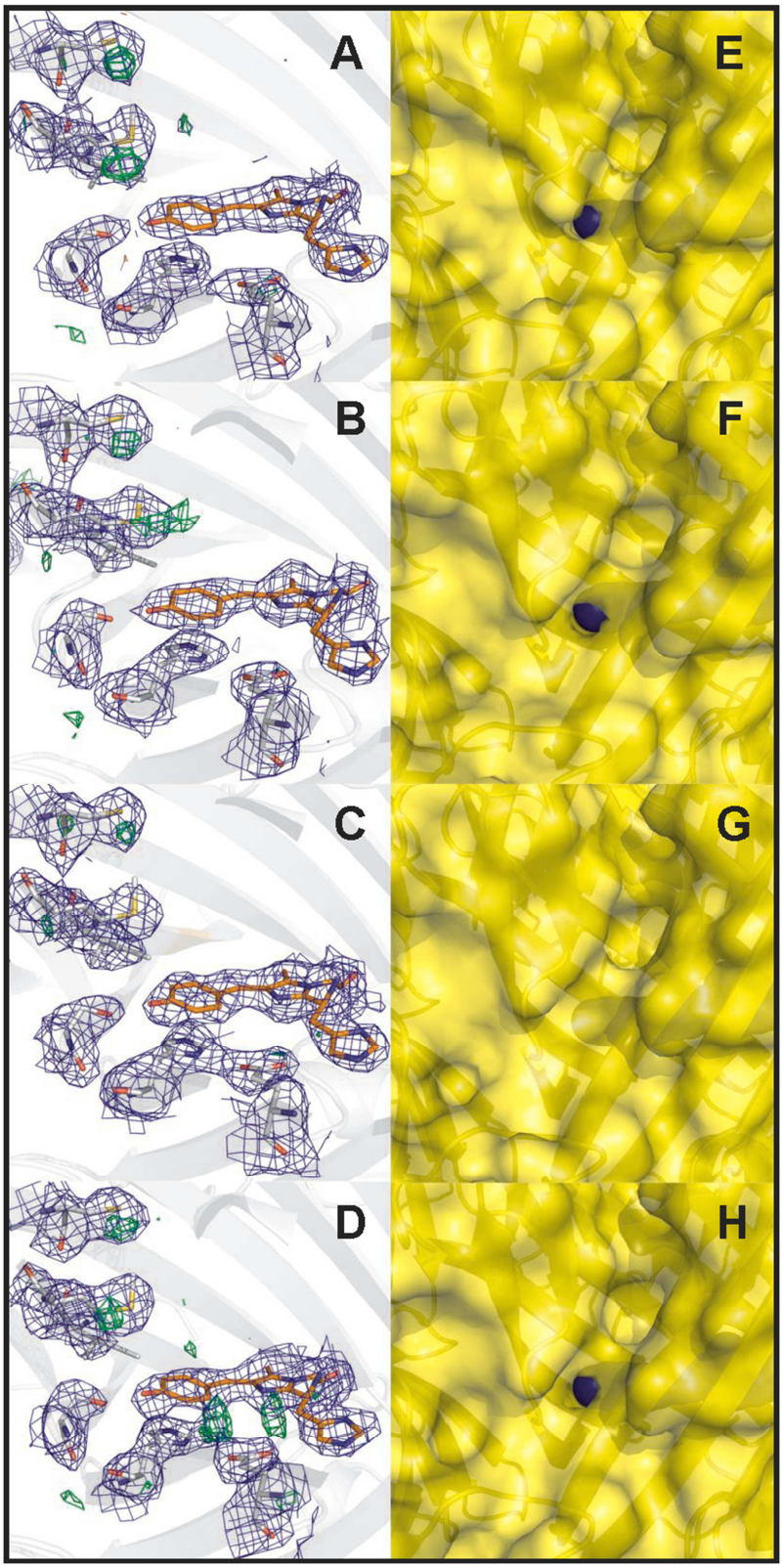

Figure S6. (A-D) Structural changes in monomers A to D induced by low-intensity photobleaching. $2F_{obs}$-F_{calc} (1 σ) and F_{obs}-F_{calc} (± 3.0 σ) electron density maps are shown as blue and green/red meshes respectively. No negative density is observed. (E-H) Surface view of monomers A to D of the IrisFP β-barrel. No access to the chromophore through the surface is visible in monomer C, which might explain the absence of significant sulfoxidation detected on Met159 in that monomer.

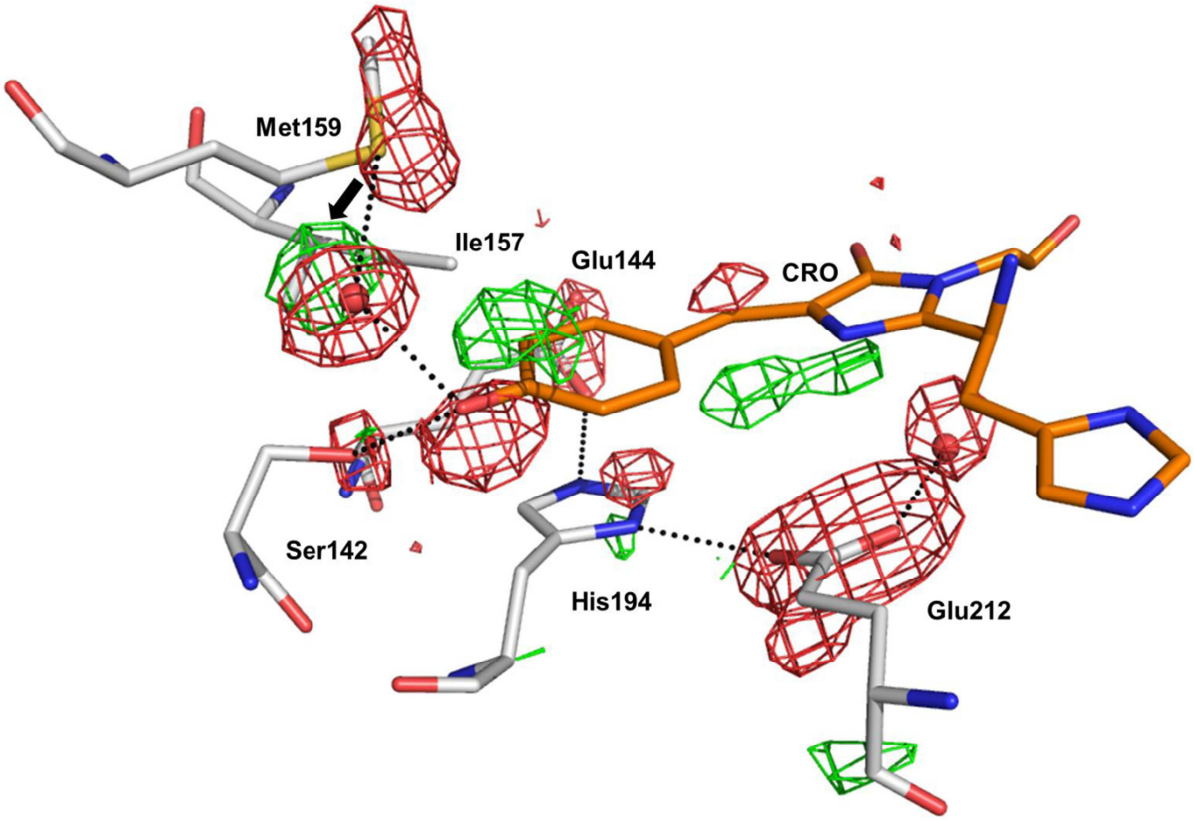

Figure S7. Structural modifications resulting from X-Ray-induced photobleaching. A NCS-averaged experimental electron difference density map is displayed. Positive density is shown in green (+6 σ) and negative density is shown in red (-6 σ), overlaid on the structure of the intact IrisFP chromophore pocket (PDB code 2VVH).

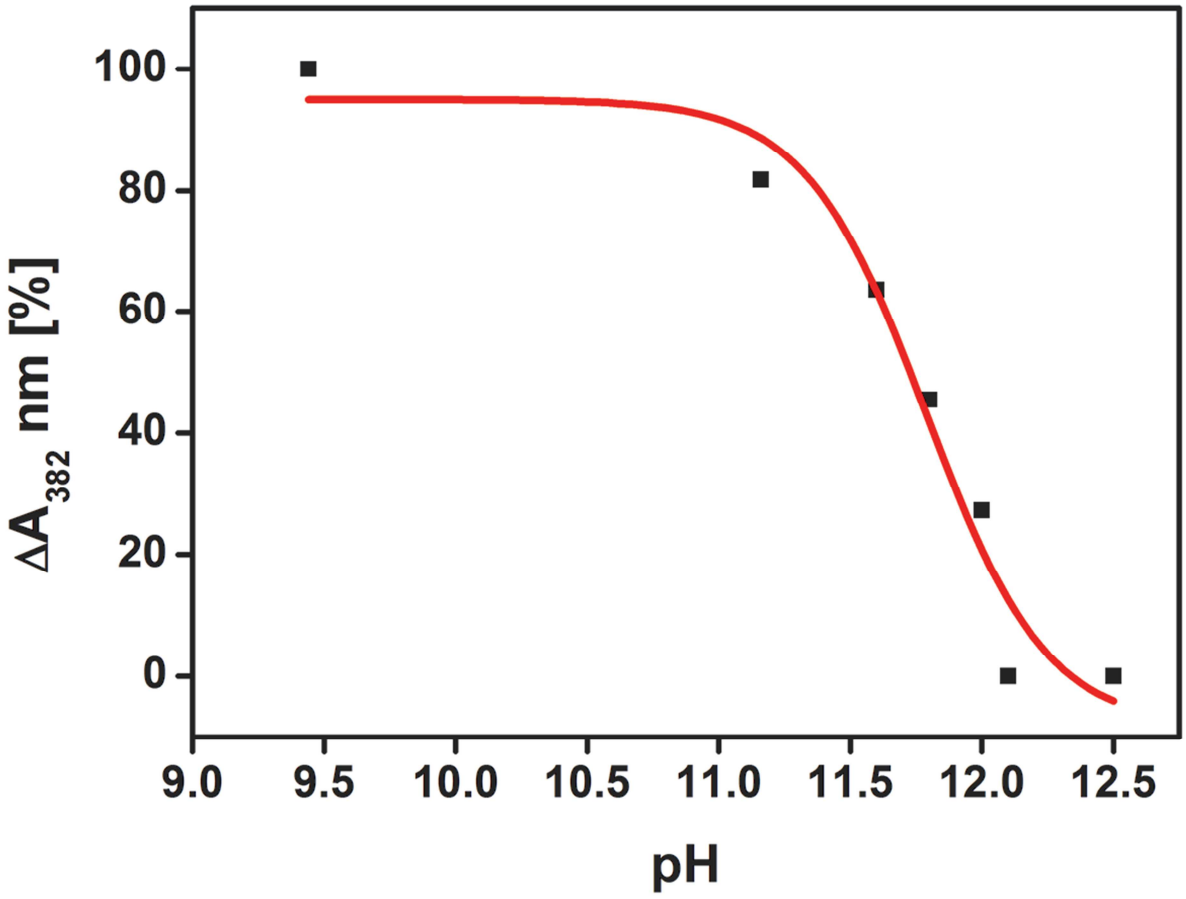

Figure S8. pH titration of the neutral absorption band of IrisFP solution samples, following low-intensity photobleaching. A Henderson-Hasselbalch fit (red curve) yields a pKa of 11.9 ± 0.2 for the oxidation-photobleached chromophore. Note that progressive protein denaturation makes the measurement of absorption values at pH >11 increasingly unreliable.

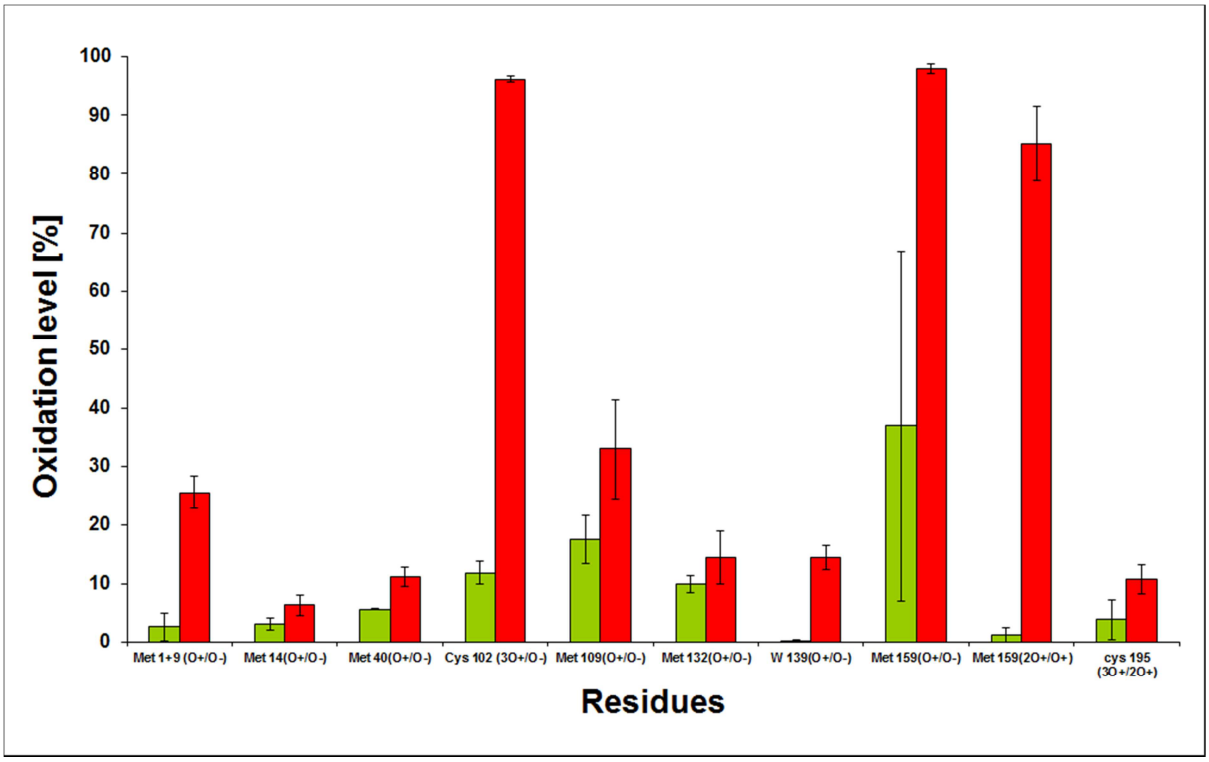

Figure S9. Mass spectrometry analysis of oxidation in non-illuminated IrisFP (green bar) and low-intensity-illuminated (red bar) samples. Only peptides identified in both non-oxidized and oxidized forms by the Mascot software are shown. Peptides displaying oxidation levels below 1% in both samples are not represented. Peptides containing Tyr78, Tyr211 and W86 fall in this category, although the data show a detectable increase in the oxidation level of these residues upon low-intensity-illumination. Due to sample pre-treatment (heating and digestion) before injection into the mass spectrometer, some background oxidation of sensitive residues is generally observed on the intact, non-bleached IrisFP, as is commonly the case.[19] The high scatter of oxidation state of the very sensitive Met159 from the reference sample is explained by the time dependent oxidation of the sample during the analytical process. The only way to evaluate Cys171 oxidation was through a low abundance miss-cleaved peptide. The non-oxidized form was not observed in any condition, but various oxidation states appeared in the illuminated sample. It was therefore impossible to derive a ratio for the corresponding peptide. For Cys195, the evaluation of the oxidation corresponded to the ratio of two oxidation states. Overall, these data clearly suggest that, upon low-intensity illumination, photo-oxidation occurs not only on residues close to the chromophore but also on more distant ones.

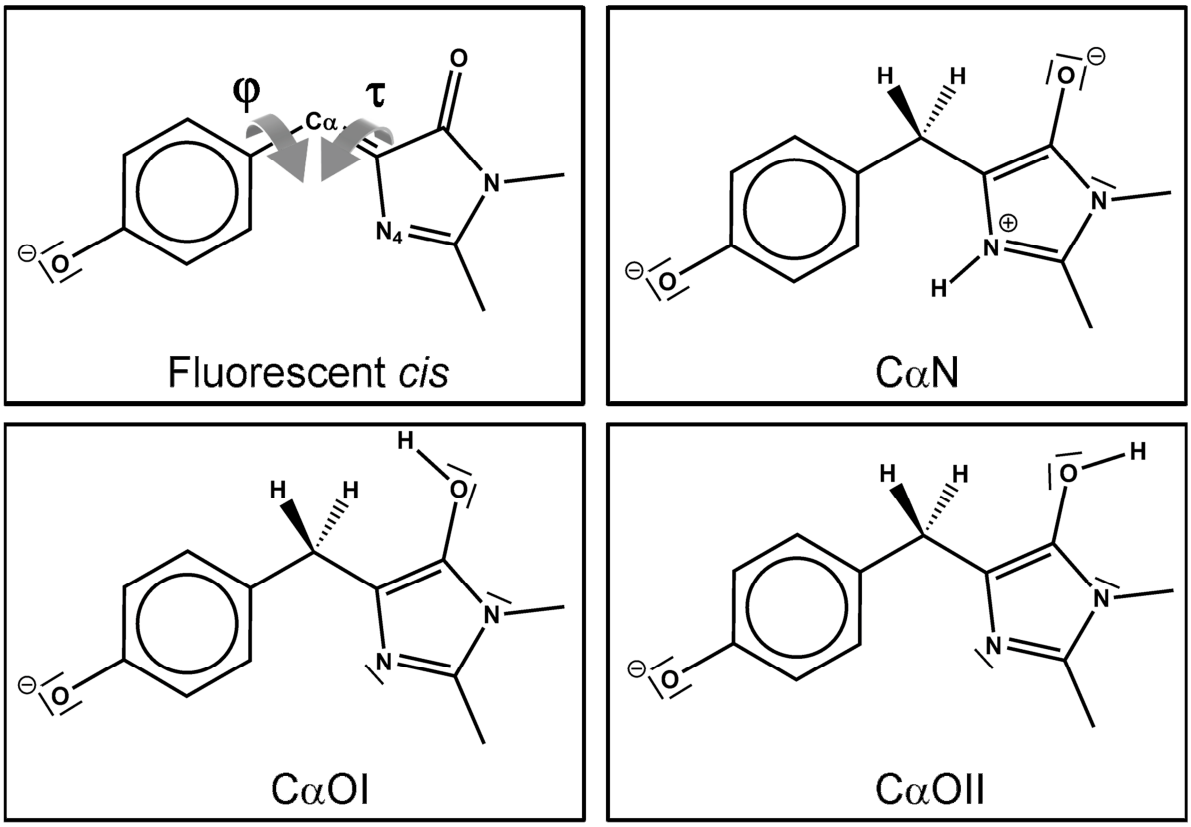

Figure S10. Lewis representation of the different chemical structures considered in this work. CαN, CαOI, CαOII describe reduced forms of the chromophore and differ by the two hydrogenated sites.

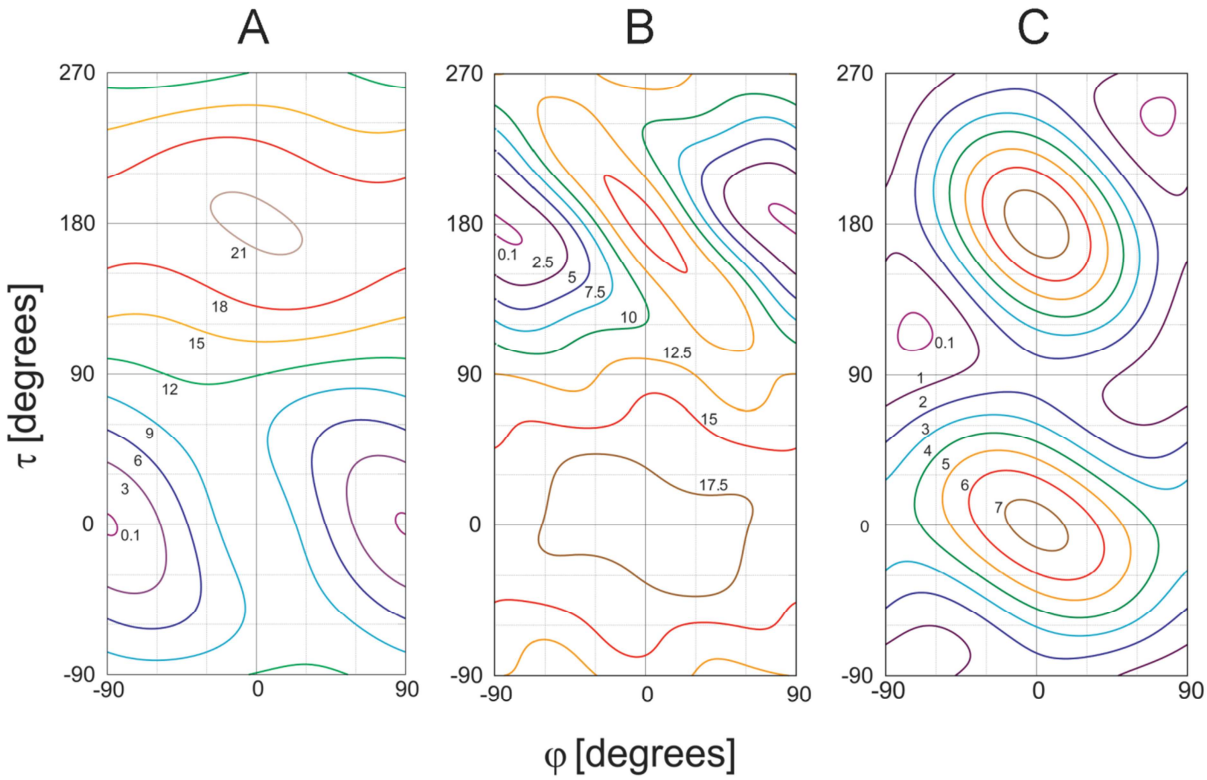

Figure S11. Potential energy surfaces (PES) for the different reduced forms of the chromophore. (A) CαN, (B) CαOI, (C) CαOII. Energies in kcal/mol.

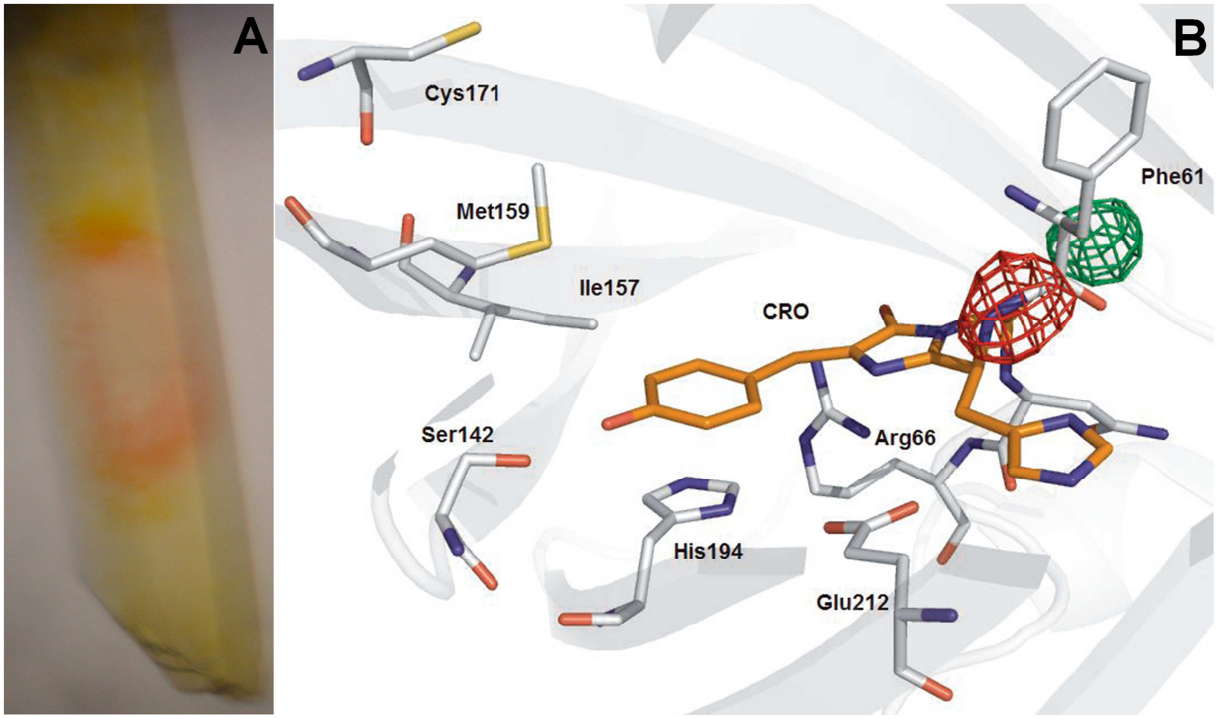

Figure S12. A: Picture of the photobleached IrisFP crystal used for X-ray data collection. Due to the larger 405 nm laser beamsize as compared to the 488 nm laser a volume peripheral to the photofatigued region underwent green-to-red photoconversion. B: $F_{calc,red}$-$F_{calc,green}$ map (± 9 σ) upon photoconversion in IrisFP: the difference density features are localized on the Phe61-His62 linkage.

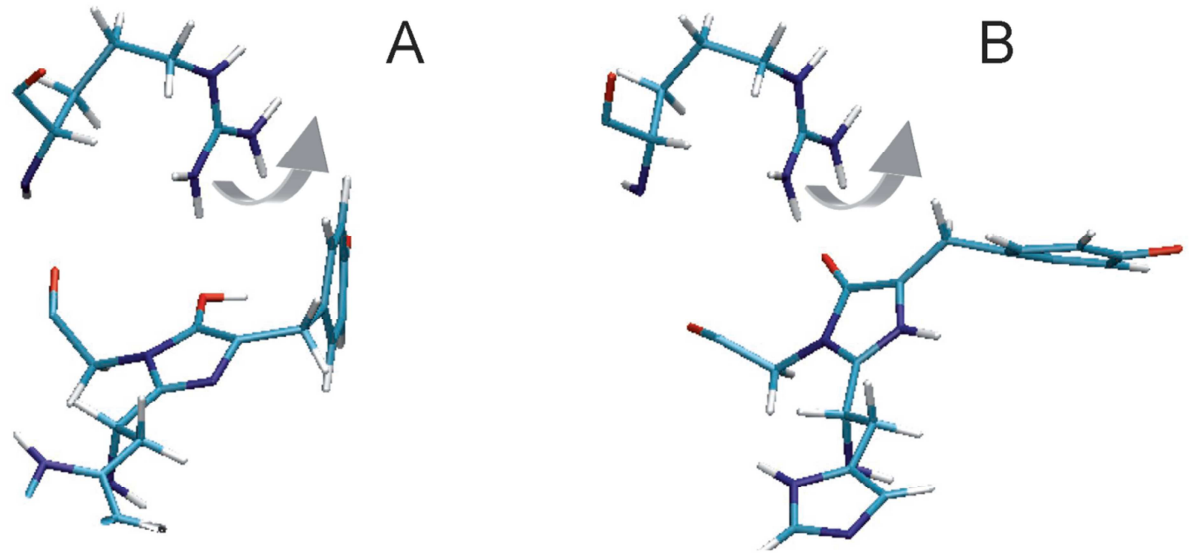

Figure S13. Snapshots extracted from molecular dynamics simulations, showing the 3D organization of the chromophore and Arg66.
(A) During CαOI simulation: τ=150° and φ=-80°. (B) During CαN simulation: τ=28° and φ=-85°. The arrow indicates the type of movement that the Arg66 side chain would undergo to reach its position in the high-intensity-photobleached structure. The phenolate hinders this movement in (A) but not in (B).

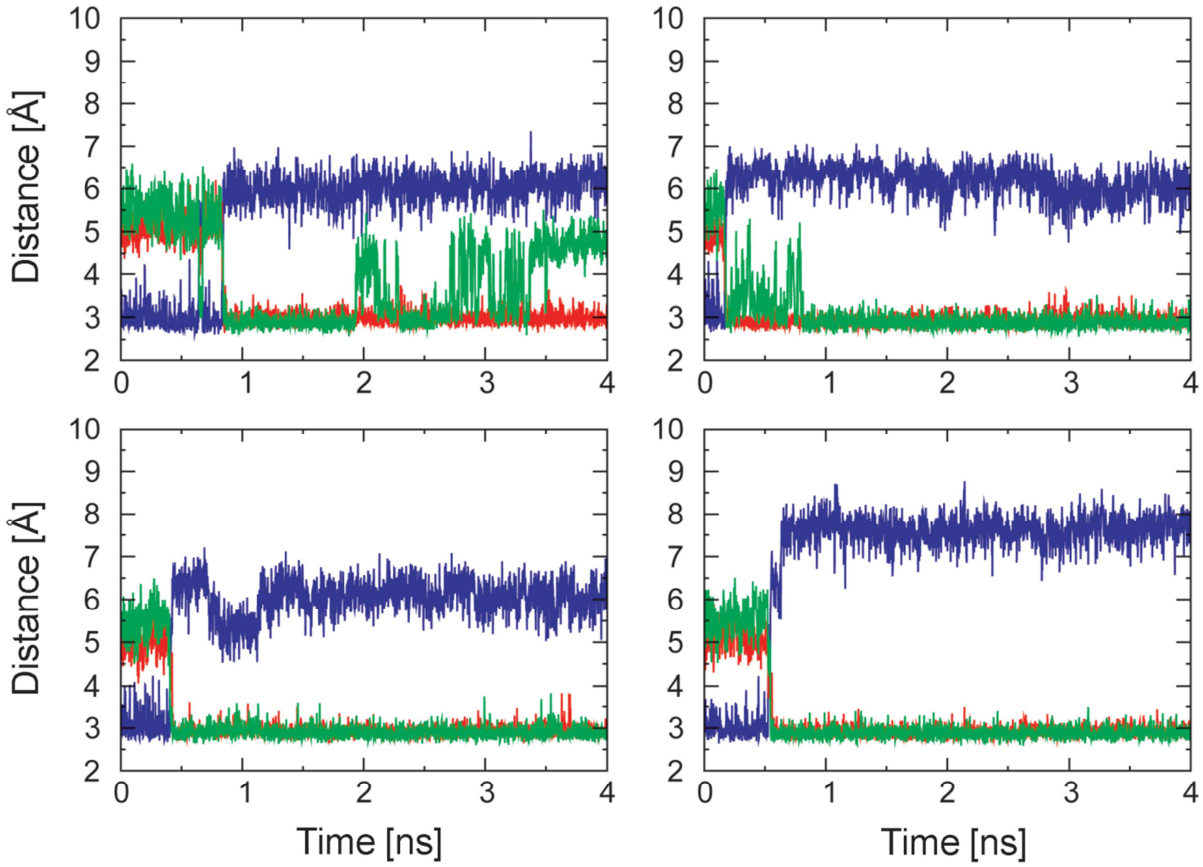

Figure S14. Characteristic distances of the H-bond network between Arg66, Glu144, His194 and Ser142, as a function of time in the four CαN simulation runs. Blue: His194(NE2)-Glu144, Red: His194(ND1)-Arg66, Green: His194(NE2)-Ser142.

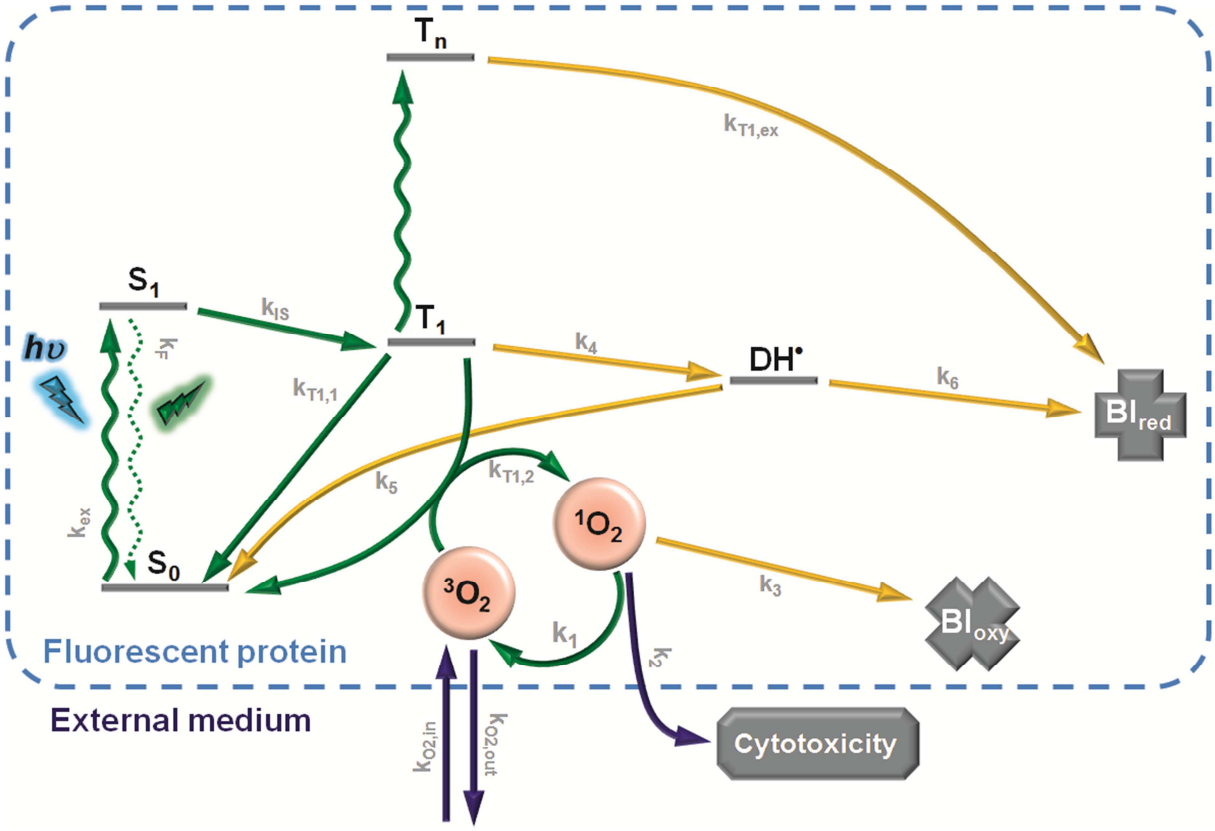

Figure S15. Putative kinetic model representative of a two-regime photobleaching in IrisFP. Description of the rate constants is provided in the SI text. Yellow arrows represent chemical steps involving e.g. electron/proton transfer or sulfoxidation reactions. Blue arrows represent entry/exit of oxygen species.

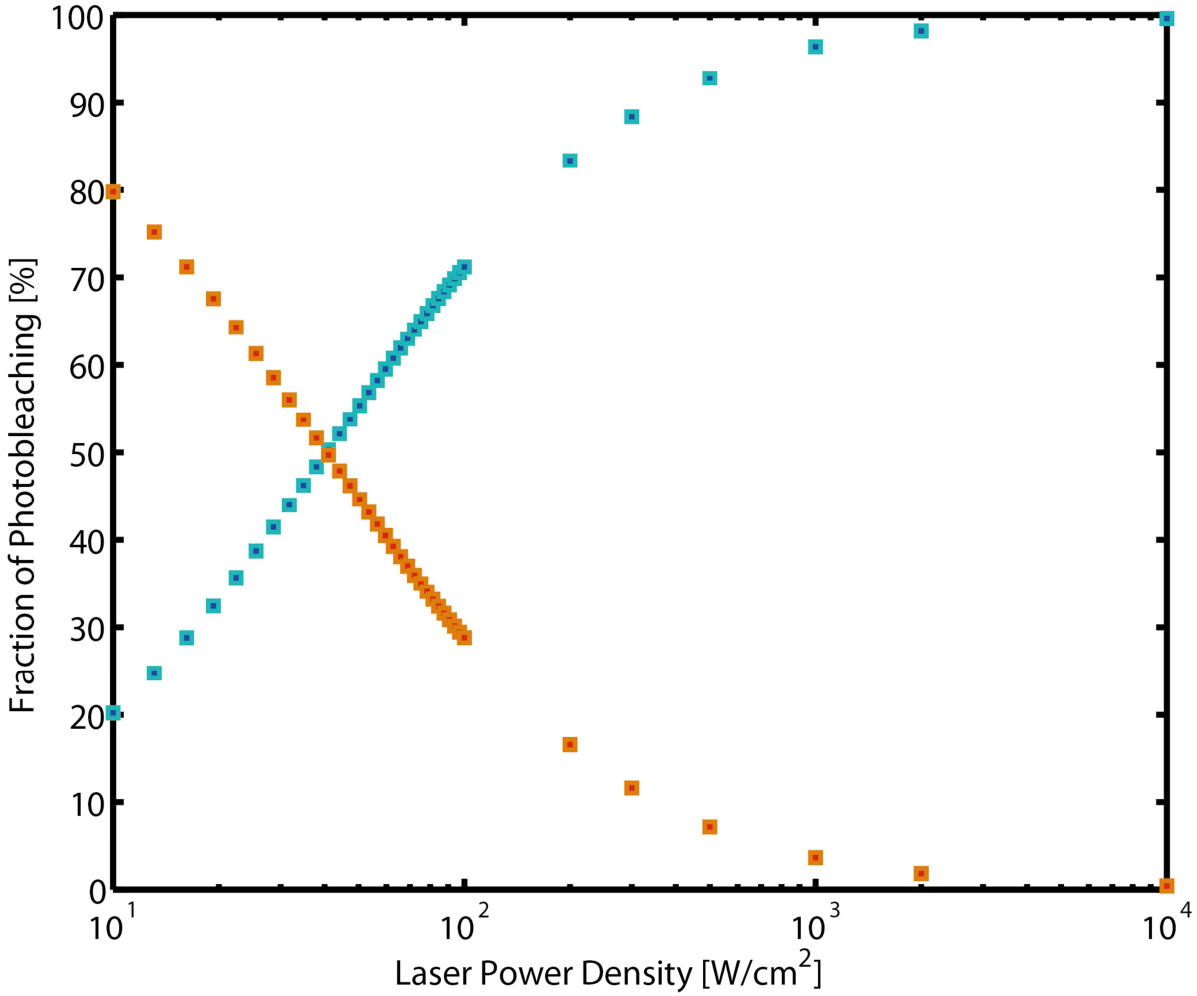

Figure S16. Power-dependence simulation of the different bleaching pathways. The fractions of photobleached protein by the respective pathways Bl_{red} (blue squares) and Bl_{oxy} (red squares) are calculated as a function of excitation power density upon illumination for a time chosen so that 15% of molecules are bleached. Rate constants described in Figure S15 were chosen as: $k_F=0.33\times10^9\ s^{-1}$, $k_{ex}=5\text{-}50\times10^3\ s^{-1}$, $k_{T1,ex}=0.15\times k_{ex}$, $k_{IS}=0.3\times10^6\ s^{-1}$, $k_1=4.0\times10^3\ s^{-1}$, $k_2=3.9\times10^6\ s^{-1}$, $k_3=1.2\times10^5\ s^{-1}$, $k_{T1,1}=5.0\times10^3\ s^{-1}$, $k_{T1,2}=1.2\times10^6\ Mol^{-1}s^{-1}$, $k_4=3.0\times10^4\ s^{-1}$, $k_5=1.0\times10^4\ s^{-1}$, $k_6=1.0\times10^1\ s^{-1}$, $k_{O2,in}=5.0\times10^7\ Mol^{-1}s^{-1}$, $k_{O2,out}=1.0\times10^5\ s^{-1}$ with $[O_2]_{medium}=200\ \mu M$.

Table S1. Crystallographic data collection and refinement statistics.

	High-intensity photobleaching	**X-ray-induced photobleaching**	**Low-intensity photobleaching**
PDB entry	4LJB	4LJC	4LJD
Data collection			
Beamline	ID14-2	ID29	PXII3
Wavelength, Å	0.933	0.997	0.999
Space group	$P\ 2_12_12_1$	$P\ 2_12_12_1$	$P\ 2_12_12_1$
Cell dimensions			
a, Å	86.09	86.64	85.99
b, Å	96.41	96.81	96.53
c, Å	140.03	140.69	140.19
Resolution, Å	47.32-1.9 (2.0-1.9)	48.41-1.86 (1.96-1.86)	47.34-2.5 (2.64-2.5)
$*R_{sym}$, %	6.8 (42.2)	6.2 (42.5)	7.5 (49.4)
Mean $I/\sigma(I)$	11.4 (3.2)	10.4 (2.5)	11.8 (2.7)
Completeness, %	99.2 (99.2)	99.3 (98.6)	97.8 (97.5)
Redundancy	4.2 (4.1)	3.3 (3.2)	3.4 (3.5)
No. of unique reflections	91193 (13214)	99096 (14169)	40095 (5752)
Wilson B factor, $Å^2$	34.9	24.8	55.6
Refinement			
# R_{work}/R_{free}	0.34/0.38	0.20/0.24	0.20/0.25
Average B factor, ($Å^2$)	27.9	27.0	29.0
Rmsd			
Bond length, (Å)	0.009	0.012	0.006
Bond angles, (°)	1.52	1.63	0.93
Ramachandran statistics (%)			
Favored	99.4	100	99.1
Allowed	0.6	0	0.9
Outliers	0	0	0

$*R_{sym} = \Sigma j \Sigma h |I_{h,j} - \langle Ih \rangle| / \Sigma j \Sigma h\ I_{h,j}$

$R_{work} = \Sigma h |F_{obs} - F_{cal}| / \Sigma h F_{obs,}$ R_{free} is calculated with a small fraction (5 %) of reflections chosen to be part of a test group.

Values in parentheses refer to the highest resolution shell.

Table S2. Mass spectrometry analysis of IrisFP decarboxylation.

	Decarboxylation (E212)
#Native IrisFP	0%
#Low energy solution	3.4%
*Low energy solution (anaerobic)	18.8%
¤High energy *in crystallo*	26%

#,*,¤ : Different digestion times used. (Due to the amount of sample necessary for mass-spectrometry analysis, high-energy experiments in the solution state (requiring highly focused laser beams) could not be successfully conducted.)

Table S3. Distances in the crystallographic structures (chain A).

	X- ray bleached structure	**High-intensity photo-bleached structure**
Glu144(OE1)-His194(NE2)	**2.9**	5.8
Glu144(OE1)-Arg66(NE)	3.3	**3.0**
Arg66(NH1)-CRO(O)	**3.2**	6.4
Arg66(NH2)-CRO(O)	**2.9**	7.2
Arg66(NH1)-His194(ND1)	5.4	**3.1**
Arg66(NH1)-Glu144(OE1)	3.8	**2.8**
His194(NE2)-Ser142(OG)	5.9	**2.9**

CRO(O) : oxygen atom of the imidazolinone ring of the chromophore. Bold characters: distances in qualitative agreement with the existence of a hydrogen bond. Distances in (Å)

Table S4. Molecular dynamics results and crystallographic structures.

	Switching between Arg66 and His194?	**Calculated switching time [ps]**	**τ [°]**	**φ [°]**
MD simulations on the chemical structures of the chromophore				
Cis (planar)	Yes	10	-4 (6)	-4 (6)
CαN	Yes	830	30 (15)	-85 (11)
	Yes	170	28 (15)	-85 (11)
	Yes	410	22 (14)	-85 (11)
	Yes	550	22 (16)	-85 (11)
CαOI	No	-	173 (9)	-75 (8)
	No	-	166 (8)	-71 (9)
	No	-	167 (8)	-77 (8)
CαOII	No	-	150 (8)	-60 (9)
	No	-	142 (8)	-60 (10)
	Yes	5	127 (12)	-69 (9)
Crystallographic structures				
X-ray bleached structure	No	-	[25,33]	[-41,-14]
High-intensity photo-bleached structure	Yes	ND	[4,43]	[-48,-12]

Numbers in parenthesis are the standard deviations in the MD simulations. The different switching times and dihedral angles values report results obtained for the different MD simulation runs. For crystallographic structures the interval covered by the values taken in chains A, B, C and D is given.

Abstract of article 2

Based on our previous results on the IrisFP photobleaching mechanism, we have identified that Glu212 is importantly involved in the high-intensity illumination photobleaching pathway and Met159 is importantly involved in the low-intensity illumination photobleaching pathway. Therefore, thanks to Xavier HENRY (Pneumo lab, IBS), we obtained IrisFP-E212Q and IrisFP-M159A mutants with the intent to improve the resistance against photofatigue under high- or low-intensity illumination, respectively. It is well-known that Glu212 has a very important role during the chromophore maturation. During the dehydration step, the carboxyl group of this Glutamate serves as a proton donor to the hydroxyl leaving group. Replacing Glu212 by Gln hindered chromophore maturation, leaving us too little protein to perform complicated experiment. This phenomenon was already observed before in Hydrozoan EGFP (Sniegowski et al., 2005). Therefore we turned our focus to the IrisFP-M159A mutant and investigated it. We transformed plasmidic DNA into *E.coli* cells for expression and then we were able to purify the IrisFP-M159A protein. The native crystallographic structure was resolved; photophysical characterization and comparative photofatigue experiments to its parent protein *in vitro* and *in vivo* were performed.

As expected, the IrisFP-M159A mutant displays an enhanced photoresistance under low-intensity illumination under various conditions: in solution, in PVA gel, in fixed and live *E.coli* cells. This enhanced photoresistance by the single mutation of Met159 confirms our finding in the previous paper that under low-intensity illumination, the sulfoxidation of nearby sulfur-containing Met159 is the predominant reason of photobleaching.

The same experiments were also carried out in PVA gel and in *E.coli* cells under high-intensity illumination. We also observed a photoresistance enhancement in fixed and live cells, which suggests that Met159 plays an unknown role in high-intensity illumination photobleaching. From this study, we cannot completely understand the role of Met159 under high-intensity illumination conditions. Further investigation should be carried out.

Rational Design of Enhanced Photoresistance in a Photoswitchable Fluorescent Protein

Chenxi Duan[1,2,3], Martin Byrdin[1,2,3], Mariam El Kathib [1,2,3], Xavier Henry[1,2,3], Virgile Adam[*,1,2,3] and Dominique Bourgeois[*,1,2,3]

[1]*Univ. Grenoble Alpes, IBS, F-38044 Grenoble, France,* [2] *CNRS, IBS, F-38044 Grenoble, France,*

[3]*CEA, IBS, F-38044 Grenoble, France*

* E-mail Addresses of corresponding authors:

dominique.bourgeois@ibs.fr

virgile.adam@ibs.fr

ABSTRACT: Fluorescent proteins are particularly susceptible to photobleaching, the permanent loss of fluorescence emission resulting from photodestruction of the chromophore. In the case of Reversibly Switchable Fluorescent Proteins (RSFPs), which can be switched back and forth between a non-fluorescent and a fluorescent state, the achievable number of switching cycles is limited by photobleaching, a process known as photofatigue. Photofatigue has become a crucial limitation in a number of advanced applications based on repeated photoswitching of RSFPs, notably in the field of super-resolution fluorescence microscopy. Here, based on our previous structural investigation of photobleaching mechanisms in IrisFP, an RSFP also capable of green-to-red photoconversion, we present the rational design of a single-mutant IrisFP-M159A that displays considerably enhanced photostability. The results suggest that, under moderate illumination intensities, photobleaching of IrisFP-like Anthozoan fluorescent proteins such as EosFP, Dendra or Dronpa derivatives is mainly driven by an oxygen-dependent mechanism resulting in the irreversible sulfoxidation of methionine 159. The photofatigue decay profiles of IrisFP and its photoresistant mutant IrisFP-M159A were investigated in different experimental conditions, *in vitro* and *in cellulo*. Although the performance of the mutant was found to be always superior, the results showed switching behaviors strongly dependent on the nanoenvironment. Thus, in general, assessment of photostability and switching properties of RSFPs should be carried out in real experimental conditions.

1. Introduction

Fluorescent proteins (FPs) have become essential tools in fluorescence imaging. PhotoTransformable Fluorescent Proteins (PTFPs) constitute an important subset of the FP family, displaying specific photophysical properties such as photoactivation, photoconversion and photoswitching. Because their fluorescence states are controllable by light, PTFPs have largely contributed to revolutionize the field of fluorescence imaging in recent years [1,2,3]. Amongst PTFPs, Reversibly Switchable Fluorescent Proteins (RSFPs) [4] offer the widest panel of applications. RSFPs can be switched back and forth between a fluorescent and a nonfluorescent state, which has recently led to the development of a number of smart methods including reversible data biostorage [5,6], photochromic FRET [7] and a variety of nanoscopy approaches. Amongst the latter, photochromic

Stochastic Optical Fluctuation Imaging (pcSOFI) [8], Nonlinear Structured Illumination Microscopy (NSIM) [9] and REversible Saturable Optical Linear Fluorescence Transitions (RESOLFT) [10] critically rely on the ability of the RSFPs to perform a high number of switching cycles. For example, in RESOLFT nanoscopy, a confocal setup is used and at each scanner position, a donut-shaped beam with a central zero intensity is applied to switch off the RSFP labels at the periphery of the Point Spread Function (PSF). A probe beam is then applied to readout the fluorescence from the labels that are still in their on-state at the center of the PSF, followed by a reset beam to restore the on-state over the entire PSF. To achieve a high spatial resolution, small laser-scanning steps are chosen and a given RSFP is thus submitted to many photoswitching cycles (typically ~100 to achieve a spatial resolution of 1/10 of the PSF width in both X and Y dimensions), requiring a strong resistance to photofatigue in addition to other key parameters such as a high fluorescence brightness and a high switching contrast.

Continued engineering efforts have been dedicated to the development of RSFPs with improved photophysical properties [1,3,4]. Structural views of the chromophore isomerization based switching mechanism have facilitated the rational design of RSFPs switching at various rates [11,12,13]. In contrast, the lack of a precise understanding of photobleaching mechanisms has only allowed the engineering of photoresistant variants by directed-evolution approaches [13,14]. Nonetheless, the development of hydrozoan RSFPs based on EGFP and EYFP has resulted in fatigue-resistant switchers such as rsEGFP [6] and Dreiklang [15] and recently rsEGFP2 [16] has been shown to display high photostability and fast switching speed, thus largely increasing the potential of RESOLFT nanoscopy.

Photobleaching in fluorescent proteins is caused by the irreversible photodestruction of the chromophore or alteration of neighboring residues. However, the underlying photochemical mechanisms remain incompletely understood. A recent study of IrisFP [17], a tetrameric RSFP of Anthozoan origin, showed that two completely different photobleaching mechanisms can happen depending only on the intensity of the excitation light [18]. IrisFP is a single mutant of EosFP (EosFP-F173S), is both switchable and photoconvertible, and presents high sequence identity and structural similarity to well-known PTFPs such as mEos2, Dendra2 or Dronpa. Under relatively high-intensity illumination conditions (> 0.1 kW/cm², typical of single molecule localization based nanoscopy), photobleaching of IrisFP is caused by decarboxylation of the strictly conserved Glu212 (IrisFP numbering) coupled to an sp^2-to-sp^3 hybridization change of the central carbon atom of the chromophore methylene bridge and an extensive rearrangement of the H-bond network surrounding the chromophore. In contrast, under low-intensity illumination conditions (~0.01 kW/cm², typical of standard widefield fluorescence imaging), Met159, a highly conserved residue in anthozoa PTFPs located next to the chromophore hydroxybenzylidene moiety, undergoes a sulfoxidation reaction that results in trapping the chromophore in a permanent nonfluorescent protonated state. Sulfoxidation of Met159 follows from the production of singlet oxygen within the chromophore pocket due to triplet-

triplet reaction of the excited chromophore with molecular oxygen. Thus, Met159 was identified as a key residue in IrisFP photobleaching under oxygenated conditions.

Here, we replaced Met159 by Alanine in IrisFP in order to increase photofatigue resistance at least under low intensity illumination condition. A structural view of IrisFP-M159A is presented and photofatigue experiments in solution, in polyvinyl-alcohol (PVA) gels and in bacterial cells were performed at low and high illumination intensities to compare the achieved performance of the designed variant with that of its parent protein.

2. Materials and Methods

Expression and purification

The M159A mutation in IrisFP/pQE32 was introduced by site-directed mutagenesis with oligonucleotide primers purchased from Invitrogen (Life Technologies, Saint Aubin, France). *E.coli* BL21(DE3) bacteria were transformed by plasmidic DNA for expression of both parent and mutant His-tagged proteins. Bacterial cultures were grown at 37°C and the overexpression was induced by adding 0.1 mM IPTG once the optical density at 600 nm reached 0.6. Cultures were then incubated at 4°C for 7 days. Cells were harvested by centrifugation and resuspended pellets (150 mM NaCl/50 mM HEPES pH 7.5) were lysed by sonication. Supernatants containing crude protein extracts were purified using a pre-packed Talon metal affinity column (Clontech Laboratories, California, USA) followed by a HiLoad 16/60 Superdex 75 gel-filtration column (GE Healthcare, Pennsylvania, USA). Fractions were pooled and concentrated to 20 mg/ml.

Crystallization, X-ray data collection and data processing

Crystals of IrisFP-M159A were grown at 293 K by the hanging drop method, using a 1:1 ratio of concentrated protein and 2.1 M ammonium sulfate / 0.1 M Bicine (pH 8.1). The rod-shaped yellowish colored crystals dimensioned $50 \times 100 \times 500\ \mu m^3$. X-ray data were collected at 100 K at the European Synchrotron Radiation Facility (ESRF, Grenoble) on the beamline ID14-4 (X-ray wavelength λ = 0.939 Å) equipped with an ADSC Q315r detector. Data sets were integrated and scaled at 2.0 Å resolution with XDS [19]. The crystal structure of IrisFP-M159A (PDB ID: 4R6B) was solved by molecular replacement with Molrep [20], using the coordinates of one monomer of IrisFP (PDB ID: 2VVH) as a search model. Refinement was made with Phenix [21]. Data collection and model refinement statistics are compiled in Table 2. Figure 2 was prepared with PyMOL [22]. The structure of the protein in its switched-off state could not be obtained due to compromised diffraction after laser illumination of crystals.

Photophysical characterization in solution

Purified proteins were diluted in Tris buffer (pH 8.5) to ensure that chromophores were completely in the anionic state and concentrations were adjusted to an optical density OD = 0.1 at 488 nm. Samples were placed in a 10 mm optical path quartz cell with blackened walls and two opposite 3 x 5 mm^2 clear windows (Starna, Pfungstadt, Germany). The cell was filled to the upper limit of the window, closed with a plastic stopper and placed between optical fibers, coupled to excitation lasers on one side and, via a 500 nm cutoff filter (EdgeBasic, Semrock), to a CCD-based spectrometer (AvaSpec-ULS2048L, Avantes, Eerbeek, the Netherlands) on the other side. The switching-off laser (488 nm, CrystaLaser, Reno, USA) also served for readout and thus was on permanently, whereas the activation laser (405 nm, CrystaLaser, Reno, USA) was only on during periods of on-switching. High-resolution photoswitching cycles were recorded by placing a microlens array (Thorlabs) between the fiber output and the quartz cuvette entry window so as to produce a fully homogenized excitation beam. Data were recorded for ~1 h with a cycle time of 10 min and an on-switching duration of 3 min. (405 nm: 1.3 mW/cm², 488 nm 8 mW/cm²). For photofatigue experiments, sufficient laser power densities could not be obtained with the microlens array, which thus was replaced with a collimating lens despite the loss of homogenized beam profiles. Photofatigue was studied for >18 h with a cycle time of 20 s and an on-switching duration of 3 s. (405 nm: 0.03 W/cm², 488 nm 0.04 W/cm²). Laser powers were measured behind the exit window of the water-filled cell.

Microscopy setup

Photobleaching experiments were performed on an inverted microscope (IX-81, Olympus) with a 100× oil immersion objective equipped with a NPS nosepiece (Olympus). Samples were illuminated by circularly polarized 488-nm (Spectra-Physics, Santa Clara, USA) and 405-nm (CrystaLaser, Reno, USA) gaussian-shaped laser beams with FWHM of ~20 μm at the focal plane. For low-intensity photofatigue experiments, continuous illumination at 488 nm (40 W/cm²) and alternating illumination at 405 nm (2.3 W/cm²) were performed with 15-ms frames recorded every 75 ms. Each cycle was 3-s long (off-to-on: 0.3 s, on-to-off 2.7 s). Each experiment consisted of 1000 switching cycles. For high-intensity photofatigue experiments, continuous illumination at 488 nm (400 W/cm²) and alternating illumination at 405 nm (10.8 W/cm²) were performed with 5-ms frames recorded every 25 ms. Each cycle was 250 ms long (off-to-on: 25 ms, on-to-off: 225 ms). Each experiment consisted of 600 switching cycles. Proper synchronization of laser timing and frame acquisition by the EMCCD camera (Evolve 512, Roper, USA) was realized with Labview.

Photofatigue in PVA gel

Purified proteins were diluted to micromolar concentration in a solution of 1% PVA (Mowiol 4-88, Sigma-Aldrich) in Tris buffer at pH 8.5. Glass slides were coated with a solution of PVA containing the protein of interest to form a thin film, which was let to dry for 1-4 hours. The dried matrix ensured an efficient embedding of the proteins, preventing their diffusion.

Photofatigue in cellulo

E.coli BL21(DE3) bacteria were transformed by plasmidic DNA coding for each of the two proteins and bacterial cultures were grown at 37°C until reaching an optical density at 600 nm between 0.4 and 0.8. For fixed-cell experiments, three consecutive centrifugations were performed. Cells were first resuspended in PBS buffer and then in paraformaldehyde (%4 w/v) for 30 min for fixation. Finally, paraformaldehyde was washed by the last centrifugation and cells were resuspended in PBS. The fixed cells were immobilized by incubating the bacterial suspension during 1h at room temperature on chitosan-coated glass slides. For live-cell experiments, after a centrifugation at 150 rpm, cells were resuspended in 80 µL LB medium. 10 µL of the cell suspension were spread on a freshly prepared 1-mm thick agarose pad (2 % w/v agarose / PBS pH 7.5) on a slide and incubated for 10 mn at room temperature. A cover slide was then placed over the pad and sealed before the measurements.

Fluorescence quantum yield and pKa measurements

Excitation and emission spectra were recorded with a Synergy H4 Hybrid microplate reader (Bio-Tek, Winooski, USA). The fluorescence quantum yield of IrisFP-M159A was calculated by the method described by Williams *et al.* [23]

Extraction of photoswitching parameters

Image processing was achieved with ImageJ (Rasband, W.S., ImageJ, U. S. National Institutes of Health, Bethesda, Maryland, USA, http://imagej.nih.gov/ij/, 1997-2014). Background subtraction was achieved in the following manner: In PVA the measured EMCCD-offset of 500 counts was subtracted; for *in-cellulo* experiments, non-transformed cells were mixed with transformed cells so that a correct background corresponding to the EMCCD offset plus the autofluorescence signals from the bacteria and the LB medium (for live cells) could be substracted. To obtain photofatigue profiles, the average fluorescence signal inside a region of interest contouring a chosen transformed cell was computed and the average fluorescence signal inside a region of interest contouring a nearby non-transformed cell was subtracted, using ImageJ.

On- and off-switching quantum yields were obtained by fitting individual switching cycles with a simple kinetic model involving one-to-one reversible conversion between the on and off state. However, in the case of PVA and fixed cells, as molecules may not be excited at the same rate in a rigid medium, the model allowed for a variable anisotropic distribution of the chromophore dipoles. Also, the fitting model was designed to take into account the limited time-resolution afforded by the used integrating detectors. Model fitting and further processing of the photofatigue decay profiles was done in Matlab (see Supporting Information).

3. Results

Photophysical and structural characterization of IrisFP-M159A

To test the hypothesis according to which photobleaching of IrisFP under moderate illumination intensity mainly results from sulfoxidation of Met159, we produced the single mutant Met159Ala (IrisFP-M159A) with the expectation that resistance to photofatigue should be enhanced. Mutation of Met159 in several RSFPs has previously been shown to affect various photophysical properties, such as the off- and on-switching rates in Dronpa-2 (Met159Thr) and Dronpa-3 (Met159Ala) [12,24], blue shifting of excitation/emission spectra in bsDronpa (Met159Cys) [25], or reversal of switching mode in Padron (Met159Tyr) [25]. Thus, to evaluate such possible effects in addition to fatigue resistance, we carried out an extensive biophysical characterization of IrisFP-M159A and compared the results with IrisFP. IrisFP-M159A has its excitation and emission maxima at 484 nm and 513 nm (Figure 1), slightly blue shifted by 4 nm and 3 nm as compared to IrisFP [17], respectively, and giving rise to a 29 nm Stokes shift (Table 1). IrisFP-M159A shows a 12 % higher extinction coefficient than its parent at physiological pH (pH 7.3), but a significantly reduced fluorescence quantum yield, resulting in a decreased brightness by a factor of ~2.4. At physiological pH, no neutral absorbance peak around 400 nm is observed, suggesting a low chromophore pKa. Indeed, a pH titration of the absorption bands of IrisFP-M159A revealed a pKa of 4.7, significantly lower than IrisFP (pKa=5.7) (Figure 1).

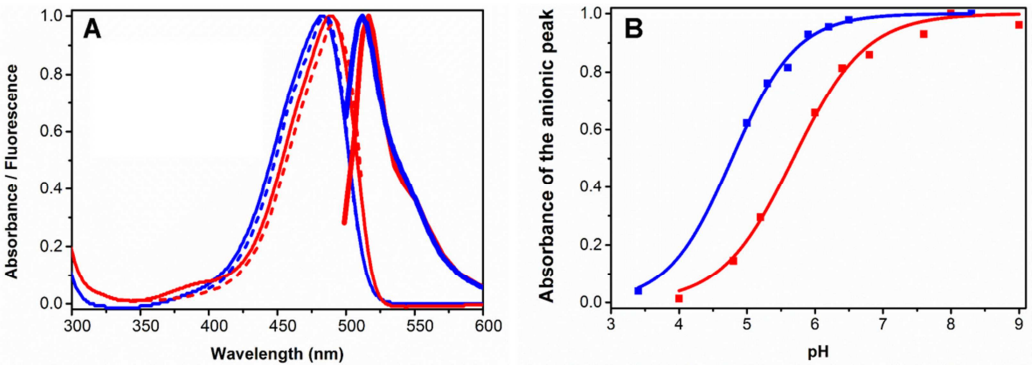

Figure 1. The mutation M159A in IrisFP only moderately affects its spectra but acidifies its chomophore. (A) Absorption (solid), excitation (dashes) and emission (bold) spectra of IrisFP (red) and IrisFP-M159A (blue) at pH 7.3. Absorption and excitation maxima peak at 488 nm for IrisFP and 484 nm for IrisFP-M159A. Emission spectra show a maximum at 516 and 513 nm for IrisFP and IrisFP-M159, respectively. (B) Titration curves of IrisFP (red) and IrisFP-M159A (blue), demonstrating a clear acidification of the mutant's chromophore. Measurement points (squares) are fitted by the Henderson-Hasselbalch equation (lines), which yields pKa values of 5.7 for IrisFP and 4.7 for IrisFP-M159A.

Table 1. Photophysical properties of IrisFP and IrisFP–M159A.

		IrisFP	**IrisFP-M159A**
On-state	Absorbance maximum [nm]	488	484
	Emission maximum [nm]	516	513
	Extinction coefficient at anionic peak (ε) [$M^{-1}.cm^{-1}$]	52200	62800
	Fluorescence quantum yield	0.43	0.18
	Brightness (relative to EGFP)	0.68	0.28
	pKa	5.7	4.7
Off-state	Absorption maximum [nm]	390	390
	Extinction coefficient at neutral peak (ε) [$M^{-1}.cm^{-1}$]	27342	29363

The overall crystallographic structure of the IrisFP-M159A mutant, obtained at 2.0 Å resolution, is nearly identical to that of the parent protein, with an rms deviation over all C_α atoms of only 0.174 Å. The interface between monomers is entirely preserved so that IrisFP-M159A is, as IrisFP, an obligate tetramer. Inspection of the chromophore and its surrounding residues (Figure 2) shows only minimal rearrangements. Because alanine has a side chain much shorter than that of methionine, a water molecule (Wat2) is found to fill up the cavity created by mutagenesis. Together with Wat2, two water molecules already present in the IrisFP structure (Wat1 and Wat3) are slightly moved to accommodate a new H-bond chain linking the phenolate moiety of the chromophore to Ser173. Ser173 is slightly shifted towards Ala159.

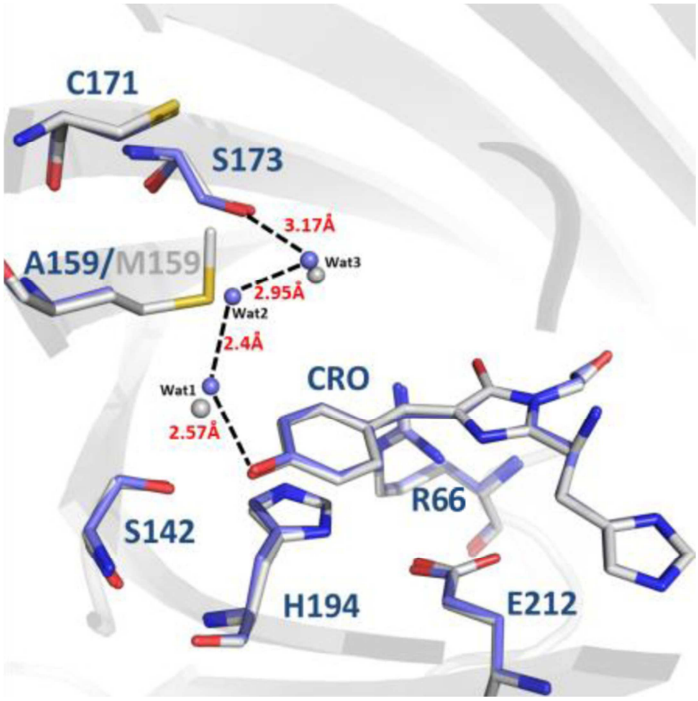

Figure 2. Crystallographic structure of IrisFP-M159A (light blue) overlaid with that of IrisFP (gray). The chromophore and neighboring residues are shown in stick mode, water molecules are represented as balls, and dashed lines represent the newly formed H-bonds chain between the phenolate moiety of the chromophore and Ser173.

Despite the newly established hydrogen bond network, the absence of Met159 likely results in a reduced rigidity of the chromophore environment promoting non-radiative de-excitation pathways and consistent with the observation of a lower fluorescence quantum yield in the mutant. Moreover, in the absence of Met159, the electrostatic environment of the chromophore hydroxybenzylidene moiety is altered, which likely accounts for the reduced pKa and slightly blue-shifted excitation spectrum.

Table 2. Crystallographic data collection and refinement statistics.

PDB entry	4R6B
Data collection	
Beamline	ID14-4
Wavelength, Å	0.939
Space group	P $2_12_12_1$
Cell dimensions	
a, Å	86.70
b, Å	96.35
c, Å	139.43
Resolution, Å	46.47-2.00 (2.11-2.0)
*R_{sym}, %	9.0 (45.1)
Mean $I/\sigma(I)$	10.0 (2.7)
Completeness, %	100.0 (100.0)
Redundancy	4.9 (5.0)
No. of unique reflections	79546 (11489)
Wilson B factor, $Å^2$	22.4
Refinement	
# R_{work}/R_{free}	0.20/0.23
Average B factor, ($Å^2$)	25
Rmsd	
Bond length, (Å)	0.011
Bond angles, (°)	1.18
Ramachandran statistics (%)	
Favored	93.9
Allowed	6.1
Outliers	0

*$R_{sym} = \Sigma j \Sigma h |I_{h,j} - \langle Ih \rangle| / \Sigma j \Sigma h\ I_{h,j}$

$R_{work} = \Sigma h |F_{obs} - F_{cal}| / \Sigma h F_{obs,}$ R_{free} is calculated with a small fraction (5 %) of reflections chosen to be part of a test group.

Values in parentheses refer to the highest resolution shell.

Switching behavior and photofatigue studies in solution

A first comparative investigation of the switching behavior of IrisFP-M159A and IrisFP was performed in solution. Purified protein solutions were placed in a quartz cuvette, with concentrations adjusted to provide identical optical density at 488 nm (OD=0.1). First, a very low laser power density (6 mW/cm² at 488 nm) was applied in order to record high resolution switching kinetics over a few cycles (300 points per cycle). As its parent, IrisFP-M159A displays negative photoswitching, that is, off-switching results from illumination at the peak excitation wavelength. The extracted quantum yields for off- and on-switching, the off- and on-switching brightness (product of switching quantum yield by extinction coefficient at the switching wavelength) and the switching contrast (ratio of emitted fluorescence in the on and off states) are shown in Table 3. It is seen that the off-switching

quantum yield of IrisFP-M159A is about 4 times that of IrisFP, consistent with the idea that the larger flexibility of the mutant protein should facilitate *cis-trans* isomerization of the chromophore. The on-switching quantum yield of IrisFP-M159A, however, is about 30% lower than that of IrisFP, despite the apparent higher rate of on-switching (Figure 3). This is due to the fact that, as the 488 nm laser is kept on during on-switching to allow proper monitoring of the emitted fluorescence, the apparent rate is the sum of the actual on- and off- switching rates. For the two proteins, the switching kinetics follow an almost ideal monophasic behavior, suggesting a homogeneous population of molecules and a one-to-one switching behavior between the on-state and the off-state under these experimental conditions.

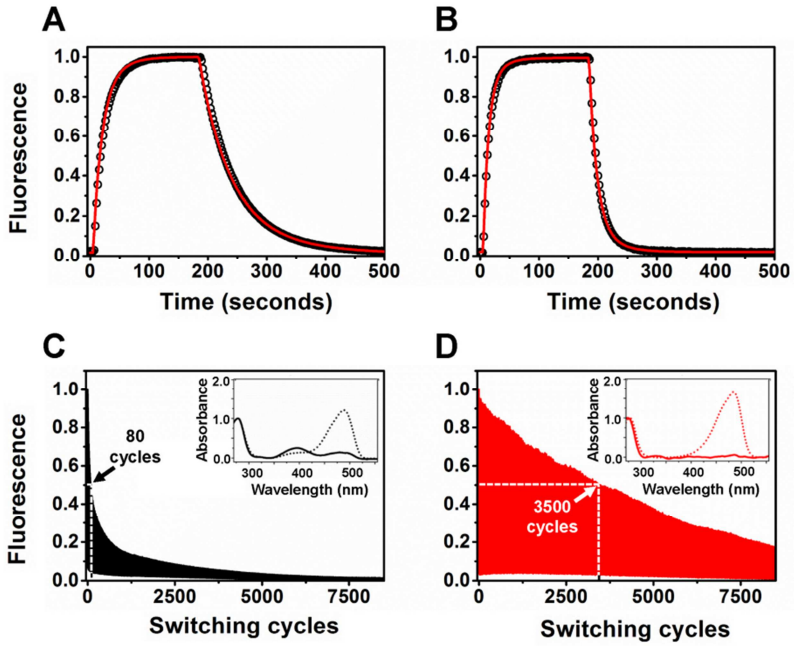

Figure 3. Photofatigue of IrisFP and IrisFP-M159A in solution. A single switching cycle is shown (black circles) for IrisFP (A) and for IrisFP-M159A (B) along with their fits (red curves). A series of such switching cycles is recorded by integrating the fluorescence signal during the exposure of IrisFP (C) and IrisFP-M159A (D) samples to alternating 488-nm (0.04 W/cm²) / 405-nm (0.03 W/cm²) laser illuminations. At such low intensities in solution IrisFP-M159A demonstrates a >40-fold improvement in the achievable number of switching cycles as compared to its parent. Insets show absorption spectra before (dashed lines) and after (solid lines) photofatigue of the samples. IrisFP presents an absorption band at ~390 nm due to chromophore protonation consecutive to sulfoxidation of Met-159, while this feature is absent in the spectrum of IrisFP-M159A.

Table 3. Photoswitching behavior in solution.

	IrisFP	**IrisFP-M159A**
On-to-off switching quantum yield	0.005	0.019
Off-to-on switching quantum yield	0.15	0.11
On-to-off switching brightness [$\Phi_{\text{On-to-off switching}} \times \varepsilon_{488}$]	261 (1)[c]	1193 (4.57)[c]
Off-to-on switching brightness [$\Phi_{\text{Off-to-on switching}} \times \varepsilon_{405}$]	4101 (1) [c]	3230 (0.78)[c]
Switching contrast [$\text{Fluorescence}_{on}/\text{Fluorescence}_{off}$] [a]	65.7	72.9
Photofatigue half decay [cycles]	80	3500
Photoresistance enhancement [b]	5.2	
Thermal recovery half-time [h]	2.5	0.5

[a] Calculated over the first halftime of the photofatigue decay
[b]Calculated from the ratio of the integrated photofatigue decays × extinction coefficients at anionic peaks taken from Table 1.
[c]Values between parentheses are normalized to IrisFP.

Photofatigue experiments were then performed on IrisFP and IrisFP-M159A, for about 8000 cycles with moderate time resolution (20 points/cycle, 0.04 W/cm² at 488 nm). The photofatigue kinetics are shown in Figure 3C and 3D. IrisFP showed a much faster photofatigue decay than the M159A mutant: its fluorescence was halved after ~80 cycles whereas it took about 3500 cycles to achieve the same decrease with the mutant. The photofatigue decay of IrisFP is clearly biphasic, which suggests the possible buildup of a long-lived dark state retarding photofatigue during the slow phase of the experiment through a shelving effect. It is important to note that the difference in the number of achievable cycles by a factor of ~43 is not representative of the true difference in photostability between the two proteins, due to the fact that IrisFP-M159A switches more rapidly. Indeed, it can be estimated by integrating the emitted fluorescence signal along the photofatigue decay curve and correcting for the difference in extinction coefficient that IrisFP-M159A is about 5.2 times more photostable than its parent protein under these experimental conditions. Furthermore, since IrisFP-M159A also has a reduced fluorescence quantum yield, its total photon budget is only ~1.8 times that of IrisFP.

Comparative absorbance spectra recorded before and after photofatigue decay of the two proteins show that, whereas a substantial increase in the neutral band peaking at around 390 nm is observed for IrisFP after photofatigue, this is not the case for the mutant, which in contrast displays a completely flat spectrum (Figure 3C, 3D, inset). We previously have shown that the increase in absorption at 390 nm by IrisFP upon photofatigue at low illumination intensity follows from sulfoxidation of Met159, trapping the chromophore in a nonfluorescent protonated state. The present data thus confirms that no such trapping occurs in IrisFP-M159A, which most likely accounts for the observed superior photofatigue resistance of this mutant.

Switching behavior and photofatigue studies in vitro and in cellulo

It is now recognized that the switching behavior of RSFPs strongly depends on both illumination and nanoenvironmental conditions [16,26]. Therefore, we next carried out photofatigue decay experiments *in vitro* and *in cellulo* at two different illumination intensities (~40 W/cm² and ~400 W/cm²), aiming at comparing the behavior of the two proteins. All results are summarized in Figure 4 and Table 4. At high illumination intensity, our EMCCD camera based setup did not provide sufficient time-resolution to follow individual switching cycles with sufficient accuracy, so that only the envelope of the fluorescence decay along the photofatigue profiles are reported. At low illumination intensity, individual switching cycles could be monitored and the available time resolution, depending on the investigated conditions (see below), was generally sufficient to achieve a coarse extraction of the on- and off-switching brightness.

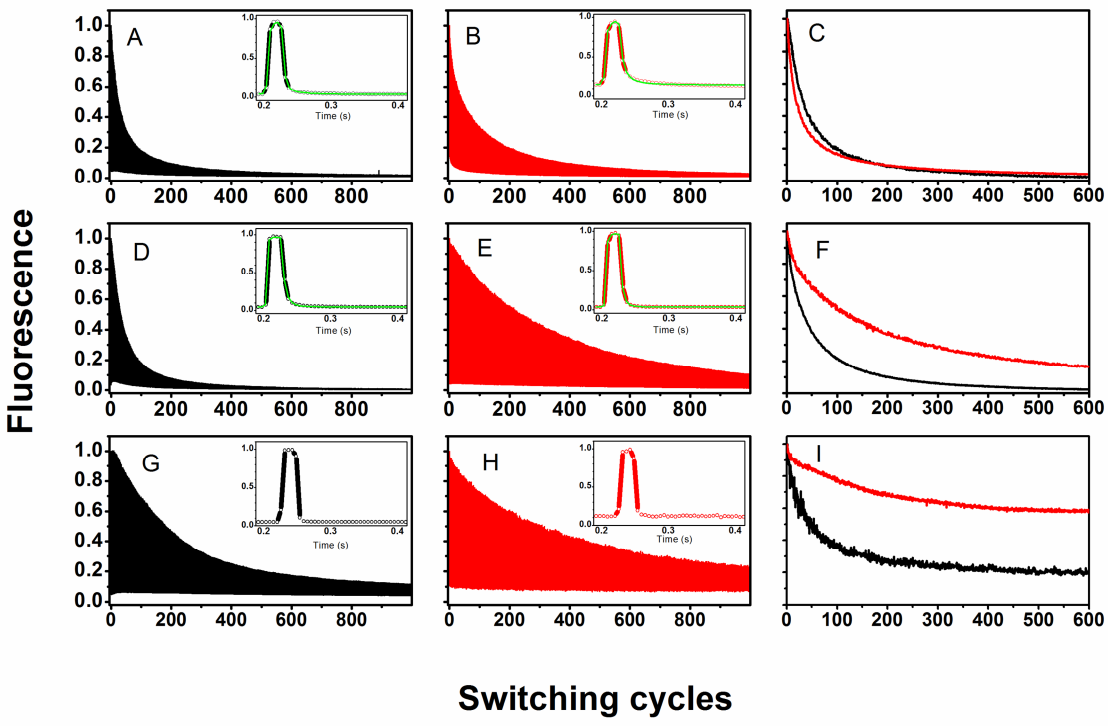

Figure 4. Photofatigue of IrisFP (black) and IrisFP-M159A (red) embedded in a PVA gel (A-C), in fixed bacteria (D-F) and in live bacteria (G-I) at low (~40 W/cm², left and central column) and high (~400 W/cm², right column) intensity 488 nm illumination. The insets show individual switching cycles. Green lines: model fits from which the switching yields reported in Table 4 were extracted.

A first set of experiments were performed in polyvinyl-alcohol (PVA) gels. Interestingly, the switching speed of both proteins appeared to be strongly reduced as compared to solution studies (Table 4). The photofatigue half decay of IrisFP was reduced by a factor of ~3 as compared to solution studies and, surprisingly, that of IrisFP-M159A was decreased by a factor of nearly 80. This finding is corroborated by the observation that the switching kinetics of the mutant was dramatically slowed down, to the point that in PVA the global behavior of the M159A mutant became relatively similar to

that of its parent. Nevertheless, a slight photoresistance enhancement by a factor of ~1.9 was still obtained with the mutant protein. Under high-intensity illumination, the two proteins also behaved similarly, with IrisFP even showing a slightly slower photofatigue decay. Of interest is the complex shape of the overall photofatigue decay profiles of the two proteins recorded under low illumination conditions. These profiles exhibit a clear biphasic decay of the fluorescence maxima and an intriguing evolution of the fluorescence minima at early time points, pointing at complex photophysical processes taking place. Overall, these data suggest that PVA strongly modifies the switching behavior of IrisFP and its mutant possibly due to reduced oxygen access, redox effect that are known to be promoted by this polymer [27,28,29], or motional restriction. In fact, although macromolecules are expected to freely tumble in the aqueous cavities within the PVA gel, we observed that individual switching cycles were best fitted with a kinetic model that assumes fixed dipole orientations of the fluorescent proteins.

Table 4. Conditions and parameters for IrisFP and M159A photofatigue experiments *in vitro* and *in cellulo*.

Matrix	Power density [a]	Protein	Off-to-on switching brightness [b] [$cm^{-1}.M^{-1}$]	On-to-off switching brightness [b] [$cm^{-1}.M^{-1}$]	Switching contrast [c]	Photo-fatigue half decay [cycles]	Photo-resistance enhance ment [d]
PVA gel	Low	IrisFP	440 (0.11)[e]	≈ 52 (0.20)[e]	18	25	1.9
		IrisFP-M159A	820 (0.20)[e]	≈ 25 (0.10)[e]	10	45	
	High	IrisFP	ND	ND	ND	31	ND
		IrisFP-M159A	ND	ND	ND	17	
Fixed cells	Low	IrisFP	1900 (0.46)[e]	≈ 36 (0.14)[e]	16	33	6.1
		IrisFP-M159A	880 (0.21)[e]	≈ 56 (0.21)[e]	22	248	
	High	IrisFP	ND	ND	ND	35	ND
		IrisFP-M159A	ND	ND	ND	115	
Live cells	Low	IrisFP[f]	≥ 1400 (0.34)[e]	≥ 52 (0.20)[e]	14	178	2.0
		IrisFP-M159A[f]	ND	ND	8	315	
	High	IrisFP	ND	ND	ND	54	ND
		IrisFP-M159A	ND	ND	ND	> 600	

[a] High corresponds to 400 W/cm^2, low corresponds to 40 W/cm^2
[b] Calculated as the product of switching quantum yield and absorption coefficient taken from Table 1
[c] Calculated over the first halftime of the photofatigue decay
[d] Calculated from the ratio of the integrated photofatigue decays × extinction coefficients taken from Table 1
[e] Values between parentheses are normalized to IrisFP in solution (Table 3)
[f] Determination of switching brightness limited by time resolution
ND: Not determined

Next, we recorded photofatigue decay profiles in fixed *E. coli* BL21(DE3) cells. Again, the switching speed of both proteins appeared to be strongly reduced as compared to solution studies. However IrisFP-M159A displayed a well behaved photofatigue decay profile under low illumination conditions and was found to exhibit a much greater number of switching cycles than its parent protein under both illumination conditions. The photoresistance enhancement of IrisFP-M159A in fixed cells

under low illumination intensity exceeds that of IrisFP by a factor of ~6.1. As in PVA, individual switching cycles were best fitted with a kinetic model assuming fixed dipole orientations of the fluorophores. This is consistent with the hypothesis that cross-linking by paraformaldehyde in fixed cells may prevent tumbling of macromolecules.

Finally, photofatigue data were recorded in live *E. coli* cells. In this case, it appeared that the switching kinetics of both proteins were too rapid to allow reliable fitting of individual cycles, suggesting that in such environment, the fluorescent protein markers adopt a behavior close to that in solution. Inspection of the switching cycles also suggests that molecules freely tumble when expressed in the cytoplasm of live *E. coli* cells. Consistent with faster switching, the achievable number of photoswitching cycles by both proteins was found higher than in PVA or fixed cells, and the photo resistance enhancement achieved by IrisFP-M159A was estimated to be ~2.0.

It is worth noting that a switching contrast much lower than in solution was observed in all tested conditions, and particularly in live cells. Such lower contrast may result from the higher laser power densities used in widefield illumination conditions, but this issue remains to be explored.

4. Discussion and Conclusion

In this work, we have shown that rational engineering of an RSFP by a single mutation leads to significantly enhanced photoresistance. As expected from our previous structural investigation [18], the M159A mutation in IrisFP increased fatigue resistance at low laser illumination intensities (< ~40 W/cm²). This is explained by the suppression of a sulfoxidation reaction that in the IrisFP parent protein results in trapping the chromophore irreversibly in a nonfluorescent protonated state. The mechanism that leads to sulfoxidation of Met159 likely involves quenching of the chromophore triplet state by oxygen, which releases highly reactive singlet oxygen within the chromophore pocket. Singlet oxygen is prone to attack any neighboring sulfur group, and thus rapidly reacts with the nearby Met159. The observed enhancement in fatigue resistance by a factor > 5 in solution reaches beyond expectations, considering that other sources of photobleaching certainly exist (e.g. destabilization of the protein scaffold by oxidation reactions involving singlet oxygen and other residues such as cysteins, tryptophans or tyrosines). Thus, the Met159 sulfoxidation pathway appears to be the major source of photobleaching in IrisFP in solution and at low illumination intensities, and this conclusion may also hold for popular phototransformable fluorescent proteins such as mEos2, Dronpa or Dendra2, which all have a methionine at position 159 located next to the chromophore. However, in PVA and in *E. coli* cells, the increase in photoresistance afforded by the M159A mutation was variable (Table 4) suggesting that the complex nanoenvironment in these samples may promote other photobleaching pathways.

The M159A mutation in IrisFP also resulted in about a 4-fold faster off-switching speed, which is similar to the effect obtained in e.g. Dronpa variants [12,24]. The combination of more rapid

switching and enhanced photoresistance yielded a considerable increase in the number of achievable on-off switching cycles, reaching a factor > 40 in solution. In PVA and in *E. coli* cells, the situation was again different: a strong decrease of the switching speed of the two proteins was noticed and the enhancement in the number of achievable switching cycles by the mutant was not so high (factors of ~2, ~7.5 and ~1.8 in PVA, fixed cells and live cells, respectively).

Under high illumination intensities (~0.4 kW/cm²), the improvement in photostability achieved in the M159A-IrisFP mutant could not be assessed due to the limited time-resolution of our experimental setup, which did not allow to accurately monitor individual switching cycles. Nevertheless, the gain in the number of on-off switching cycles achieved by IrisFP-M159A was on average reduced as compared to low light-level conditions (with the intriguing exception of live cells, Table 4). This is consistent with the hypothesis that other photobleaching pathways predominate at high illumination intensities. We indeed observed that at such intensities photobleaching in IrisFP essentially proceeds through a consecutive two-photon absorption process (CTPA) that leads to disruption of chromophore π-conjugation through decarboxylation of the fully conserved Glu212 residue, without involving Met159 nor the presence of oxygen [18]. Yet, the improvement in photofatigue decay achieved by IrisFP-M159A at high intensities suggests that Met159 could indirectly participate in this redox based photobleaching mechanism.

Overall, our data suggest that IrisFP-M159A, or preferably monomeric variants less prone to impair fused protein function such as NijiFP-M159A, Dendra2-M159A [11], or pcDronpa2-M159A [30], could facilitate the use of advanced techniques based on photochromism such as pcFRET [7], OLID microscopy [31] or pcSOFI [8].

Our widefield-based setup did not allow testing IrisFP and its mutant under the experimental conditions of RESOLFT nanoscopy. Based on our results and on the published switching properties of rsEGFP and rsEGFP2, which exhibit ~1100 and ~2100 cycles, respectively, before half decay in polyacrylamide [16], we speculate that the latter RSFPs remain superior for RESOLFT nanoscopy. However, the successful use of Dronpa-M159T with this technique [32] suggests that IrisFP-like M159A variants could still perform well under RESOLFT conditions. The use of mIris-M159A or NijiFP-M159A could thus open the door to the development of two-color pulse-chase RESOLFT nanoscopy [33].

The putative superior photofatigue resistance of EGFP-like RSFPs could be explained by two factors. First, rsEGFP and its derivatives do not have sulfur containing residues in their chromophore pocket, *de facto* achieving the same effect as the one we rationally engineered in the case of IrisFP-M159A. Second, Glu222 decarboxylation in these proteins may not necessarily result in photobleaching, as suggested by the observation that such decarboxylation rather activates proteins of the GFP family [34], the most notable example being photoactivatable PA-GFP [35]. Nevertheless, a precise understanding of the strong photoresistance of rsEGFP and its variants calls for a structural characterization of these proteins in their on and off states as well as in their photofatigued states.

In conclusion, we have shown that Met159 plays a critical role in controlling the photostability of IrisFP and possibly other RSFPs of anthozoan origin. Importantly, the photoswitching behavior of RSFPs appears to be strongly influenced by the local nanoenvironment, consistent with the growing evidence that, despite embedding by the β-barrel matrix, the photophysics of fluorescent protein's chromophores is largely controlled by the external environment. In particular we observed that PVA gels or the use of paraformaldehyde for cell fixation drastically changed the photoswitching properties of IrisFP and its mutant. The rationale behind such observation remains to be investigated, but could involve redox effects or reduced conformational freedom. Finally, the complex shape of photofatigue decay profiles observed in this work suggests the existence of subtle photophysical processes that could, in particular, involve the formation of long-lived dark states yet to be characterized.

5. Acknowledgment

We thank Stefan Jakobs and Tim Grotjohann for insightful discussions. D.B. acknowledges financial support by the ANR (ANR-2011-BSV5-012-01 NOBLEACH).

6. References

1. Adam V, Berardozzi R, Byrdin M, Bourgeois D (2014) Phototransformable fluorescent proteins: Future challenges. Current Opinion in Chemical Biology 20: 92-102.
2. Shcherbakova DM, Sengupta P, Lippincott-Schwartz J, Verkhusha VV (2014) Photocontrollable Fluorescent Proteins for Superresolution Imaging. Annual Review of Biophysics 43: 303-329.
3. Adam V (2014) Phototransformable fluorescent proteins: which one for which application? Histochem Cell Biol 142: 19-41.
4. Bourgeois D, Adam V (2012) Reversible photoswitching in fluorescent proteins: A mechanistic view. Iubmb Life 64: 482-491.
5. Adam V, Mizuno H, Grichine A, Hotta J, Yamagata Y, et al. (2010) Data storage based on photochromic and photoconvertible fluorescent proteins. J Biotechnol 149: 289-298.
6. Grotjohann T, Testa I, Leutenegger M, Bock H, Urban NT, et al. (2011) Diffraction-unlimited all-optical imaging and writing with a photochromic GFP. Nature 478: 204-208.
7. Subach FV, Zhang L, Gadella TW, Gurskaya NG, Lukyanov KA, et al. (2010) Red fluorescent protein with reversibly photoswitchable absorbance for photochromic FRET. Chem Biol 17: 745-755.
8. Dedecker P, Mo GC, Dertinger T, Zhang J (2012) Widely accessible method for superresolution fluorescence imaging of living systems. Proc Natl Acad Sci U S A 109: 10909-10914.
9. Rego EH, Shao L, Macklin JJ, Winoto L, Johansson GA, et al. (2012) Nonlinear structured-illumination microscopy with a photoswitchable protein reveals cellular structures at 50-nm resolution. Proc Natl Acad Sci U S A 109: E135-143.
10. Hofmann M, Eggeling C, Jakobs S, Hell SW (2005) Breaking the diffraction barrier in fluorescence microscopy at low light intensities by using reversibly photoswitchable proteins. Proc Natl Acad Sci U S A 102: 17565-17569.
11. Adam V, Moeyaert B, David CC, Mizuno H, Lelimousin M, et al. (2011) Rational design of photoconvertible and biphotochromic fluorescent proteins for advanced microscopy applications. Chem Biol 18: 1241-1251.

12. Stiel AC, Trowitzsch S, Weber G, Andresen M, Eggeling C, et al. (2007) 1.8 A bright-state structure of the reversibly switchable fluorescent protein Dronpa guides the generation of fast switching variants. Biochem J 402: 35-42.
13. Chang H, Zhang M, Ji W, Chen J, Zhang Y, et al. (2012) A unique series of reversibly switchable fluorescent proteins with beneficial properties for various applications. Proc Natl Acad Sci U S A 109: 4455-4460.
14. Shaner NC, Lin MZ, McKeown MR, Steinbach PA, Hazelwood KL, et al. (2008) Improving the photostability of bright monomeric orange and red fluorescent proteins. Nat Methods 5: 545-551.
15. Brakemann T, Stiel AC, Weber G, Andresen M, Testa I, et al. (2011) A reversibly photoswitchable GFP-like protein with fluorescence excitation decoupled from switching. Nat Biotechnol 29: 942-947.
16. Grotjohann T, Testa I, Reuss M, Brakemann T, Eggeling C, et al. (2012) rsEGFP2 enables fast RESOLFT nanoscopy of living cells. eLife 1: e00248.
17. Adam V, Lelimousin M, Boehme S, Desfonds G, Nienhaus K, et al. (2008) Structural characterization of IrisFP, an optical highlighter undergoing multiple photo-induced transformations. Proc Natl Acad Sci U S A 105: 18343-18348.
18. Duan C, Adam V, Byrdin M, Ridard J, Kieffer-Jaquinod S, et al. (2013) Structural evidence for a two-regime photobleaching mechanism in a reversibly switchable fluorescent protein. J Am Chem Soc 135: 15841-15850.
19. Kabsch W (2010) XDS. Acta Crystallogr D Biol Crystallogr 66: 125-132.
20. Vagin A, Teplyakov A (2010) Molecular replacement with MOLREP. Acta Crystallogr D Biol Crystallogr 66: 22-25.
21. Adams PD, Afonine PV, Bunkoczi G, Chen VB, Davis IW, et al. (2010) PHENIX: a comprehensive Python-based system for macromolecular structure solution. Acta Crystallographica Section D 66: 213-221.
22. Ordog R (2008) PyDeT, a PyMOL plug-in for visualizing geometric concepts around proteins. Bioinformation 2: 346-347.
23. Williams ATR, Winfield SA, Miller JN (1983) Relative fluorescence quantum yields using a computer-controlled luminescence spectrometer. Analyst 108: 1067-1071.
24. Ando R, Flors C, Mizuno H, Hofkens J, Miyawaki A (2007) Highlighted generation of fluorescence signals using simultaneous two-color irradiation on Dronpa mutants. Biophys J 92: L97-99.
25. Andresen M, Stiel AC, Folling J, Wenzel D, Schonle A, et al. (2008) Photoswitchable fluorescent proteins enable monochromatic multilabel imaging and dual color fluorescence nanoscopy. Nat Biotechnol 26: 1035-1040.
26. Endesfelder U, Malkusch S, Flottmann B, Mondry J, Liguzinski P, et al. (2011) Chemically Induced Photoswitching of Fluorescent Probes—A General Concept for Super-Resolution Microscopy. Molecules 16: 3106-3118.
27. Avilov S, Berardozzi R, Gunewardene MS, Adam V, Hess ST, et al. (2014) *In cellulo* Evaluation of Phototransformation Quantum Yields in Fluorescent Proteins Used As Markers for Single-Molecule Localization Microscopy. PLoS ONE 9: e98362.
28. Yeow EK, Melnikov SM, Bell TD, De Schryver FC, Hofkens J (2006) Characterizing the fluorescence intermittency and photobleaching kinetics of dye molecules immobilized on a glass surface. J Phys Chem A 110: 1726-1734.
29. Zondervan R, Kulzer F, Orlinskii SB, Orrit M (2003) Photoblinking of rhodamine 6G in poly(vinyl alcohol): Radical dark state formed through the triplet. Journal of Physical Chemistry A 107: 6770-6776.
30. Moeyaert B, Nguyen Bich N, De Zitter E, Rocha S, Clays K, et al. (2014) Green-to-red photoconvertible Dronpa mutant for multimodal super-resolution fluorescence microscopy. ACS Nano 8: 1664-1673.
31. Marriott G, Mao S, Sakata T, Ran J, Jackson DK, et al. (2008) Optical lock-in detection imaging microscopy for contrast-enhanced imaging in living cells. Proc Natl Acad Sci U S A 105: 17789-17794.

32. Testa I, Urban NT, Jakobs S, Eggeling C, Willig KI, et al. (2012) Nanoscopy of living brain slices with low light levels. Neuron 75: 992-1000.
33. Fuchs J, Bohme S, Oswald F, Hedde PN, Krause M, et al. (2010) A photoactivatable marker protein for pulse-chase imaging with superresolution. Nat Methods 7: 627-630.
34. van Thor JJ, Gensch T, Hellingwerf KJ, Johnson LN (2002) Phototransformation of green fluorescent protein with UV and visible light leads to decarboxylation of glutamate 222. Nat Struct Biol 9: 37-41.
35. Henderson JN, Gepshtein R, Heenan JR, Kallio K, Huppert D, et al. (2009) Structure and mechanism of the photoactivatable green fluorescent protein. J Am Chem Soc 131: 4176-4177.

Supplementary information

Rational Design of Enhanced Photoresistance in a Photoswitchable Fluorescent Protein

Chenxi Duan[1,2,3], Martin Byrdin[1,2,3], Mariam El Kathib [1,2,3], Xavier Henry[1,2,3], Virgile Adam[*,1,2,3] and Dominique Bourgeois[*,1,2,3]

Description of the fitting model

A simple kinetic model involving one-to-one reversible conversion between the on and off states was used to extract the on- and off-switching quantum yields:

$$\mathrm{ON} \underset{k_{-1} \times \Phi_{ON}}{\overset{k_1 \times \Phi_{OFF}}{\rightleftharpoons}} \mathrm{OFF}$$

Where k_1 and k_{-1} are the excitation rate constants during the switching-off and switching-on processes, respectively, and Φ_{OFF} and Φ_{ON} are the quantum yields for off-switching and on-switching. A proper evaluation of the dipole-orientation-dependent molecular excitation rates is necessary.

Case of tumbling molecules:

The excitation rate [s^{-1}] of a rapidly tumbling molecule is given by: $k = \varepsilon P \lambda \frac{(10^{-6}) Ln(10)}{N_A hc}$

where ε [$M^{-1}cm^{-1}$] is the extinction coefficient of the considered species (*ON* or *OFF* molecules) at the excitation wavelength λ [nm], P [Wcm^{-2}] is the laser power-density

(assumed to be uniform throughout the illuminated sample), N_A is the Avogadro number, h is the Planck constant and c is the speed of light.

The model then simply writes:

$$\frac{d[ON](t)}{dt} = -k_1\phi_{OFF}[ON](t) + k_{-1}\phi_{ON}[OFF](t)$$

$$[ON](t) + [OFF](t) = C_0$$

where C_0 is the total concentration of the fluorescent protein.

During switching-off periods (488 nm laser on and 405 nm laser off), we have:

$$k_1 = k_1^{488}, k_{-1} = k_{-1}^{488}$$

Note that k_{-1}^{488} corresponds to residual on-switching due to absorption at 488 nm of the OFF state. This residual on-switching may not be negligible, and will essentially determine the observed switching contrast. k_{-1}^{488} depends on the extinction coefficient ε_{OFF}^{488} ie the absorption of the OFF state at 488 nm, which is unknown but can be fitted from the data.

During switching-on periods (488 nm laser on and 405 nm laser on), we have:

$$k_1 = k_1^{488} + k_1^{405}, k_{-1} = k_{-1}^{488} + k_{-1}^{405}$$

As k_1^{488} is very large as compared to k_1^{405} because ε_{ON}^{488}, the absorption of the ON state at 488 nm, is much larger than ε_{ON}^{405} (which is also unknown), and the illumination power density at 488 nm is typically much higher than that at 405 nm, k_1^{405} is neglected.

The emitted fluorescence is then:

$$F(t) \propto [ON](t)$$

To take into account the limited time resolution of the EMCCD detector, the detected signal at every frame is then integrated over the frametime:

$$S^{EMCCD}(frame) \propto \int_{frametime} F(t)dt$$

<u>*Case of fixed molecules:*</u>

For a fixed oriented molecule with spherical coordinates θ and φ, the excitation rate of the absorbance dipole is angle dependent. For a circularly polarized laser beam whose electromagnetic field is assumed to be parallel to the objective focal plane, the excitation rate is given by: $k(\theta) = \frac{3}{2}k\cos^2\theta$, where θ is measured from the focal plane. The model then writes:

$$\frac{d[ON(\theta)](t)}{dt} = -k_1(\theta)\phi_{OFF}[ON(\theta)](t) + k_{-1}(\theta)\phi_{ON}[OFF(\theta)](t)$$

$$[ON(\theta)](t) + [OFF(\theta)](t) = C_0(\theta)$$

$$C_0(\theta) = \frac{\cos(\theta)}{\int \cos(\theta) d\theta} C_0$$

For each θ the calculations proceeds in the same way, however, the fluorescence is not emitted isotropically, so that based on Fourkas et al (Opt Lett 26: 211-213, 2001), the detected signal is:

$$F(t) \propto \int [ON(\theta)](t) E(\theta) d\theta$$

with the detection efficiency $E(\theta)$ taking the form:

$$E(\theta) = a + b \sin^2(\theta)$$

Case of variable tumbling propensity:

In real situations, molecules might be partially tumbling. We modeled this case as the fixed molecule case except that the excitation rates were then obtained as weighted averages of those rates for fully tumbling and fixed molecules.

$$k(\theta) = w \frac{3}{2} k \cos^2 \theta + (1 - w) k$$

where *w* is a tumbling propensity.

Abstract of article 3

This publication is a book chapter published in “Methods in Molecular Biology” (Duan et al., 2014a). In this review, we first present the development of RSFPs and classify RSFPs into three groups, negative RSFPs, positive RSFPs and decoupled RSFP. Then we present suitable approaches for the investigation of photoswitching mechanisms including X-ray crystallography, NMR, UV-vis optical spectroscopy or vibrational spectroscopy. Most importantly, like indicated in the title, we especially focused on the structural basis of all three different kinds of RSFPs. We took IrisFP, Padron and Dreiklang as examples to explain the photoswitching mechanisms in negative RSFPs, positive RSFPs and decoupled RSFPs, respectively. A large fraction of the paper was dedicated to present the uses of RSFPs such as PhotoActivated Localization Microscopy (PALM), pcSOFI, RESOLFT, Saturated Structured Illumination Microscopy (SSIM), bi-photochromic Pulse Chase, reversible data storage, optogenetics, viscosity sensing, photochromic FRET. At the end of this chapter, we presented some future perspectives for RSFPs. In fact, this review could serve as a better introduction to my thesis.

Chapter 12

Structural Basis of Photoswitching in Fluorescent Proteins

Chenxi Duan, Virgile Adam, Martin Byrdin, and Dominique Bourgeois

Abstract

Fluorescent proteins have revolutionized life sciences because they allow noninvasive and highly specific labeling of biological samples. The subset of "phototransformable" fluorescent proteins recently attracted a widespread interest, as their fluorescence state can be modified upon excitation at defined wavelengths. The fluorescence emission of Reversibly Switchable Fluorescent Proteins (RSFPs), in particular, can be repeatedly switched on and off. RSFPs enable many new exciting modalities in fluorescence microscopy and biotechnology, including protein tracking, photochromic Förster Resonance Energy Transfer, super-resolution microscopy, optogenetics, and ultra-high-density optical data storage. Photoswitching in RSFPs typically results from chromophore *cis–trans* isomerization accompanied by a protonation change, but other switching schemes based on, e.g., chromophore hydration/dehydration have also been discovered. In this chapter, we review the main structural features at the basis of photoswitching in RSFPs.

Key words Fluorescent proteins, Photoswitching, Dronpa, RSFPs, Protein dynamics, *cis–trans* Isomerization, Proton transfer, Super-resolution microscopy

Abbreviations

GFP	Green fluorescent protein
YFP	Yellow fluorescent protein
FPs	Fluorescent proteins
PTFPs	Phototransformable fluorescent proteins
RSFPs	Reversibly switchable fluorescent proteins
PCFPs	Photoconvertible fluorescent proteins
PAFPs	Photoactivatable fluorescent proteins
ESPT	Excited state proton transfer
KIE	Kinetic isotope effect
p-HBI	4-(*p*-Hydroxybenzylidene)-5-imidazolinone
pcFRET	Photochromic Förster resonance energy transfer
QM/MM	Quantum mechanics/molecular mechanics
SMLM	Single molecule localization microscopy
PALM	Photoactivated localization microscopy
STORM	Stochastic optical reconstruction microscopy
STED	Stimulated emission depletion

Sidney Cambridge (ed.), *Photoswitching Proteins: Methods and Protocols*, Methods in Molecular Biology, vol. 1148,
DOI 10.1007/978-1-4939-0470-9_12,

RESOLFT	Reversible saturable optical linear fluorescence transitions
SSIM	Saturated structured illumination microscopy
(pc)SOFI	(Photochromic) stochastic optical fluctuation imaging
IR	Infra-red
HSQC	Heteronuclear single quantum coherence
XFEL	X-Ray-free electron laser

1 Introduction

Fluorescent proteins (FPs) have become indispensable tools to investigate the interrelations between cell structure, function, and dynamics [1]. Their three-dimensional structure is quite simple: the peptide chain forms an 11-stranded β-barrel resembling a "soda can," which wraps around a three-residues-based endogenous chromophore (Fig. 1). This 4-(*p*-hydroxybenzylidene)-5-imidazolinone (*p*-HBI) chromophore only requires oxygen as an external cofactor to become mature. A stunning palette of fluorescent proteins displaying a wide range of emission colors (450–650 nm) has been engineered, typically by rational or random mutagenesis of the chromophore itself or of its close environment [2]. The discovery of FPs from Anthozoan species (e.g., corals or anemones), which exhibit a high structural similarity but only a small sequence identity (<30 %) with the more classical Hydrozoan FPs (e.g., jellyfishes), launched the development of red fluorescent proteins [3], and considerably boosted FP research in recent years.

In addition to suitable colors, useful FPs should exhibit a high expression level, fast maturation, and high fluorescence brightness so that they can be imaged with sufficient signal-to-noise ratio soon after cell transfection. Furthermore, they should be monomeric and should not induce cytotoxicity, to avoid cellular dysfunction. Importantly, they should be photostable and possible modifications of their fluorescence properties as a function of light excitation or environmental parameters (e.g., pH, redox potential, oxygen level) should be understood.

The protonation state of the *p*-hydroxybenzylidene moiety of the chromophore plays a key role in the fluorescence properties of FPs. Two protonation states can generally be adopted, the proportion of which is determined by the interactions with neighboring residues in the chromophore pocket and may (or not) vary with pH. The protonated (neutral) chromophore absorbs in the so-called "A-band," whereas the deprotonated (anionic) chromophore absorbs in the "B-band" (Fig. 1). For a green-emitting FP, those bands usually peak at ~400 nm and ~490 nm, respectively. In their anionic state, FPs are typically highly fluorescent, whereas in their neutral state they are dimly or not fluorescent. However, upon excitation of the neutral state, the FP chromophore becomes a strong acid with a p*K*a near zero. Ultrafast conversion to a

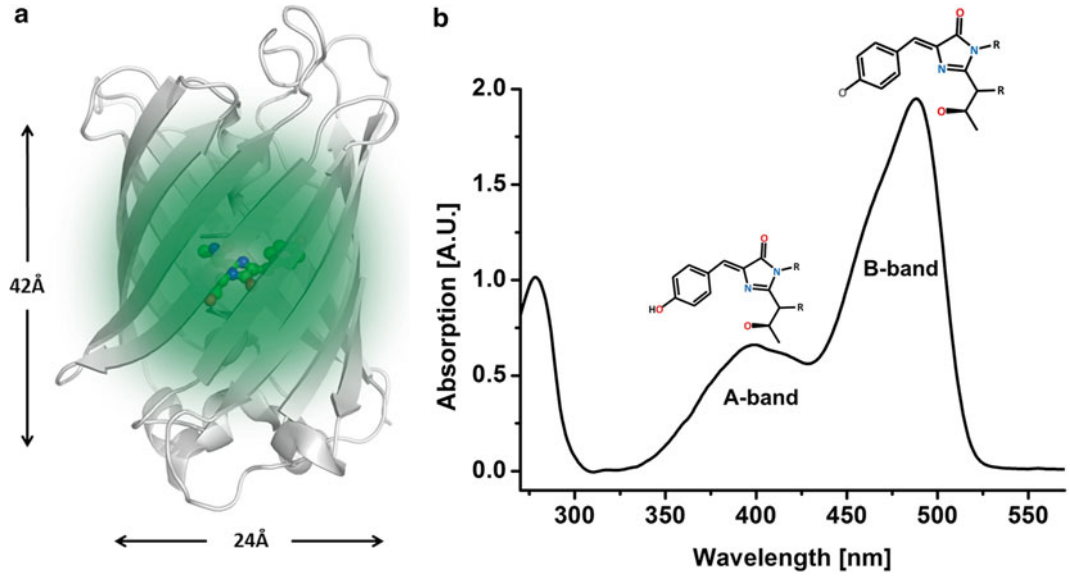

Fig. 1 Enhanced green fluorescent protein (EGFP). (**a**) The crystal structure (Protein Data Bank (PDB) ID 2Y0G) of a single chain is represented in *gray cartoons*. The green-glowing chromophore is represented in *balls* and *sticks* and *stands* in the center of the barrel. (**b**) Absorption spectrum of EGFP. Two bands are attributed to the neutral form (A-band) and the anionic form (B-band) of the chromophore. Lewis structures of the corresponding chromophore are represented as *insets*

deprotonated excited state may thus occur, resulting in high yield and strongly Stokes-shifted fluorescence.

The high fluorescence quantum yield of FPs (generally > ~0.5) is commonly attributed to the idea that the chromophore is held rigidly within the protein matrix through a set of tight non-covalent interactions. This is a too simplistic view. In fact, FPs exhibit a highly dynamic behavior, in line with their observed complex photophysics. Upon light absorption, and especially when intersystem crossing to the long-lived triplet state takes place, the FP structural plasticity may allow a number of photophysical or photochemical transformations to occur. For example, like any fluorophore, FPs undergo transient stochastic switching events to nonfluorescent dark states ("blinking"), and eventual conversion to a permanent off state ("bleaching").

In the subfamily of fluorescent proteins termed Phototransformable FPs (PTFPs), specific phototransformations can be quantitatively induced by light, which is at the basis of a number of revolutionary developments in advanced fluorescence microscopy. These PTFPs, mostly found in Anthozoan stony corals, but also engineered from Hydrozoan FPs have become the focus of intense research since a few years [4–6]. Three types of phototransformations may be distinguished in PTFPs (Fig. 2): nonreversible activation from a nonfluorescent to a fluorescent state (referred to as "photoactivation," fluorescent proteins of this

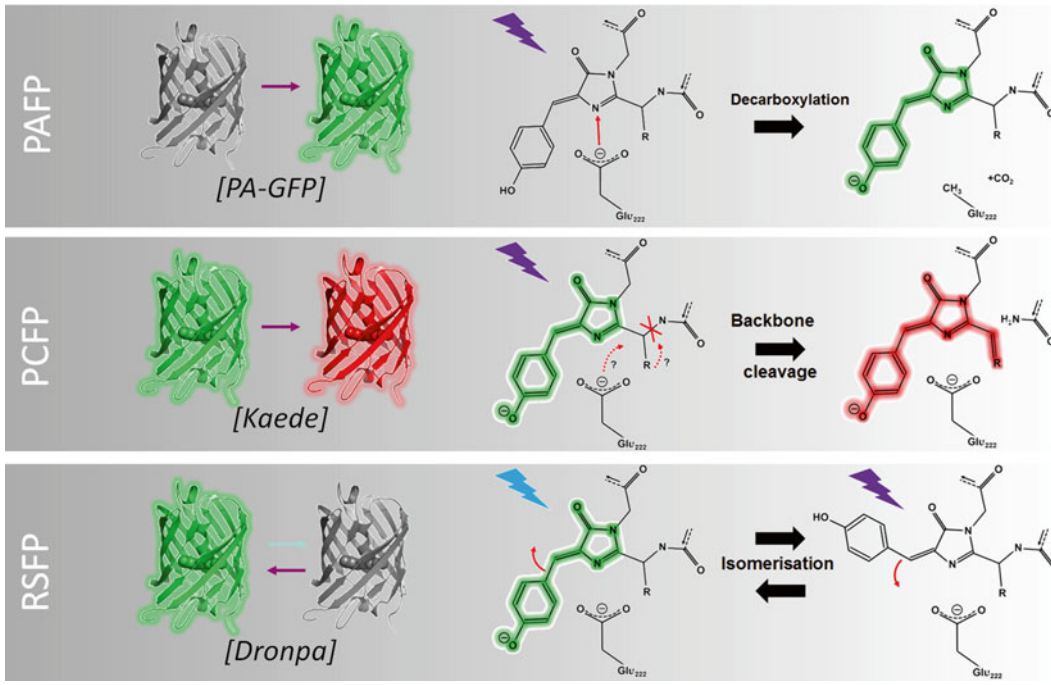

Fig. 2 Various possible reactions in phototransformable fluorescent proteins with typical examples of irreversibly photoactivatable fluorescent proteins (PAFP), irreversibly photoconvertible fluorescent proteins (PCFP), and reversibly switchable fluorescent proteins (RSFP). Photoinduced reactions occurring at the chromophore level are represented for each case. Figure reproduced from D. Bourgeois, A. Regis-Faro and V. Adam (2012), Biochemical Society Transactions, 40 531–538, © the Biochemical Society, with permission from Portland Press Limited

group are called Photoactivatable FPs (PAFPs)), nonreversible conversion between two fluorescent states with different emission colors ("photoconversion," fluorescent proteins of this group are called Photoconvertible FPs (PCFPs)), and reversible switching between a fluorescent on-state and a nonfluorescent off-state ("photoswitching," fluorescent proteins of this group are called Reversibly Switchable FPs (RSFPs)). In this chapter we give a structural perspective on the fascinating photophysical properties of RSFPs.

2 Discovery and Classification of RSFPs

A list of the currently developed RSFPs with their main photophysical properties is provided in Table 1.

The first observation of reversible photoswitching of a fluorescent protein at room temperature was made with yellow derivatives of *Aequora victoria* GFP at the single molecule [7] and at the ensemble levels [8–10]. However, photoswitching of these Hydrozoan FPs appeared limited, probably involving only minor

Table 1
Properties of well-characterized RSFPs developed to date

Class	Switching	Protein (oligomerization)	Parent protein [wild-type]	Source organism	Chromophore triad	λ_{max} ex/em[a](nm)	ε[a] ($M^{-1}.cm^{-1}$)	Φ_{fluo}[a]	Brightness[b]	pK_a	Φ_{sw}[a] On-off	Φ_{sw}[a] Off-on	Actinic light (nm) On-off	Actinic light (nm) Off-on	Ref.
Anthozoans	Negative	mTFP0.7 (M)	cFP484	*Clavularia* sp.	AYG	453/488	60,000	0.50	89 %	4.0	ND	ND	458	405	[31]
		mGeosC (M)	EosFP	*L. Hemprichii*	CYG	505/516	76,967	0.81	186 %	6.0	ND	ND	488	405	[34]
		mGeos-M (M)	EosFP	*L. Hemprichii*	MYG	503/514	51,609	0.85	130 %	4.5–5	ND	ND	488	405	[34]
		mGeos-S (M)	EosFP	*L. Hemprichii*	SYG	501/512	64,602	0.76	145 %	5–5.5	ND	ND	488	405	[34]
		Dronpa (M)	22G	*Echinophyllia* sp. *SC22*	CYG	503/517	94,100	0.67	188 %	5.3	3.0×10^{-4}	7.0×10^{-1}	488	405	[12, 36]
		Dronpa-2 (M)	Dronpa [22G]	*Echinophyllia* sp. *SC22*	CYG	489/515	56,000	0.28	47 %	ND	4.7×10^{-2}	ND	488	405	[29]
		Dronpa-3 (M)	Dronpa [22G]	*Echinophyllia* sp. *SC22*	CYG	489/515	58,000	0.33	57 %	ND	5.3×10^{-3}	ND	488	405	[29]
		rsFastLime (M)	Dronpa [22G]	*Echinophyllia* sp. *SC22*	CYG	496/518	39,094	0.77	89 %	ND	ND	ND	488	405	[20]
		bsDronpa (M)	Dronpa [22G]	*Echinophyllia* sp. *SC22*	CYG	460/504	45,000	0.50	67 %	ND	ND	ND	488	405	[20]
		rsCherryRev (M)	mCherry [DsRed]	*Discosoma* sp.	MYG	572/608	84,000	0.005	1 %	5.5	ND	ND	550	450	[77]
		rsTagRFP (M)	TagRFP [eqFP578]	*E. quadricolor*	MYG	567/585	36,800	0.11	12 %	6.6	ND	ND	570	445	[78]
		mEosFP M159A (M)	EosFP	*L. Hemprichii*	HYG	487/512	98,600	0.52	153 %	4.3	2.6×10^{-3}	1.5×10^{-1}	488	405	[36]
		IrisFP (T)	EosFP	*L. Hemprichii*	HYG	488/516	57,800	0.48	83 %	5.7	3.2×10^{-3}	1.5×10^{-1}	488	405	[35, 36]
		IrisFP (T)				551/580	27,000	0.50	40 %	6.8	2.0×10^{-3}	5.0×10^{-2}	561	440	
		mIrisFP (M)	EosFP	*L. Hemprichii*	HYG	486/516	74,000	0.60	132 %	5.7	2.2×10^{-3}	1.3×10^{-1}	488	405	[36, 71]
		mIrisFP (M)				546/578	26,000	0.44	34 %	7.0	4.0×10^{-4}	1.1×10^{-1}	561	440	
		NijiFP (M)	Dendra2 [DendGFP]	*Dendronephthya* sp.	HYG	469/507	41,100	0.64	78 %	7.0	1.8×10^{-3}	1.0×10^{-1}	488	405	[36]
		NijiFP (M)				526/569	42,000	0.65	81 %	7.3	1.0×10^{-3}	1.0×10^{-1}	561	440	
		Dendra2 M159A (M)	Dendra2 [DendGFP]	*Dendronephthya* sp.	HYG	471/504	51,100	0.55	84 %	6.5	1.1×10^{-3}	8.0×10^{-2}	488	405	[36]
		Dendra2 M159A (M)				528/562	45,000	0.75	100 %	6.8	3.2×10^{-3}	1.0×10^{-2}	561	440	
	Positive	Padron (M)	Dronpa [22G]	*Echinophyllia* sp. *SC22*	CYG	503/522	43,000	0.64	82 %	ND	ND	ND	405	488	[20]
		rsCherry (M)	mCherry [DsRed]	*Discosoma* sp.	MYG	572/610	80,000	0.02	5 %	6.0	ND	ND	450	550	[77]
		asFP595 (T)	–	*A. sulcata*	MYG	572/595	56,200	<0.001	<0.2 %	ND	ND	ND	450	568	[81]
		KFP1 (T)	asFP595	*A. sulcata*	MYG	590/600	59,000	0.07	12 %	ND	ND	ND	458	532	[11]
Hydrozoans	Negative	Mut2Q (M)	GFP	*A. victoria*	AYG	496/507	54,000	0.28	45 %	6.0	4.7×10^{-3}	2.6×10^{-2}	478	405	[37, 82]
		EYQ1 (M)	EYFP [GFP]	*A. victoria*	SYG	510/524	73,000	0.72	156 %	6.9	1.8×10^{-4}	6.0×10^{-2}	514	405	[37]
		rsEGFP (M)	EGFP [GFP]	*A. victoria*	TYG	493/510	47,000	0.36	50 %	6.5	ND	ND	488	405	[38]
		rsEGFP2(M)	EGFP [GFP]	*A. victoria*	AYG	478/503	61,300	0.3	60 %	5.8	ND	ND	491	405	[39]
	D[a]	Dreiklang (M)	Citrine [GFP]	*A. victoria*	GYG	511/529	83,000	0.41	101 %	7.2	ND	ND	405	365	[40]

Note: the table summarizes the photophysical properties of RSFPs in their fluorescent form

[a]Abbreviations: λ_{max} ex/em wavelength of maximum in excitation/emission spectrum; ε, molar extinction coefficient; Φ_{fluo}, fluorescence quantum yield; Φ_{sw}, photoswitching quantum yield; D, decoupled switching

[b]Brightness is the product of quantum yield and molar extinction coefficient divided by 1,000, expressed in % of the EGFP brightness

[c]Wavelengths required for reversible transitions. Background colors represent the emission colors of the proteins (left) and the colors of lights used to reversibly switch proteins (right). M, monomer; T, tetramer; NA, not applicable; ND, not determined

subpopulations of molecules. Efficient photoswitching was initially reported of the weakly fluorescent and tetrameric asFP595 from the Anthozoan sea anemone *Anemonia sulcata*. The phenomena was described as reversible "kindling," because the fluorescence emission from asFP595 was enhanced by the fluorescence excitation light (568 nm) and quenched by blue light (450 nm) [11]. The first RSFP of sufficient quality to successfully conduct biological experiments was obtained upon engineering a Pectiniidae coral FP, yielding the well-known Dronpa [12]. In contrast to asFP595, fluorescence emission in Dronpa is quenched by the excitation light (490 nm) and recovered by illumination with violet light (405 nm). A large number of mechanistic investigations were then performed on these two proteins [13–28].

In view of the growing interest of RSFPs for advanced fluorescence microscopy applications, substantial efforts were made in the last years to develop variants with improved properties such as higher fluorescence brightness (the product of fluorescence quantum yield and molar extinction coefficient), enhanced switching contrast (ratio of fluorescence emission of the on and off states), tunable switching quantum yields, increased photoresistance, or red-shifted emission (Table 1). Several new Anthozoan RSFPs were thus introduced such as a number of Dronpa variants [20, 29, 30], mTFP0.7 from *Clavuliara* sp. [31], rsTagRFP from *E. quadricolor* [32, 33], mGeos from *L. hemprichii* [34], and others (Table 1). An interesting case was IrisFP (and later NijiFP), which combines on–off photoswitching with green to red photo-conversion properties [35, 36], introducing the possibility to achieve dual color photoswitching with a single protein. Recently, Hydrozoan GFP-based RSFPs were also developed, showing that high-performance photoswitching is not restricted to Anthozoan FPs. Single-mutation of the strictly conserved Glu222 (GFP numbering) into Gln conferred high-contrast switching properties to variants of YFP [37], while a combined rational and random mutagenesis approach yielded the photoresistant rsEGFP [38] and rsEGFP2 [39].

All these RSFPs can be classified as "negative" or "positive." In negative RSFPs such as Dronpa, off-switching results from illumination at wavelengths absorbed by the protein in its on-state. In positive RSFPs such as asFP595, on-switching results from illumination at wavelengths absorbed by the protein in its on-state (Table 1). In all cases, switching is thought to primarily result from a light-induced *cis–trans* isomerization of the chromophore accompanied by a change of the *p*-hydroxybenzylidene protonation state. A different acid–base environment of the chromophore in the two isomeric states modulates its p*K*a and is key to the photoswitching function. In the fluorescent on-state, the chromophore is typically in an anionic *cis* configuration, whereas in the nonfluorescent off state it is found in a *trans* configuration, either neutral or anionic. In negative RSFPs, the *cis* configuration of the chromophore is the

thermodynamically stable form, so these proteins are typically highly fluorescent in their native state. In positive RSFPs, the nonfluorescent *trans* configurations tends to be more thermodynamically stable, although both states are sometimes observed at equilibrium, so these proteins are normally nonfluorescent or weakly fluorescent in their native state.

In 2011, Brakemann *et al.* [40] engineered YFP-derivatives previously shown to be partially switchable [10, 41] to elaborate Dreiklang, an RSFP that exhibits an entirely new mechanism which does not rely on *cis–trans* isomerization of the chromophore, but rather involves reversible chemical modifications of the imidazolinone moiety. In Dreiklang, photoswitching is neither positive nor negative but is "decoupled," meaning that fluorescence excitation exerts no influence on photoswitching.

3 Methodology for the Investigation of Photoswitching Mechanisms

Boosted by this rapidly evolving research field, increased attention has been devoted to mechanistic investigations of RSFPs with a dual goal: gaining fundamental insight into this intriguing phenomenon and rationally designing variants with enhanced photophysical properties. Several methods can be used that are briefly described below.

Confocal or wide-field fluorescence microscopy approaches based on single-molecule detection allow monitoring the stochastic nature of photoswitching. By recording many single-molecule fluorescence traces, histograms of on-times and off-times can be extracted from which key photophysical parameters such as switching quantum yields can be derived. Single-molecule investigations provide the essential advantage that subpopulations of molecules behaving differently from the average can be identified. The same illumination conditions as those used in cell microscopy experiments can be used and the influence of environmental conditions such as redox potential, pH, or oxygen level can be monitored. However, to study single molecule behavior, the RSFPs are typically attached to a glass coverslip or immobilized in a polymer substrate, which might induce deviations relative to the *in cellulo* behavior. Ultimately, despite complications due to a lower signal-to-noise ratio and a higher molecular density, these methods will be applied directly in the biological sample so as to evaluate RSFPs switching in genuine experimental conditions.

To get a high-resolution structural view of photoswitching, ensemble level techniques must be used, such as X-ray crystallography, NMR, UV–vis optical spectroscopy, or vibrational spectroscopy. The most direct view of the structural signature of photoswitching is provided by crystallography. However, the

nonstandard concepts of "kinetic" protein crystallography need to be used [42], whereby photoswitching is induced *in crystallo*. Indeed, the photoswitched chromophore is usually not stable for more than at most a few hours, a time much too short to achieve crystal growth. Thus, to generate the switched state, the crystalline sample is submitted to laser illumination, followed by flash cooling to prevent back switching and to minimize radiation damage effects during diffraction data collection. Fortunately, FPs are well-suited samples for kinetic protein crystallography, as conformational changes induced by light illumination are small enough to be compatible with crystal packing interactions, so that samples are usually not seriously deteriorated upon illumination. However, it should always be kept in mind that the crystalline state may exert an influence on the observed switching scenario, for example by selecting out a subset of conformational states not strictly representative of the in-solution behavior. This point has for example been a matter of debate concerning the structure of the off state of Dronpa [16]. 2D-NMR investigations (typically based on ^{1}H–^{15}N or ^{1}H–^{13}C HSQC experiments) have the advantage that no crystal constraints are present, so the observed conformational changes may be more genuine. However, the usually longer measuring times at room temperature make it trickier to maintain the photoswitched state in the sample. For example, prolonged illumination might be required and result in unwanted photobleaching. In all cases, X-ray or NMR structural views should be complemented by steady-state optical spectroscopy measurements so as to quantify the extent of photoswitching in the investigated samples. Optical microspectrophotometry can be applied *in crystallo*, in the absorbance, fluorescence [43], or even Raman mode [44]. It should be noted that careful spectroscopic investigations using relatively basic instruments can provide a wealth of insightful mechanistic information complementary to structural approaches [45, 46].

To gain further mechanistic insight, putative intermediate states along the photoswitching reaction pathway should be characterized in addition to the switching endpoints. Since photoswitching is typically a very rapid (subnanosecond) process, ultrafast pump-probe UV–vis or IR spectroscopy are the tools of choice to be used. However, a major difficulty is that photoswitching in RSFPs is a low yield process (10^{-4}–10^{-1}) so that the fraction of molecules that can simultaneously follow the desired photoswitching pathway is small (although a larger fraction may engage into the pathway but quickly return to the starting state or deviate to other photophysical states). This explains why almost all ultrafast spectroscopic investigations of RSFPs photoswitching so far concentrated on the back-photoswitching reaction of Dronpa which has a particularly high yield (>0.1).

Yet, another approach to track intermediates consists in performing temperature-controlled experiments. At sufficiently

low temperature, the switching reaction may not be able to be completed if thermal energy barriers are present along the pathway. In such a case, activated molecules may possibly get trapped and accumulate in an intermediate state that can then be probed structurally or spectroscopically. Such an approach was for example used to study the protein Padron [47]. Working at low temperature, however, always carries the danger that the protein conformational landscape may be altered.

Important insight into photoswitching mechanisms can also be obtained from theoretical investigations such as molecular dynamics simulations or reaction-path-finding techniques. In such studies, the RSFP is modeled with quantum mechanics/molecular mechanics (QM/MM) hybrid approaches: the chromophore and its nearby environment are described at the quantum level in the ground or excited state, whereas the rest of the protein is treated with classical force fields. Such investigations have provided a number of interesting details about fundamental properties of photoswitching [21, 27]. However, they strongly rely on available high-resolution crystallographic input structures, and it should be kept in mind that they remain restricted by necessary simplifications and assumptions, due to limited computing power. For example, modeling proton transfer reactions involving the RSFPs chromophore is difficult, as the number of atoms in the QM region can typically not be changed along simulations.

Ultrafast time-resolved crystallography experiments on RSFPs based on synchrotron Laue diffraction have so far remained unsuccessful. However, new XFEL sources offer exciting prospects to catch photoswitching in action. In the long term, the dream would be to watch single RSFPs in real time at atomic resolution, e.g., by combining femtosecond stimulated Raman scattering [48] with XFEL diffraction [49].

4 Photoswitching Mechanisms

In this section, we describe in more detail the photoswitching mechanisms as observed in negative, positive, and decoupled RSFPs. Three important remarks should be made beforehand.

First, the *p*-HBI chromophore in solution has been shown to undergo facile photoinduced *cis–trans* isomerization caused by twisting around the methylene bridge that links the two cyclic moieties (explaining the lack of fluorescence of the isolated *p*-HBI chromophore in solution) [50]. Thus, chromophore isomerization in RSFPs is primarily a manifestation of intrinsic excited state chromophore dynamics. This process is in general hindered by the protein scaffold in FPs, but it can still occur with low yield in RSFPs. Chromophore isomerization in RSFPs is a single-photon excitation process in both directions [13, 47]. However, back-switching is

also thermally driven and it should be kept in mind that some FPs are able to change the isomeric state of their chromophore in the ground state following pH changes [51, 52].

Second, the isomeric state of the chromophore in general does not dictate per se the occurrence or the lack of fluorescence. There exist FPs exhibiting strong fluorescence in the *trans* state [52, 53]. However, in positive or negative RSFPs, the nonfluorescent state has always been found to correspond to the *trans* configuration of the chromophore.

Third, the proton affinity of the chromophore hydroxybenzylidene group strongly depends on the local protein environment and therefore it is isomer dependent, both in the ground and in the excited states. Widely different chromophore p*K*a are therefore expected—and observed—in the *trans* or *cis* configurations. As chromophore protonation has a strong influence on the ability to fluoresce, this isomer-dependent p*K*a generally plays a key role in fluorescence switching.

4.1 Negative Anthozoan RSFPs: On and Off States

To describe the photoswitching mechanism in negative RSFPs, we take the example of IrisFP, which has been extensively characterized by us [35]. The X-ray structures and absorption/fluorescence spectra of the protein in its on and off states are presented in Fig. 3.

In both states, it can be seen that the chromophore is maintained by a complex set of H-bonding interactions involving Arg66, Ser142, Glu144, Ser173, Tyr177, His194, and Glu212, as well as water molecules. These residues are essentially conserved in all negative RSFPs from Anthozoa species. *cis–trans* Isomerization is accompanied by a substantial structural change of the chromophore pocket. The tightly H-bonded triad Glu144-His194-Glu212 in the *cis* configuration is replaced by the Glu144-Arg66-Glu212 triad in the *trans* configuration, with either His194 or Arg66 stabilizing the chromophore by π-stacking and π-cation interactions with the hydroxybenzylidene moiety, respectively. In the *cis* configuration, the chromophore phenolate interacts with Ser142 whose hydroxy group is protonated, thus favoring a deprotonated state. This anionic state is further favored by the interaction of Arg66 with the carbonyl group of the imidazolinone moiety, which retains electron density on that ring. Hence, the p*K*a of the *cis* chromophore in IrisFP ensures a predominantly deprotonated chromophore at physiological pH (p*K*a = 5.7). The chromophore is also found in a highly planar configuration. Thus, the conditions favoring a high fluorescence yield are fulfilled. In the *trans* configuration, a very different scenario is found, where the phenolate group is interacting with the deprotonated Glu144, and the interaction of Arg66 with the imidazolinone being disengaged. Consequently, there is a substantial change in the chromophore electrostatic environment, and the latter is found completely protonated at physiological pH, with a p*K*a > 10.

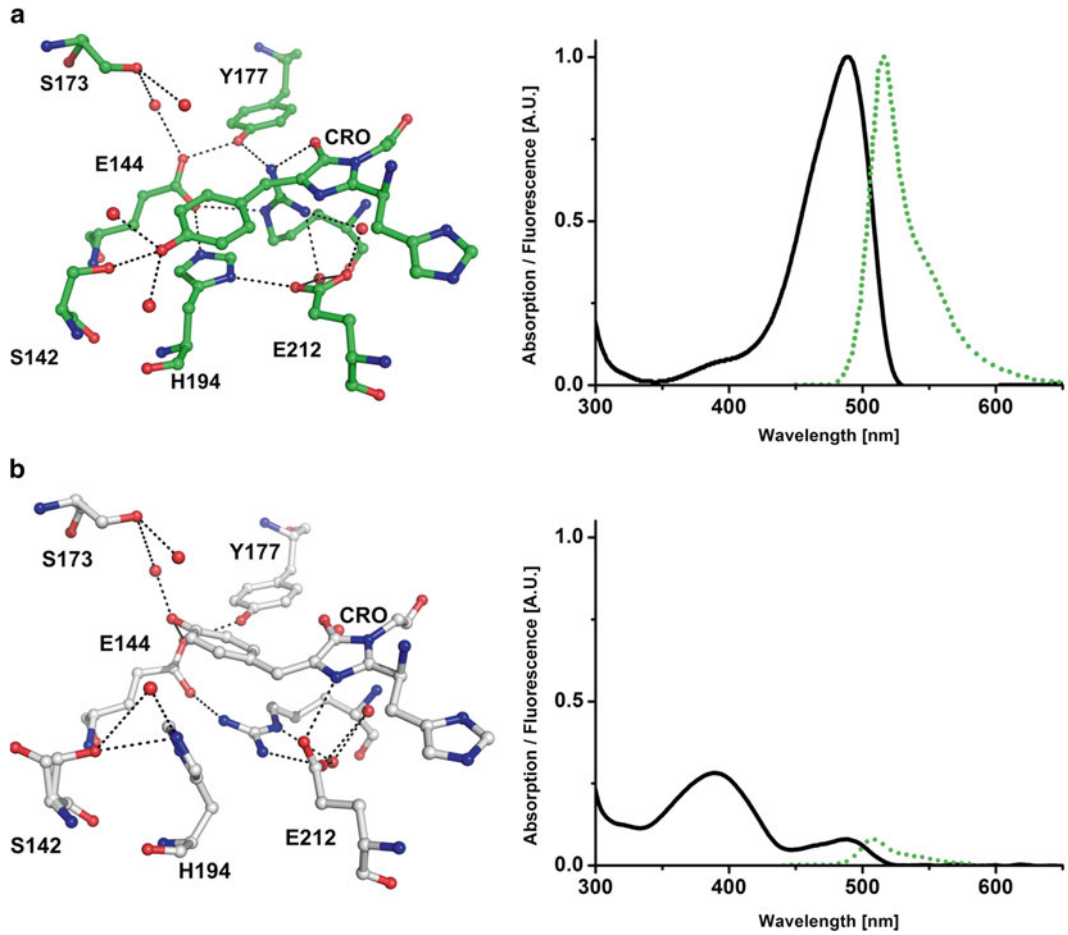

Fig. 3 Crystallographic structures of the chromophore, its microenvironment, and the corresponding spectra for IrisFP. (**a**) In the more stable fluorescent state (PDB ID 2VVH), the chromophore adopts a *cis* conformation and is deprotonated as observable by the major anionic absorption band peaking at 487 nm (*black spectrum*) that provides fluorescence peaking at 516 nm (*green dotted spectrum*). (**b**) In the dark state (PDB ID 2VVI), the 3D structure shows that the chromophore clearly adopts a *trans* conformation and is protonated as observable by the major neutral band peaking at 390 nm (*black spectrum*). The remaining fluorescence signal (*green dotted spectrum*) is due to a minor fraction of chromophores remaining in the *cis* conformation. Water molecules are represented as *red balls* and hydrogen bonds are represented as *black dotted lines*

No ESPT (excited state proton transfer) is observed and the chromophore is found to adopt a quite distorted geometry. Thus, the conditions favoring a high fluorescence yield are not fulfilled. The *trans*-conformation is thermodynamically quite stable, taking a few hours to return to the *cis*-conformation. This stems from the fact that the protein scaffold is able to accommodate the hydroxybenzylidene group of the *trans*-chromophore with overall little deformation, and by optimally rearranging the H-bond networks within the pocket. Some subtleties contribute to enhancing the stability of the *trans*-state: for example, Ser142, which maintains a strong

H-bond with the hydroxybenzylidene moiety in the *cis*-state, engages with another H-bonding partner once the chromophore has been isomerized, as a compensation. Also, Glu212 directly interacts with the imidazolinone nitrogen in the *trans*-state, providing further stabilization.

Similar schemes have been described for Dronpa [15] and mTFP0.7 [31], with some relatively minor variations. An important peculiarity of Dronpa is that upon off-photoswitching, the seventh β-strand near the chromophore becomes disordered, as shown by NMR experiments [16]. As this strand forms part of the cross-dimer interface in the tetrameric parent of Dronpa, Dronpa photoswitching modulates its propensity to multimerize at high concentration. This property was ingenuously used to develop a new optogenetic approach [54]. Likewise, researchers took advantage of the flexibility-mediated photoswitching of Dronpa to develop a viscosity measurement assay [55].

4.2 Positive Anthozoan RSFPs: On and Off States

Padron is a positive RSFP engineered from Dronpa [30, 56]. The two essential Met159Tyr and Val157Gly mutations were sufficient to completely reverse the switching properties of Dronpa (hence the name "Padron"). The X-ray structures and absorption/fluorescence spectra of Padron in its on and off states are presented in Fig. 4. In the on state, the configurations of the chromophore and of its immediate environment do not differ much from Dronpa or IrisFP. However, Ser142 adopts a different conformation than in Dronpa, which might be responsible for the substantial increase in the proton affinity of the chromophore hydroxybenzylidene moiety. Indeed, the chromophore exhibits a p*K*a of 6.0 (5.3 for Dronpa), meaning that at physiological pH a significant fraction of the switched-on Padron molecules are protonated and nonfluorescent. In the *trans* state, structural differences with negative RSFPs are striking: Tyr159 now establishes an H-bonding interaction with the chromophore phenolate, which maintains the latter in an anionic state, with a p*K*a of 4.5. His193, Arg66, and Glu211 (equivalent to His194, Arg66, and Glu212 in IrisFP) do not change their conformation relative to the *cis* state, possibly because of the shifted location of Ser142, and this may in turn result in the severe torsion of the *trans* chromophore. Thus, the *trans* chromophore is nonfluorescent but exhibits an absorption spectrum similar to that of the fluorescent on state (although somewhat broader presumably due to a larger conformational freedom).

4.3 Positive and Negative Anthozoan RSFPs: Reaction Pathways

Photoswitching kinetics and pathways in RSFPs are controlled by the potential energy surfaces that connect the on and off states of the chromophore. The chromophore isomer conformation and protonation, in the ground and excited state, as well as the protein environment, are all involved. Therefore, modifying the chromophore composition, or its environment, allows tuning properties

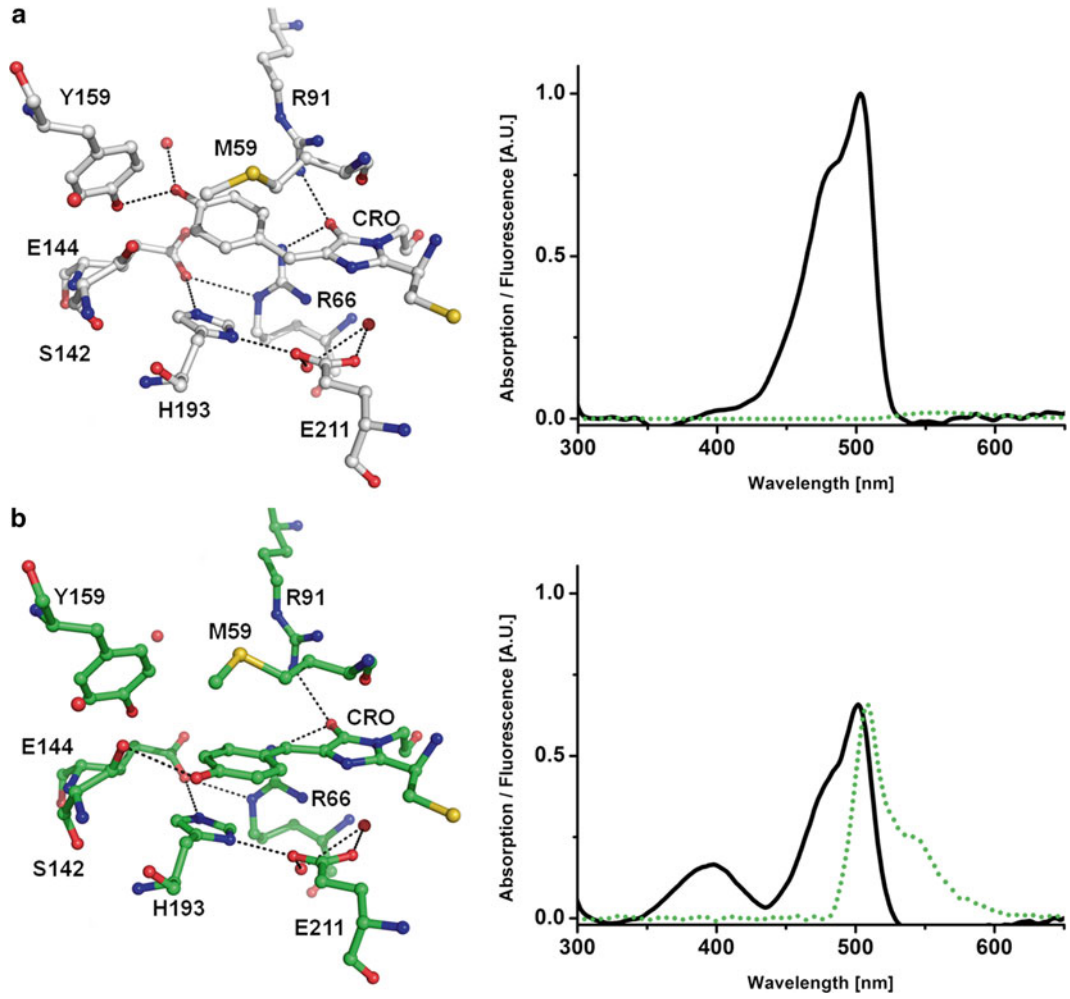

Fig. 4 Crystallographic structures of the chromophore, its microenvironment, and the corresponding spectra for Padron. (**a**) In the more stable dark state (PDB ID 3ZUF) the 3D structure shows that the chromophore adopts a trans conformation and is deprotonated as indicated by the major anionic absorption band peaking at 503 nm (*black spectrum*). (**b**) In the fluorescent state (PDB ID 3ZUJ) the chromophore clearly adopts a *cis* conformation. Absorption spectra reveal two bands, one peaking at 390 nm and corresponding to the neutral fraction and one peaking at 503 nm and corresponding to the anionic fluorescent fraction peaking at 518 nm. Water molecules are represented as red balls and hydrogen bonds are represented as *black dotted lines*

such as photoswitching rates, photon outputs, photostability, or pH-sensitivity. For example, Chang et al. [34] engineered the mGeos negative RSFPs by modifying the first position of the chromophore tripeptide and found that mGeos-M (with a methionine at this position) had the highest number of photons emitted per switching cycle amongst all green RSFPs. Likewise, Adam et al. [36] modified the protein environment of the photo-convertible EosFP and Dendra2 PCFPs to engineer bi-photochromic variants with differing properties.

In both positive and negative RSFPs, the exact order of events and the presence of intermediate states along the reaction pathway have been investigated. Because of its high quantum yield (~0.5), the back switching reaction in Dronpa could be experimentally interrogated by ultrafast spectroscopy. ESPT to an intermediate state I was proposed to occur, consistent with the observation of a significant kinetic isotope effect (KIE) using deuterated samples [18]. In line with this view, theoretical calculations proposed that isomerization and deprotonation events during Dronpa off-on switching are concerted [21]. This view is also consistent with the elegant theoretical model of Olsen et al. [57], which suggests that to promote efficient photoswitching, the protein environment should restrict torsion around the methylene phenoxy bond (P-bond) and promote torsion around the imidazolinone bond (I-bond) through suitable acid–base chemistry. However, these findings were recently questioned by a Fourier Transform infrared study (FTIR) in which a *cis* protonated ground state intermediate was evidenced, strongly suggesting that deprotonation of the chromophore rather occurs as a subsequent step to isomerization [23]. These contradictory observations show that the interpretation of ultrafast spectroscopic data is a delicate issue and corroborates the fact that many interrelated factors control photoswitching in RSFPs, the exact roles of which are difficult to disentangle. Moreover, hidden processes may take place and further complicate the matter: as an example, the recent study of Gayda et al. [45] on a mutant of IrisFP (called mIrisGFP) revealed that the neutral *cis* chromophore of mIrisGFP can isomerize to the neutral *trans* state much more efficiently than the anionic *cis* chromophore (consistent with a barrierless mechanism predicted by the Olsen model [57]). This phenomenon however typically remains unnoticed, as back switching by the same illumination wavelength (405 nm) is even more efficient, bringing back the neutral *trans* chromophore "immediately" to the *cis* configuration. Several different switching processes may thus occur in parallel, even if at the ensemble level the spectroscopic footprint remains steady. Overall, the precise photoswitching mechanism of negative RSFPs still remains to be elucidated completely.

In positive RSFPs, work has been done on Padron and asFP595. A study of the asFP595-Ala143Ser mutant (displaying an enhanced fluorescence quantum yield) by molecular dynamics suggested that on-switching was linked to chromophore *trans–cis* isomerization via a Hula-Twist mechanism, in which both I and P bonds change in a concerted manner to minimize the volume swept by the chromophore during switching [14]. This view is however difficult to reconcile with the Olsen theory of isomerization through I-bond flip. *Ab initio* calculations and QC/MM molecular dynamics simulations in asFP595 suggested that *trans–cis* isomerization occurs in the neutral state of the chromophore, followed by a dark state equilibration to a zwitterionic fluorescent *cis* state [27]. In Padron, a different scenario was observed: two fluorescent intermediates

along the on-switching pathway could be cryo-trapped [47]. The combined spectroscopic and crystallographic data suggested that *trans–cis* isomerization of the chromophore occurs entirely in the anionic state and precedes protonation. These experimental findings are in line with the latest results by FTIR in Dronpa [23]. They are also interesting in terms of structural protein dynamics. First, they reveal that full *trans–cis* isomerization of the Padron chromophore is possible at 100 K, a temperature at which protein dynamical breathing is essentially stalled. As heat dissipation upon photon absorption occurs on the picosecond timescale, a transiently "hot" chromophore could account for this observation. Second, it was observed that protonation of the chromophore following isomerization only took place above the glass transition temperature (~200 K), suggesting that protonation involves exchange with the surrounding solvent. The fact that Padron can be efficiently photoswitched at cryo-temperature opens interesting potential applications such as cryo-nanoscopy [47].

Overall, as for negative RSFPs, the mechanisms governing fluorescence switching in positive RSFPs are still not entirely understood. The extent by which these mechanisms differ between members of each family also remains to be evaluated.

4.4 Hydrozoan RSFPs

Surprisingly little structural information is available on RSFPs evolved from GFP derivatives. Amongst several pieces of indirect evidence, studies by vibrational spectroscopy [58] suggest that a chromophore *cis–trans* isomerization process similar to that found in Anthozoan RSFPs also takes place in these proteins. However structural evidence for a *trans* chromophore in Hydrozoan RSFPs is still lacking.

4.5 Decoupled Switching in Hydrozoan RSFPs: Dreiklang

Positive and negative RSFPs are not optimal in that laser-light used for fluorescence excitation also induces switching. The protein Dreiklang, evolved from the GFP variant Citrine, nicely overcomes this problem [40]. In Dreiklang, excitation at 514 nm does not induce significant off-switching, whereas near UV-light at 365 and 405 nm result in on and off switching, respectively. The existence of such decoupling had already been hinted at in previous experiments with EYFP [10, 41]. In Dreiklang, this behavior was deliberately exacerbated by random mutagenesis, resulting in an unprecedented switching mechanism. Combined crystallographic and mass spectroscopy analyzes provided evidence that light-induced hydration-dehydration of the chromophore caused switching by disrupting the π-conjugated electron system (Fig. 5). Hydration of the C_{65} atom of the imidazolinone moiety appeared to be facilitated by the proper positioning of a water molecule (Wat_A) held in place by hydrogen bonding between Tyr203 and Glu222 and putatively replaced in the switched-off state by another water molecule (Wat_B) garnered from the environment. However, the exact roles of the 4 mutations (Val61Leu, Phe64Ile, Tyr145His,

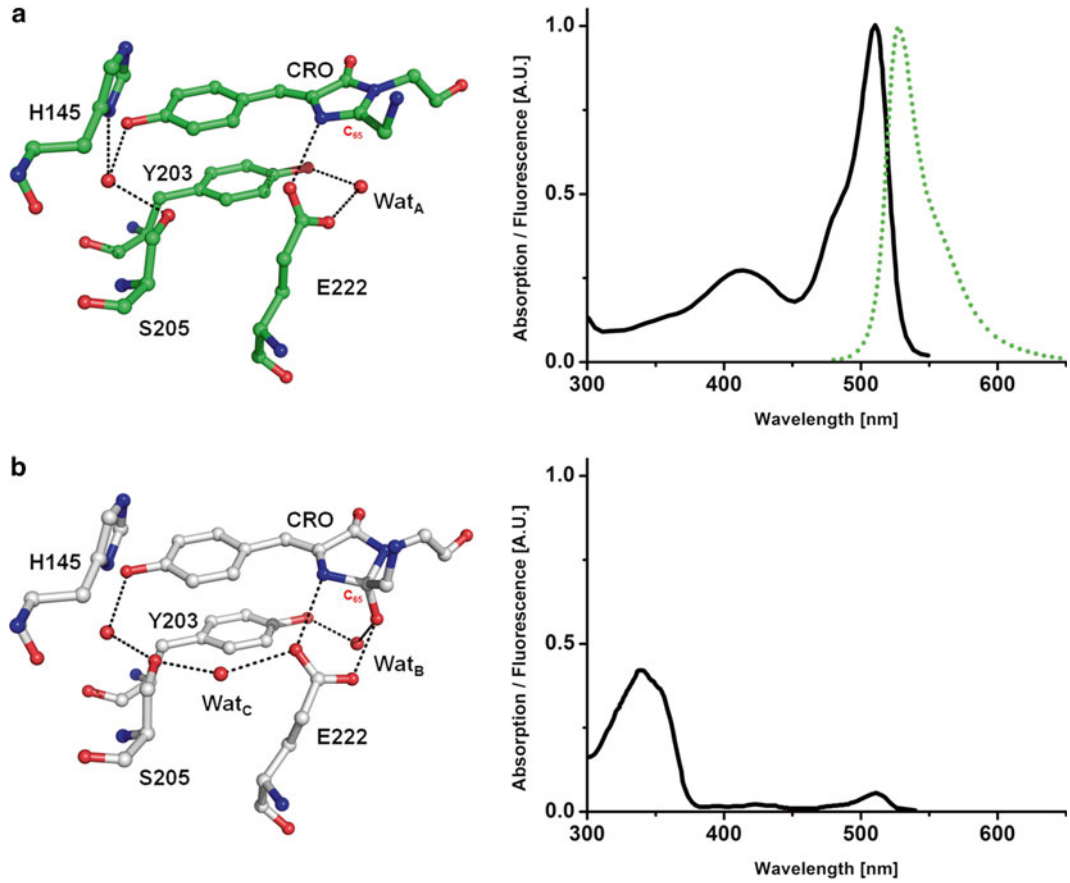

Fig. 5 Crystallographic structures of the chromophore, its microenvironment, and the corresponding spectra for Dreiklang. (**a**) In the more stable fluorescent state (PDB ID 3ST4), the chromophore adopts a *cis* conformation and is deprotonated as observable by the major anionic absorption band peaking at 515 nm (*black spectrum*) that provides fluorescence at 529 nm (*green dotted spectrum*). (**b**) In the dark state (PDB ID 3ST3) the water molecule Wat_A is found to hydrate the carbon C_{65}, distorting the geometry of the imidazolinone ring. Absorption spectra reveal that both the neutral and the anionic forms have been converted to a blue-shifted absorption band peaking at 340 nm. Water molecules are represented as *red balls* and hydrogen bonds are represented as *black dotted lines*

and Asn146Asp) relative to Citrine remain to be established. Also, the use of UV-light to induce on- and off-switching is prone to generate cytotoxicity. It is also not clear yet how the hydration/dehydration processes can be light-activated in the protonated state of the chromophore.

5 Using RSFPs in Advanced Fluorescence Applications

Many exciting fields of science are nowadays explored by using photoswitchable fluorescent proteins, including super-resolution fluorescence microscopy (*see* Chapter 16 of this volume),

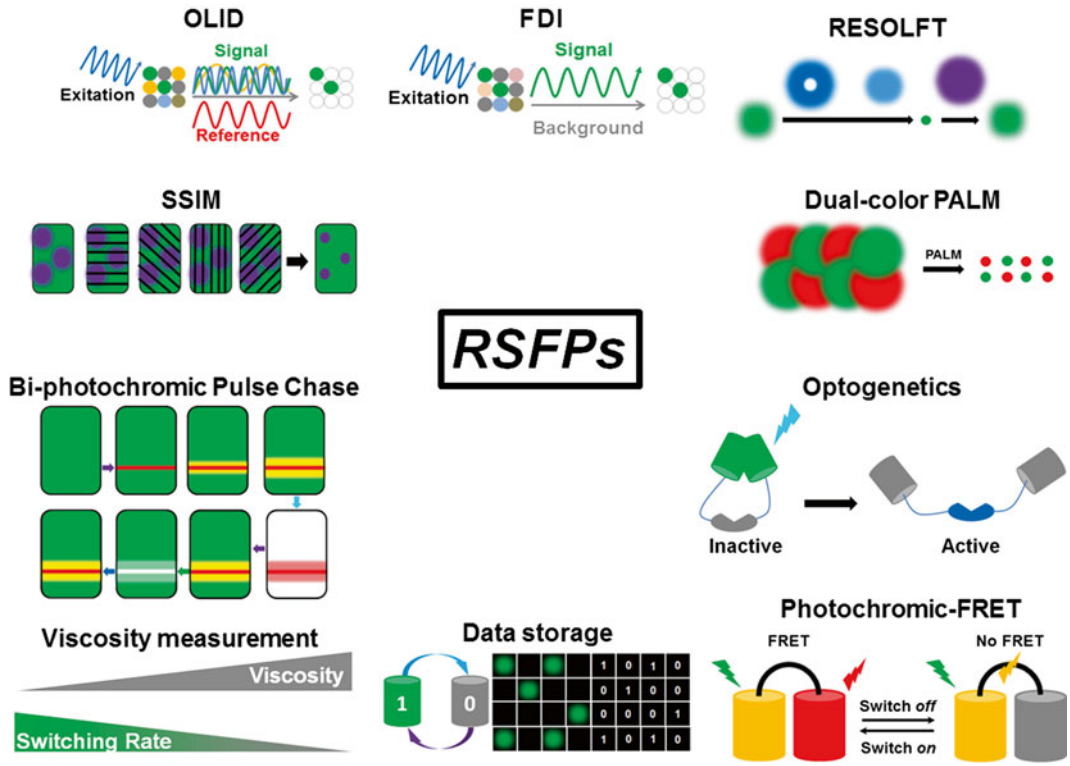

Fig. 6 Panoply of possible applications using RSFPs in super-resolution imaging and biotechnology. *OLID* optical lock-in detection, *FDI* frequency domain imaging

optogenetics, optical lock-in detection, frequency-domain imaging, sensor developments and biotechnological applications (Fig. 6). Some examples are described below.

5.1 Super-Resolution Fluorescence Microscopy by Single Molecule Localization

Single molecule localization microscopy (SMLM) was developed in 2006 with techniques such as photoactivated localization microscopy (PALM) [59, 60] and stochastic optical reconstruction microscopy (STORM) [61]. These super-resolution techniques are conceptually identical but use either phototransformable FPs (PALM) or blinking organic dyes (STORM) as highlighters. SMLM is nowadays very popular in that it does not require a complex instrumental setup and provides the best spatial resolutions currently achievable. Irreversible photoconvertible FPs are generally preferred for PALM applications over RSFPs because they typically emit more photons per localized spot and are less prone to complications due to multiple localizations of a single molecule. Multicolor PALM, however, is difficult to achieve with PCFPs only, as currently available members do not display a large spectral separation. A solution to this problem has been found by achieving dual-labeling with a green-to-red PCFP such as EosFP and an RSFP such as Dronpa. The method relies on a sequential acquisition protocol: all EosFP molecules are first photoconverted to

their red-emitting state by 405-nm irradiation and detected by 561-nm illumination with minimal effects on the Dronpa molecules that are visualized subsequently with alternating 488 and 405-nm illumination. This protocol succeeded in colocalizing a variety of proteins of interest [62, 63].

Interestingly, the rich photophysics of RSFPs also allow acquiring dual-labeling "false-multicolor" PALM data [30]. This can be accomplished by distinguishing RSFPs variants of similar colors based on properties such as positive vs. negative switching, or different photoswitching rates.

The capacity of RSFPs to produce intense fluctuations of their emission signal recently permitted their application into a variant of SMLM called stochastic optical fluctuation imaging (SOFI) (*see* Chapter 17 of this volume). In its standard version, SOFI takes advantage of natural fluorescence flickering to enhance image resolution [64]. Photochromic SOFI (pcSOFI) [65] demonstrates improved signal-to-noise contrast and a two- to threefold enhancement of the spatial resolution compared to diffraction-limited images, thanks to the possibility of precisely controlling the "flickering" (switching) of RSFPs.

5.2 Nonlinear Microscopy Applications

RSFPs can be advantageously used in nonlinear imaging because the saturation of their switching transitions leads to distinct minima/maxima of fluorescence depending on the illumination pattern, even with low light intensities.

In confocal illumination mode, the concept of REversible Saturable Optical Linear Fluorescence Transitions (RESOLFT) [66] has been proposed as an alternative to the well-known STimulated Emission Depletion (STED) microscopy. In STED, a donut-shaped laser spot applied immediately after excitation by a diffraction-limited laser spot depletes emission of a standard fluorophore except for the central zero-intensity region of the donut beam. The diameter of the resulting effective point spread function decreases with increasing intensities of the donut-shaped beam, thus providing enhanced resolution. However, an enormous power density is required for this beam (typically MW/cm^2). Instead, when RESOLFT is used in combination with RSFPs [67, 68], the donut-shaped beam serves to switch off the label, a process which is not limited by the fluorescence lifetime. Thus, albeit at the expense of a reduced time-resolution, this allows a huge decrease (up to six orders of magnitude) of the light intensity needed to break the diffraction barrier as compared to STED microscopy. This considerably reduces potential cytotoxic effects.

Increasing spatial resolution in RESOLFT implies achieving a higher number of switching cycles of the RSFP, while improving time resolution requires higher switching yields. The engineering of the well-known EGFP into rsEGFP [38] created an RSFP with much faster photoswitching rates than Dronpa and with a much

enhanced photoresistance, comparable to that of its parent EGFP. Recent modifications of this variant resulted in an even faster RSFP, named rsEGFP2, in which, as compared to rsEGFP, the mutations Val150Ala and Ser205Asn have been back-mutated and the first amino acid of the chromophore was modified (Thr65Ala) [39]. RsEGFP2 allows the application of RESOLFT microscopy with no more light than in conventional confocal microscopy and at unprecedented speed.

Similarly, very weak illumination intensities can be used when RSFPs are employed in combination with Saturated Structured Illumination Microscopy (SSIM), a nonlinear version of SIM [69]. In this wide-field imaging technique, the sample is illuminated with a sine-shaped wavefront (structured illumination) that is modulated in phase and angle. From the interferences between the patterned illumination and the spatial response of the fluorescent sample (Moiré fringes) a resolution increase by a factor of 2 can be achieved. To push the resolution further with standard fluorophores, very intense illumination is required to saturate the singlet excited state S_1, producing sharp fluorescent fringes. The use of RSFPs such as Dronpa relies on saturating the long-lived off state instead of the short-lived S_1, alleviating the need for high intensities [70].

5.3 Advanced Microscopy and Biotechnology with Bi-photochromic FPs

Biphotochromic FPs combine the photophysical properties of both PCFPs and RSFPs into single PTFPs. IrisFP [35] was the first member of this family: it can be irreversibly photoconverted from green to red and reversibly switched off in either the green or the red state. The monomeric variant mIrisFP was successfully used as a tool for two-color super-resolved pulse-chase imaging experiments [71]. In this technique, a fraction of the molecules are first photoconverted to their red-emitting state and let to diffuse within the cell. Using photochromic-based PALM, both the unphotoconverted (green) and photoconverted (red) molecules are then tracked at nanometric precision. Improved biphotochromic variants have been recently engineered [36]. In particular, NijiFP is a variant of the monomeric PCFP Dendra2 and demonstrated promising properties: low tendency to oligomerize, good spectral contrast between green and red states, and excellent photoswitching capability of the two forms.

PTFPs have been used to demonstrate the concept of biological data-storage, possibly in 3D [72]. Notably, rsEGFP has been shown to provide a remarkable support for rewritable ultrahigh density data storage [38]. Biphotochromic FPs open the route to quaternary data storage applications. Photoconverting to the red state half of a biphotochromic FP substrate spread on a surface, it becomes possible to achieve four optical combinations by switching off or on the green and red molecules. A base-4 encoding system is obtained: dark + dark = 0, dark + green = 1, dark + red = 2, red + green = 3, equivalent in binary code to 00, 01, 10, and 11, respectively.

5.4 Optogenetics

The use of RSFPs in optogenetics was recently introduced as an exquisite tool to control specific cellular activities through reversible photoswitching [54]. Dronpa is a monomeric RSFP, but it was derived from a tetrameric parent. A single mutant of Dronpa (Lys145Asn), called PDM1-4 [73], was shown to exhibit a propensity to tetramerize in the switched-on state, whereas it remains monomeric in the off state. The crystallographic structure of PDM1-4 revealed a rigidified tetramer interface, consistent with this finding [74]. A mixture of PDM1-4 and Dronpa was then shown to promote light-induced dimer-to-monomer conversion rather than tetramer-to-monomer conversion with PDM1-4 alone. The idea, then, consists in fusing a protein of interest (POI) at one end with PDM1-4 and at the other end with Dronpa. In the on-state, the two RSFP domains interact, "caging" the POI, while in their off state they split, restoring the POI activity. The method was applied to intersectin, a guanine nucleotide exchange factor that activates Cdc42. Upon 490-nm illumination, activation of Cdc42 by uncaged intersectin was monitored through the growth of filopodia, an obvious morphological change that was observed concomitantly with the disappearance of Dronpa fluorescence due to switching. Using the same concept, it was possible to design a light inducible NS3-4A protease in the hepatitis C virus (HCV).

5.5 Viscosity Sensing

The interrelation between Dronpa photoswitching and β-barrel plasticity allowed yet another surprising application of this RSFP, this time as a sensor for solvent viscosity. Hydrodynamic changes exerted on Dronpa by an increasing viscosity were found to reduce the photoswitching rate of its chromophore [55]. Moreover, the authors demonstrated that fast-switching variants and more specifically Dronpa[Val157Ile/Met159Ala], named Dronpa-3 [29], are especially sensitive to viscosity changes: the photoswitching rate of Dronpa-3 slowed down by a factor of 4 when the glycerol concentration was increased from 0 to 90 %. This makes Dronpa-3 an efficient genetically-encoded reporter for microviscosity in vivo as demonstrated in the case of chromatin: a slightly more viscous environment was repeatedly measured when cells were in mitosis.

5.6 Photochromic FRET (pcFRET)

The synthesis of photochromic organic fluorescent dyes allowed, a decade ago, the development of a novel approach for quantitative Förster resonance energy transfer (FRET) [75, 76]. In this photochromic FRET (pcFRET) approach, modulations of fluorescence emission by a donor molecule can be induced by reversible switching of a photochromic acceptor, allowing quantitative and repeatable determination of the FRET efficiency between two molecules without the need to apply corrections based on reference images.

The recent engineering of the red-shifted RSFPs rsCherryRev [77] and rsTagRFP [78] allowed the conception of similar pcFRET

experiments using solely genetically encoded reporters. Coupled to EYFP as a donor, rsTagRFP revealed to be an excellent photochromic acceptor [78] and allowed a precise quantification of protein–protein interactions within living cells.

6 Conclusion: Future Prospects for RSFPs

Reversibly switchable FPs are astonishing macromolecules that nowadays play a key role in state-of-the-art techniques based on light-induced protein manipulation.

In contrast to photoconvertible FPs that are found in nature, all RSFPs known so far are man-made, developed on the basis of FPs from both the Anthozoan and the Hydrozoan classes. Thus, there is probably little functional advantage to such switching capabilities in marine organisms. On the contrary, an incredibly wide palette of applications has already been found by researchers, in the fields of advanced fluorescence microscopy and biotechnology.

The mechanism underlying switching in RSFPs is generally based on *cis–trans* photoinduced isomerization of the chromophore coupled with a protonation change. However, there are subtle differences between members, and despite significant progress in the last years, reaction pathways and intermediate states possibly involved are still under debate.

An important aspect of future research in RSFPs photophysics will be to understand how blinking and bleaching, these phenomena that are so characteristic in all FPs, interfere with photoswitching. Although hints have been provided already [79, 80], these stochastic events are difficult to capture and characterize. Yet, they are fundamental in the quest for future optimization of RSFPs, together with other properties, such as red-shifted fluorescence or decoupled switching.

Our knowledge of fluorescent proteins is constantly growing. However, experience has shown that the complex architecture of the β-barrel and its links to the chromophore is intricate to a degree that success in developing improved variants on the basis of rational design alone has been so far the exception rather than the rule. It will be interesting to see if multi-residue rational design of a PTFP will eventually be successful, knowing that directed evolution approaches are currently bound to miss a large fraction of possible synergistic combinations of mutations.

Whatever the engineering approaches, surprising new properties will continue to emerge and, based on these, the palette of new RSFPs-based applications will continue to grow, so it is worth to stay tuned for amazing new developments.

References

1. Dedecker P, De Schryver FC, Hofkens J (2013) Fluorescent proteins: shine on, you crazy diamond. J Am Chem Soc 135(7):2387–2402. doi:10.1021/ja309768d
2. Chudakov DM, Matz MV, Lukyanov S, Lukyanov KA (2010) Fluorescent proteins and their applications in imaging living cells and tissues. Physiol Rev 90(3):1103–1163. doi:10.1152/physrev.00038.2009
3. Subach FV, Verkhusha VV (2012) Chromophore transformations in red fluorescent proteins. Chem Rev 112(7):4308–4327. doi:10.1021/cr2001965
4. Lippincott-Schwartz J, Patterson GH (2009) Photoactivatable fluorescent proteins for diffraction-limited and super-resolution imaging. Trends Cell Biol 19(11):555–565. doi:S0962-8924(09)00199-8 [pii]10.1016/j.tcb.2009.09.003
5. Bourgeois D, Adam V (2012) Reversible photoswitching in fluorescent proteins: a mechanistic view. IUBMB Life 64(6):482–491. doi:10.1002/iub.1023
6. Bourgeois D, Regis-Faro A, Adam V (2012) Photoactivated structural dynamics of fluorescent proteins. Biochem Soc Trans 40:531–538. doi:10.1042/bst20120002
7. Dickson RM, Cubitt AB, Tsien RY, Moerner WE (1997) On/off blinking and switching behaviour of single molecules of green fluorescent protein. Nature 388(6640):355–358
8. Sinnecker D, Voigt P, Hellwig N, Schaefer M (2005) Reversible photobleaching of enhanced green fluorescent proteins. Biochemistry 44(18):7085–7094
9. Nifosi R, Ferrari A, Arcangeli C, Tozzini V, Pellegrini V, Beltram F (2003) Photoreversible dark state in a tristable green fluorescent protein variant. J Phys Chem B 107(7):1679–1684. doi:10.1021/Jp0266852
10. McAnaney TB, Zeng W, Doe CF, Bhanji N, Wakelin S, Pearson DS, Abbyad P, Shi X, Boxer SG, Bagshaw CR (2005) Protonation, photobleaching, and photoactivation of yellow fluorescent protein (YFP 10C): a unifying mechanism. Biochemistry 44(14):5510–5524
11. Chudakov DM, Feofanov AV, Mudrik NN, Lukyanov S, Lukyanov KA (2003) Chromophore environment provides clue to "kindling fluorescent protein" riddle. J Biol Chem 278(9):7215–7219
12. Ando R, Mizuno H, Miyawaki A (2004) Regulated fast nucleocytoplasmic shuttling observed by reversible protein highlighting. Science 306(5700):1370–1373. doi:10.1126/science.1102506
13. Habuchi S, Ando R, Dedecker P, Verheijen W, Mizuno H, Miyawaki A, Hofkens J (2005) Reversible single-molecule photoswitching in the GFP-like fluorescent protein Dronpa. Proc Natl Acad Sci U S A 102(27):9511–9516
14. Andresen M, Wahl MC, Stiel AC, Grater F, Schafer LV, Trowitzsch S, Weber G, Eggeling C, Grubmuller H, Hell SW, Jakobs S (2005) Structure and mechanism of the reversible photoswitch of a fluorescent protein. Proc Natl Acad Sci U S A 102(37):13070–13074. doi:10.1073/pnas.0502772102
15. Andresen M, Stiel AC, Trowitzsch S, Weber G, Eggeling C, Wahl MC, Hell SW, Jakobs S (2007) Structural basis for reversible photoswitching in Dronpa. Proc Natl Acad Sci U S A 104(32):13005–13009. doi:10.1073/pnas.0700629104
16. Mizuno H, Mal TK, Walchli M, Kikuchi A, Fukano T, Ando R, Jeyakanthan J, Taka J, Shiro Y, Ikura M, Miyawaki A (2008) Light-dependent regulation of structural flexibility in a photochromic fluorescent protein. Proc Natl Acad Sci U S A 105(27):9227–9232. doi:0709599105 [pii] 10.1073/pnas.0709599105
17. Dedecker P, Hotta J, Ando R, Miyawaki A, Engelborghs Y, Hofkens J (2006) Fast and reversible photoswitching of the fluorescent protein Dronpa as evidenced by fluorescence correlation spectroscopy. Biophys J 91(5):L45–L47
18. Fron E, Flors C, Schweitzer G, Habuchi S, Mizuno H, Ando R, Schryver FC, Miyawaki A, Hofkens J (2007) Ultrafast excited-state dynamics of the photoswitchable protein Dronpa. J Am Chem Soc 129(16):4870–4871
19. Wilmann PG, Turcic K, Battad JM, Wilce MC, Devenish RJ, Prescott M, Rossjohn J (2006) The 1.7 A crystal structure of Dronpa: a photoswitchable green fluorescent protein. J Mol Biol 364(2):213–224
20. Stiel AC, Trowitzsch S, Weber G, Andresen M, Eggeling C, Hell SW, Jakobs S, Wahl MC (2007) 1.8 A bright-state structure of the reversibly switchable fluorescent protein Dronpa guides the generation of fast switching variants. Biochem J 402(1):35–42
21. Li X, Chung LW, Mizuno H, Miyawaki A, Morokuma K (2010) A theoretical study on the nature of on- and off-states of reversibly photoswitching fluorescent protein Dronpa: absorption, emission, protonation, and Raman. J Phys Chem B 114(2):1114–1126. doi:10.1021/jp909947c

22. Li X, Chung LW, Mizuno H, Miyawaki A, Morokuma K (2010) Primary events of photodynamics in reversible photoswitching fluorescent protein Dronpa. J Phys Chem Lett 1(23):3328–3333. doi:10.1021/Jz101419p
23. Warren MM, Kaucikas M, Fitzpatrick A, Champion P, Timothy Sage J, van Thor JJ (2013) Ground-state proton transfer in the photoswitching reactions of the fluorescent protein Dronpa. Nat Commun 4:1461. http://www.nature.com/ncomms/journal/v4/n2/suppinfo/ncomms2460_S1.html
24. Quillin ML, Anstrom DM, Shu X, O'Leary S, Kallio K, Chudakov DM, Remington SJ (2005) Kindling fluorescent protein from Anemonia sulcata: dark-state structure at 1.38 A resolution. Biochemistry 44(15): 5774–5787
25. Schüttrigkeit TA, von Feilitzsch T, Kompa CK, Lukyanov KA, Savitsky AP, Voityuk AA, Michel-Beyerle ME (2006) Femtosecond study of light-induced fluorescence increase of the dark chromoprotein asFP595. Chem Phys 323(2–3):149–160. doi:10.1016/j.chemphys.2005.09.039
26. Schafer LV, Groenhof G, Klingen AR, Ullmann GM, Boggio-Pasqua M, Robb MA, Grubmuller H (2007) Photoswitching of the fluorescent protein asFP595: mechanism, proton pathways, and absorption spectra. Angew Chem Int Ed 46(4):530–536
27. Schafer LV, Groenhof G, Boggio-Pasqua M, Robb MA, Grubmuller H (2008) Chromophore protonation state controls photoswitching of the fluoroprotein asFP595. PLoS Comput Biol 4(3):e1000034. doi:10.1371/journal.pcbi.1000034
28. Grigorenko BL, Polyakov IV, Savitsky AP, Nemukhin AV (2013) Unusual emitting states of the kindling fluorescent protein: appearance of the cationic chromophore in the GFP family. J Phys Chem B 117(24):7228–7234. doi:10.1021/jp402149q
29. Ando R, Flors C, Mizuno H, Hofkens J, Miyawaki A (2007) Highlighted generation of fluorescence signals using simultaneous two-color irradiation on Dronpa mutants. Biophys J 92(12):L97–L99. doi:biophysj.107.105882 [pii] 10.1529/biophysj.107.105882
30. Andresen M, Stiel AC, Folling J, Wenzel D, Schonle A, Egner A, Eggeling C, Hell SW, Jakobs S (2008) Photoswitchable fluorescent proteins enable monochromatic multilabel imaging and dual color fluorescence nanoscopy. Nat Biotechnol 26(9):1035–1040. doi:nbt.1493 [pii] 10.1038/nbt.1493
31. Henderson JN, Ai HW, Campbell RE, Remington SJ (2007) Structural basis for reversible photobleaching of a green fluorescent protein homologue. Proc Natl Acad Sci U S A 104(16):6672–6677
32. Subach FV, Zhang L, Gadella TW, Gurskaya NG, Lukyanov KA, Verkhusha VV (2010) Red fluorescent protein with reversibly photoswitchable absorbance for photochromic FRET. Chem Biol 17(7):745–755. doi:10.1016/j.chembiol.2010.05.022 S1074-5521(10)00213-9 [pii]
33. Pletnev S, Subach FV, Dauter Z, Wlodawer A, Verkhusha VV (2012) A structural basis for reversible photoswitching of absorbance spectra in red fluorescent protein rsTagRFP. J Mol Biol 417(3):144–151. doi:10.1016/j.jmb.2012.01.044
34. Chang H, Zhang M, Ji W, Chen J, Zhang Y, Liu B, Lu J, Zhang J, Xu P, Xu T (2012) A unique series of reversibly switchable fluorescent proteins with beneficial properties for various applications. Proc Natl Acad Sci U S A 109(12):4455–4460. doi:10.1073/pnas.1113770109
35. Adam V, Lelimousin M, Boehme S, Desfonds G, Nienhaus K, Field MJ, Wiedenmann J, McSweeney S, Nienhaus GU, Bourgeois D (2008) Structural characterization of IrisFP, an optical highlighter undergoing multiple photo-induced transformations. Proc Natl Acad Sci USA 105(47):18343–18348. doi:0805949105 [pii] 10.1073/pnas.0805949105
36. Adam V, Moeyaert B, David CC, Mizuno H, Lelimousin M, Dedecker P, Ando R, Miyawaki A, Michiels J, Engelborghs Y, Hofkens J (2011) Rational design of photoconvertible and biphotochromic fluorescent proteins for advanced microscopy applications. Chem Biol 18(10):1241–1251. doi:10.1016/j.chembiol.2011.08.007
37. Bizzarri R, Serresi M, Cardarelli F, Abbruzzetti S, Campanini B, Viappiani C, Beltram F (2010) Single amino acid replacement makes Aequorea victoria fluorescent proteins reversibly photoswitchable. J Am Chem Soc 132(1):85–95. doi:10.1021/ja9014953
38. Grotjohann T, Testa I, Leutenegger M, Bock H, Urban NT, Lavoie-Cardinal F, Willig KI, Eggeling C, Jakobs S, Hell SW (2011) Diffraction-unlimited all-optical imaging and writing with a photochromic GFP. Nature 478(7368):204–208. doi:10.1038/nature10497
39. Grotjohann T, Testa I, Reuss M, Brakemann T, Eggeling C, Hell SW, Jakobs S (2012) rsEGFP2 enables fast RESOLFT nanoscopy of living cells. ELife 1 1:e00248. doi:10.7554/eLife.00248.00001
40. Brakemann T, Stiel AC, Weber G, Andresen M, Testa I, Grotjohann T, Leutenegger M, Plessmann U, Urlaub H, Eggeling C, Wahl MC, Hell SW, Jakobs S (2011) A reversibly

photoswitchable GFP-like protein with fluorescence excitation decoupled from switching. Nat Biotechnol 29(10):942–947. doi:10.1038/nbt.1952

41. Faro AR, Adam V, Carpentier P, Darnault C, Bourgeois D, de Rosny E (2010) Low-temperature switching by photoinduced protonation in photochromic fluorescent proteins. Photochem Photobiol Sci 9(2):254–262. doi:10.1039/b9pp00121b
42. Bourgeois D, Royant A (2005) Advances in kinetic protein crystallography. Curr Opin Struct Biol 15(5):538–547. doi:S0959-440X(05)00150-8 [pii] 10.1016/j.sbi.2005.08.002
43. Royant A, Carpentier P, Ohana J, McGeehan J, Paetzold B, Noirclerc-Savoye M, Vernede X, Adam V, Bourgeois D (2007) Advances in spectroscopic methods for biological crystals. 1. Fluorescence lifetime measurements. J Appl Cryst 40:1105–1112. doi:10.1107/S0021889807044196
44. Carpentier P, Royant A, Ohana J, Bourgeois D (2007) Advances in spectroscopic methods for biological crystals. 2. Raman spectroscopy. J Appl Cryst 40:1113–1122. doi:10.1107/S0021889807044202
45. Gayda S, Nienhaus K, Nienhaus GU (2012) Mechanistic insights into reversible photoactivation in proteins of the GFP family. Biophys J 103(12):2521–2531
46. Adam V, Nienhaus K, Bourgeois D, Nienhaus GU (2009) Structural basis of enhanced photoconversion yield in green fluorescent protein-like protein dendra2. Biochemistry 48(22):4905–4915. doi:10.1021/bi900383a
47. Faro AR, Carpentier P, Jonasson G, Pompidor G, Arcizet D, Demachy I, Bourgeois D (2011) Low-temperature chromophore isomerization reveals the photoswitching mechanism of the fluorescent protein Padron. J Am Chem Soc 133(41):16362–16365. doi:10.1021/ja207001y
48. Fang C, Frontiera RR, Tran R, Mathies RA (2009) Mapping GFP structure evolution during proton transfer with femtosecond Raman spectroscopy. Nature 462(7270):200–204. doi:10.1038/nature08527
49. Chapman HN, Fromme P, Barty A, White TA, Kirian RA, Aquila A, Hunter MS, Schulz J, DePonte DP, Weierstall U, Doak RB, Maia FR, Martin AV, Schlichting I, Lomb L, Coppola N, Shoeman RL, Epp SW, Hartmann R, Rolles D, Rudenko A, Foucar L, Kimmel N, Weidenspointner G, Holl P, Liang M, Barthelmess M, Caleman C, Boutet S, Bogan MJ, Krzywinski J, Bostedt C, Bajt S, Gumprecht L, Rudek B, Erk B, Schmidt C, Homke A, Reich C, Pietschner D, Struder L, Hauser G, Gorke H, Ullrich J, Herrmann S, Schaller G, Schopper F, Soltau H, Kuhnel KU, Messerschmidt M, Bozek JD, Hau-Riege SP, Frank M, Hampton CY, Sierra RG, Starodub D, Williams GJ, Hajdu J, Timneanu N, Seibert MM, Andreasson J, Rocker A, Jonsson O, Svenda M, Stern S, Nass K, Andritschke R, Schroter CD, Krasniqi F, Bott M, Schmidt KE, Wang X, Grotjohann I, Holton JM, Barends TR, Neutze R, Marchesini S, Fromme R, Schorb S, Rupp D, Adolph M, Gorkhover T, Andersson I, Hirsemann H, Potdevin G, Graafsma H, Nilsson B, Spence JC (2011) Femtosecond X-ray protein nanocrystallography. Nature 470(7332):73–77. doi:10.1038/nature09750
50. Yang JS, Huang GJ, Liu YH, Peng SM (2008) Photoisomerization of the green fluorescence protein chromophore and the meta- and para-amino analogues. Chem Commun (Camb) 11:1344–1346. doi:10.1039/b717714c
51. Pletnev S, Shcherbo D, Chudakov DM, Pletneva N, Merzlyak EM, Wlodawer A, Dauter Z, Pletnev V (2008) A crystallographic study of bright far-red fluorescent protein mKate reveals pH-induced cis-trans isomerization of the chromophore. J Biol Chem 283(43):28980–28987. doi:M800599200 [pii] 10.1074/jbc.M800599200
52. Violot S, Carpentier P, Blanchoin L, Bourgeois D (2009) Reverse pH-dependence of chromophore protonation explains the large stokes shift of the red fluorescent protein mKeima. J Am Chem Soc 131(30):10356–10357. doi:10.1021/ja903695n
53. Petersen J, Wilmann PG, Beddoe T, Oakley AJ, Devenish RJ, Prescott M, Rossjohn J (2003) The 2.0-A crystal structure of eqFP611, a far red fluorescent protein from the sea anemone Entacmaea quadricolor. J Biol Chem 278(45):44626–44631
54. Zhou XX, Chung HK, Lam AJ, Lin MZ (2012) Optical control of protein activity by fluorescent protein domains. Science 338(6108):810–814. doi:10.1126/science.1226854
55. Kao Y-T, Zhu X, Min W (2012) Protein-flexibility mediated coupling between photoswitching kinetics and surrounding viscosity of a photochromic fluorescent protein. Proc Natl Acad Sci U S A. doi:10.1073/pnas.1115311109
56. Brakemann T, Weber G, Andresen M, Groenhof G, Stiel AC, Trowitzsch S, Eggeling C, Grubmuller H, Hell SW, Wahl MC, Jakobs S (2010) Molecular basis of the light-driven switching of the photochromic fluorescent protein Padron. J Biol Chem 285(19):14603–14609. doi:M109.086314 [pii] 10.1074/jbc.M109.086314

57. Olsen S, Lamothe K, Martinez TJ (2010) Protonic gating of excited-state twisting and charge localization in GFP chromophores: a mechanistic hypothesis for reversible photoswitching. J Am Chem Soc 132(4):1192–1193. doi:10.1021/ja907447k
58. Luin S, Voliani V, Lanza G, Bizzarri R, Amat P, Tozzini V, Serresi M, Beltram F (2009) Raman study of chromophore states in photochromic fluorescent proteins. J Am Chem Soc 131(1):96–103. doi:10.1021/ja804504b 10.1021/ja804504b [pii]
59. Betzig E, Patterson GH, Sougrat R, Lindwasser OW, Olenych S, Bonifacino JS, Davidson MW, Lippincott-Schwartz J, Hess HF (2006) Imaging intracellular fluorescent proteins at nanometer resolution. Science 313(5793):1642–1645
60. Hess ST, Girirajan TP, Mason MD (2006) Ultra-high resolution imaging by fluorescence photoactivation localization microscopy. Biophys J 91(11):4258–4272
61. Rust MJ, Bates M, Zhuang X (2006) Sub-diffraction-limit imaging by stochastic optical reconstruction microscopy (STORM). Nat Methods 3(10):793–796
62. Shroff H, Galbraith CG, Galbraith JA, White H, Gillette J, Olenych S, Davidson MW, Betzig E (2007) Dual-color superresolution imaging of genetically expressed probes within individual adhesion complexes. Proc Natl Acad Sci U S A 104(51):20308–20313. doi:10.1073/pnas.0710517105
63. Hsu CJ, Baumgart T (2011) Spatial association of signaling proteins and F-actin effects on cluster assembly analyzed via photoactivation localization microscopy in T cells. PLoS One 6(8):e23586. doi:10.1371/journal.pone.0023586
64. Dertinger T, Colyer R, Iyer G, Weiss S, Enderlein J (2009) Fast, background-free, 3D super-resolution optical fluctuation imaging (SOFI). Proc Natl Acad Sci U S A 106(52):22287–22292. doi:10.1073/pnas.0907866106
65. Dedecker P, Mo GCH, Dertinger T, Zhang J (2012) Widely accessible method for superresolution fluorescence imaging of living systems. Proc Natl Acad Sci U S A 109(27):10909–10914. doi:10.1073/pnas.1204917109
66. Hell SW, Dyba M, Jakobs S (2004) Concepts for nanoscale resolution in fluorescence microscopy. Curr Opin Neurobiol 14(5):599–609
67. Dedecker P, Hotta J, Flors C, Sliwa M, Uji-i H, Roeffaers MB, Ando R, Mizuno H, Miyawaki A, Hofkens J (2007) Subdiffraction imaging through the selective donut-mode depletion of thermally stable photoswitchable fluorophores: numerical analysis and application to the fluorescent protein Dronpa. J Am Chem Soc 129(51):16132–16141. doi:10.1021/ja076128z
68. Hofmann M, Eggeling C, Jakobs S, Hell SW (2005) Breaking the diffraction barrier in fluorescence microscopy at low light intensities by using reversibly photoswitchable proteins. Proc Natl Acad Sci U S A 102(49):17565–17569
69. Gustafsson MG (2005) Nonlinear structured-illumination microscopy: wide-field fluorescence imaging with theoretically unlimited resolution. Proc Natl Acad Sci U S A 102(37):13081–13086. doi:10.1073/pnas.0406877102
70. Rego EH, Shao L, Macklin JJ, Winoto L, Johansson GA, Kamps-Hughes N, Davidson MW, Gustafsson MG (2011) Nonlinear structured-illumination microscopy with a photoswitchable protein reveals cellular structures at 50-nm resolution. Proc Natl Acad Sci U S A 109:E135–E143. doi:10.1073/pnas.1107547108
71. Fuchs J, Bohme S, Oswald F, Hedde PN, Krause M, Wiedenmann J, Nienhaus GU (2010) A photoactivatable marker protein for pulse-chase imaging with superresolution. Nat Methods 7(8):627–630. doi:10.1038/nmeth.1477
72. Adam V, Mizuno H, Grichine A, Hotta JI, Yamagata Y, Moeyaert B, Nienhaus GU, Miyawaki A, Bourgeois D, Hofkens J (2010) Data storage based on photochromic and photoconvertible fluorescent proteins. J Biotechnol 4(6):377–390. doi:S0168-1656(10)00186-0 [pii] 10.1016/j.jbiotec.2010.04.001
73. Mizuno H, Dedecker P, Ando R, Fukano T, Hofkens J, Miyawaki A (2010) Higher resolution in localization microscopy by slower switching of a photochromic protein. Photochem Photobiol Sci 9(2):239–248. doi:10.1039/b9pp00124g
74. Nguyen Bich N, Moeyaert B, Van Hecke K, Dedecker P, Mizuno H, Hofkens J, Van Meervelt L (2012) Structural basis for the influence of a single mutation K145N on the oligomerization and photoswitching rate of Dronpa. Acta Crystallogr D Biol Crystallogr 68(12):1653–1659. doi:10.1107/s0907444912039686
75. Giordano L, Jovin TM, Irie M, Jares-Erijman EA (2002) Diheteroarylethenes as thermally stable photoswitchable acceptors in photochromic fluorescence resonance energy transfer (pcFRET). J Am Chem Soc 124(25):7481–7489
76. Song L, Jares-Erijman EA, Jovin TM (2002) A photochromic acceptor as a reversible light-driven switch in fluorescence resonance energy transfer (FRET). J Photochem Photobiol Chem 150:177–185
77. Stiel AC, Andresen M, Bock H, Hilbert M, Schilde J, Schonle A, Eggeling C, Egner A, Hell SW, Jakobs S (2008) Generation of monomeric

reversibly switchable red fluorescent proteins for far-field fluorescence nanoscopy. Biophys J 95(6):2989–2997.doi:doi:biophysj.108.130146 [pii] 10.1529/biophysj.108.130146

78. Subach OM, Malashkevich VN, Zencheck WD, Morozova KS, Piatkevich KD, Almo SC, Verkhusha VV (2010) Structural characterization of acylimine-containing blue and red chromophores in mTagBFP and TagRFP fluorescent proteins. Chem Biol 17(4):333–341. doi:S1074-5521(10)00086-4 [pii] 10.1016/j.chembiol.2010.03.005
79. Adam V, Carpentier P, Violot S, Lelimousin M, Darnault C, Nienhaus GU, Bourgeois D (2009) Structural basis of X-ray-induced transient photobleaching in a photoactivatable green fluorescent protein. J Am Chem Soc 131(50):18063–18065. doi:10.1021/ja907296v
80. Roy A, Field MJ, Adam V, Bourgeois D (2011) The nature of transient dark states in a photoactivatable fluorescent protein. J Am Chem Soc 133(46):18586–18589. doi:10.1021/ja2085355
81. Lukyanov KA, Fradkov AF, Gurskaya NG, Matz MV, Labas YA, Savitsky AP, Markelov ML, Zaraisky AG, Zhao X, Fang Y, Tan W, Lukyanov SA (2000) Natural animal coloration can be determined by a nonfluorescent green fluorescent protein homolog. J Biol Chem 275(34):25879–25882
82. Abbruzzetti S, Grandi E, Viappiani C, Bologna S, Campanini B, Raboni S, Bettati S, Mozzarelli A (2005) Kinetics of acid-induced spectral changes in the GFPmut2 chromophore. J Am Chem Soc 127(2):626–635. doi:10.1021/ja045400r

CHAPTER 3

Conclusion and Perspectives

3.1. Conclusion

In 2011, little was known about the photobleaching mechanisms of fluorescent proteins. During this thesis, we extensively studied the photobleaching mechanisms of one specific RSFP (IrisFP) and, based on the results, rationally engineered a more photostable variant. Our data suggests a general photobleaching mechanism in Anthozoan PTFPs.

By combining X-ray crystallography, mass spectrometry, optical *in crystallo* spectroscopy and modeling approaches, we successfully revealed two completely different photobleaching mechanisms in IrisFP (**Fig15.**). Depending on the intensity of the excitation light, IrisFP can be photobleached by two different mechanisms. Under relatively intense excitation (~100W/cm² in this study, approaching that of PALM microscopy), photobleaching occurs via an oxygen-independent pathway. The photobleached structure shows that the chromophore and its surrounding residues are dramatically altered. The loss of chromophore fluorescence resulted from an sp^2-to-sp^3 hybridization change of the Cα atom of the chromophore methylene bridge. Together with this hybridization change, decarboxylation of the highly conserved Glu212 (IrisFP numbering) occurs, followed by an extensive rearrangement of the H-bond network surrounding the chromophore. Under low excitation illumination (~10W/cm² in this study, typical of standard widefield fluorescence imaging), an oxygen-dependent photobleaching pathway dominates. In contrast to high-intensity illumination, there are very few structural modifications. The major modification is that next to the chromophore, Met159 -a highly conserved residue in Anthozoan PTFPs- becomes sulfoxided. The triplet excited state of the chromophore can interact with dissolved molecular oxygen within the chromophore pocket, forming singlet oxygen. This singlet oxygen in turn may diffuse to the nearby Met159 that undergoes a sulfoxidation reaction. The sulfoxided Met159 creates a new strong H-bond to the chromophore hydroxybenzylidene moiety and traps the chromophore in a permanent protonated and hence non-fluorescent state. Due to the very high sequence and structure similarity to other Anthozoan PTFPs such as Dronpa, EosFP and Dendra derivatives, this two-regime photobleaching mechanism could be a common phenomenon within these protein families. From our results we make a somewhat counterintuitive prediction that at constant integrated illumination dose, perhaps less cytotoxicity could be produced because under high-intensity illumination, less reactive oxygen species are likely to be generated and released.

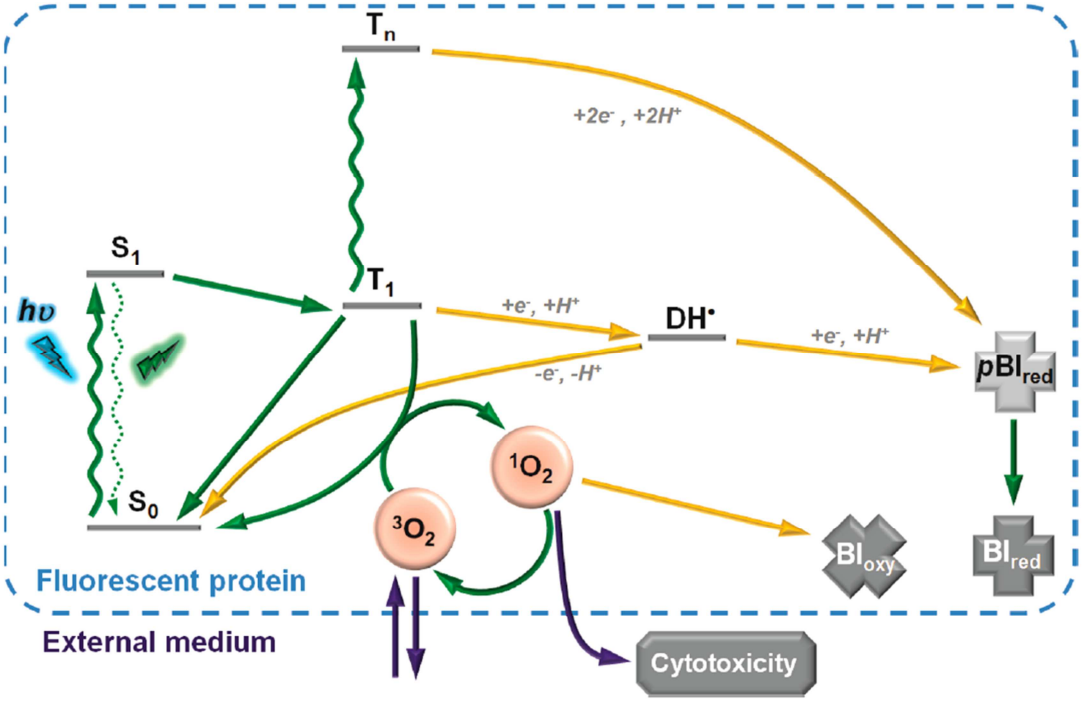

Fig15. *Proposed photophysical scheme for a two-regime photobleaching in IrisFP. Yellow arrows represent chemical steps involving electron/proton transfer or oxidation reactions. Blue arrows represent entry/exit of oxygen species.*

Based on our previous results on the IrisFP photobleaching mechanism, we rationally designed the IrisFP-M159A mutant in order to increase photoresistance against photofatigue under low-intensity illumination conditions. We obtained its native crystallographic structure and photophysically characterized IrisFP-M159A. We also investigated its photoswitching behavior and observed enhanced photoresistance in solution, in polyvinyl alcohol (PVA) gel, in fixed *E.coli* cells and in live *E.coli* cells compared to the parent protein IrisFP.

By characterizing the photophysical properties of the mutant, we found that compared to the parent, it has a lower pKa (4.7 vs. 5.7), as well as slightly blue-shifted excitation and emission maxima at 484 nm and 513 nm, respectively. However it has a lower fluorescence quantum yield and brightness.

As expected, our IrisFP-M159A mutant has a photoresistance enhancement in all investigated samples under low-intensity illumination (< 40 W/cm²). Photofatigue experiments comparing the performance of mutant and parent protein showed that the results vary a lot depending on the experimental environment. These results together with the absorption spectrum of the photofatigued sample confirm our previous hypothesis that the sulfoxidation of Met159 trapped the chromophore in a non-fluorescent state. Replacing the sulfur-containing residue by a sulfur-free residue avoids this trapping and improves the photoresistance of the protein (**Fig16.**).

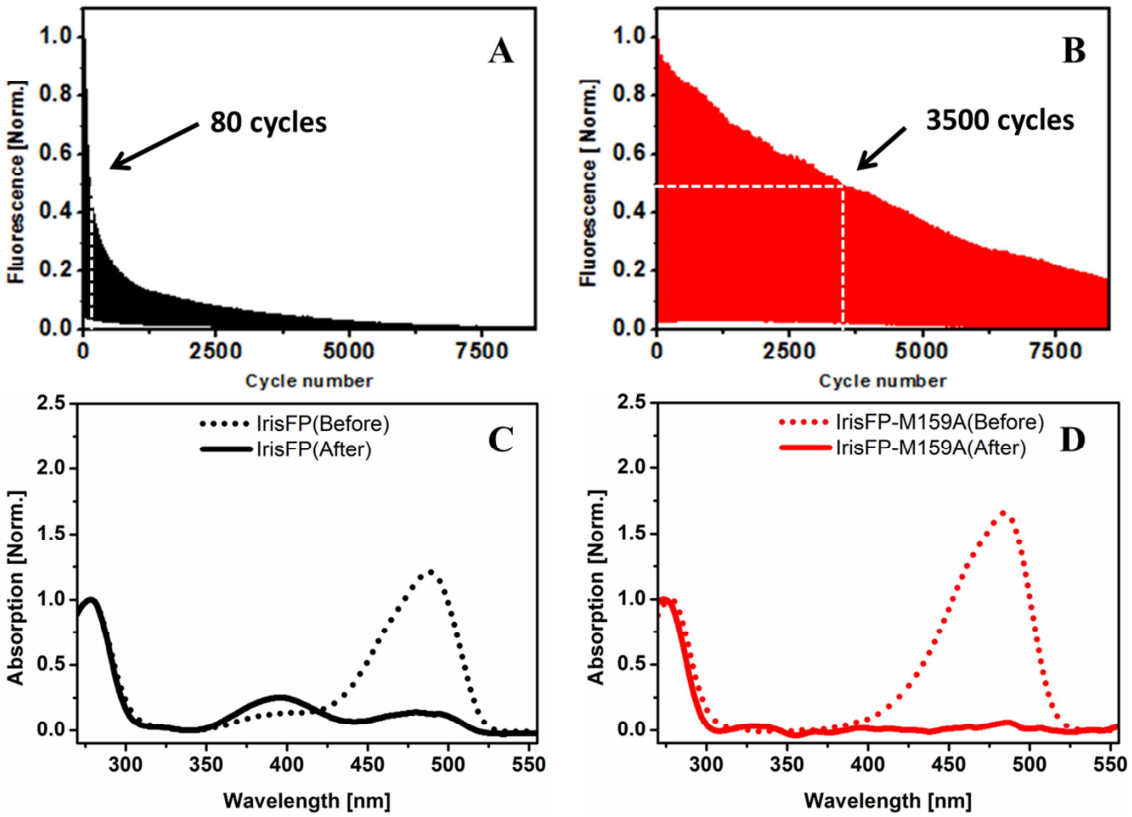

Fig16. *Fluorescence decay during photofatigue of IrisFP (A) and IrisFP-M159A (B) in solution. Absorbance of IriFP (C) and IrisFP-M159A (D) before and after photofatigue.*

3.2. Perspectives

After this thesis, we understand more about the photobleaching mechanism of RSFPs at the structural level. In the near future, we could use the same approaches to reveal the photobleaching mechanisms in Hydrozoan RSFPs and employ our findings to other proteins in order to generate new mutants with better photostability. However, there are still questions that remain unanswered that need to be investigated in the future.

1. Computer simulation of the sulfoxidation reaction of Met159 in IrisFP under low-intensity illumination conditions and the diffusion of molecular oxygen.

In our first article (Duan et al., 2013), we proposed a hypothesis of a possible sulfoxidation reaction pathway of Met159 and Cys171. Highly reactive singlet oxygen molecules are produced via a triplet-triplet energy transfer between chromophore and molecular oxygen, and then the singlet oxygen diffuses to nearby Met159, finally the sulfur-containing Met159 gets sulfoxided (Pattison et al., 2012). As the product of the reaction, a hydrogen peroxide (H_2O_2) is produced. This H_2O_2 can oxidize the nearby Cys171 (Luo et al.,

2005). Our collaborators Mikolaj FELIKS and Martin FIELD (Dynamo lab, IBS) are working on this question by using QM/MM methods. This process could be simulated to see if this reaction pathway is valid or not. Likewise, the possible diffusion pathways of the triplet/singlet oxygen molecules inside and outside the FP molecule could be explored.

2. Crystallographic structures of IrisFP-M159A after low- and high-intensity illumination photobleaching

By using the same approaches as described in our first article, we tried to obtain the photobleached crystallographic structures of IrisFP-M159A. However, those attempts were not successful. The main reason is that the mutant is more photostable and requires much more photoswitching cycles to photobleach, which introduces damage to crystals by local heating of the illuminated area. To rescue the crystal's diffraction quality, compromise conditions will have to be found for photobleaching, such as slightly cooling the crystal in the presence of oxygen.

3. Mutating Met159 in monomeric RSFPs

Our studies demonstrated an enhancement of photoresistance by a single mutation at Met159. Therefore, such a mutation could be applied to other Anthozoan RSFPs. However, IrisFP, as most other "native" RSFPs, is tetrameric and hence not very suitable for serving as a biological marker. The mutation of Met159 thus should be applied to monomeric RSFPs such as NijiFP or mIrisFP. In this context, it is noteworthy that mutations of Met159 already do exist in Dronpa variants such as Dronpa2 (Met159Thr), Dronpa3 (Met159Ala) and bsDronpa (Met159Cys). However, their photoresistance was not systematically studied. Further studies of photoresistance should be carried out. Substitution by other residues could be attempted at the Met159 position as well, to generate potentially more photostable mutants.

4. Mutant with enhanced photostability under high-intensity illumination

Although we have identified that residue Glu212 is involved in the high-intensity illumination photobleaching pathway within IrisFP, however, our E212Q mutant is not suitable for biological applications. Because of the essential role of the Glu212 residue during the chromophore maturation process, the substitution of Glu by Gln can largely slow down the maturation of the chromophore. However, in the second paper (Duan et al., 2014) we still demonstrated enhanced photostability of IrisFP-M159A in bacterial cells under such illumination condition, which suggests that Met159 has unknown indirect effect to the high-

intensity illumination photobleaching. Probably other neighboring residues are involved as well.

5. Study of Hydrozoan RSFPs photobleaching mechanisms

Although most RSFPs are originally from Anthozoan species, based on EGFP and EYFP, Jakobs's lab developed some Hydrozoan RSFPs with high switching performance such as rsEGFP, rsEGFP2 and Dreiklang, which were already successfully applied in RESOLFT nanoscopy. Despite high structure similarity between Anthozoan and Hydrozoan FPs, they share limited sequence identity. In Hydrozoan RSFPs, there is no sulfur-containing residue in the chromophore pocket. Thus the photobleaching caused by sulfoxidation of Met159 in low-intensity illumination pathway in Anthozoan RSFPs doesn't exist in Hydrozoan RSFPs. Furthermore, the decarboxylation of Glu212 (IrisFP numbering) at the origin of photobleaching in Anthozoan RSFPs probably does not to occur in Hydrozoan RSFPs either. PA-GFP is the best example displaying that the decarboxylation of Glu222 (GFP numbering) activates the chromophore and turns on the fluorescence. The Glu222 initially favors the protonation of the chromophore that hardly absorbs 488 nm light. Upon UV illumination, decarboxylation of this residue favors the deprotonation of the chromophore that emits fluorescence under excitation by 488 nm light. (Henderson et al., 2009).

6. Engineering of photostable mutants of Hydrozoan FPs

One possible photobleaching pathway in Hydrozoan FPs is that singlet oxygen diffuses to other residues more remote from the chromophore pocket and oxidizes them, which can result in photobleaching. Once the study of photobleaching mechanisms in Hydrozoan RSFPs progresses, key residues that are involved in photobleaching will be identified, and one could rationally design photostable mutants of Hydrozoan RSFPs like we did in Anthozoan RSFPs.

7. Long-lived dark state

In both articles, the photofatigue profiles display a clearly biphasic fluorescence amplitude decay suggesting that several photobleaching pathways occurs during photofatigue and that other photophysical process may be involved as well. One possible photophysical process is the establishment of a long-lived dark state with lifetime of several minutes. We speculate that, during the fast phase, a population of molecules enters in a long-lived dark state, creating a shelving effect and hence slowing down the photofatigue decay. Possibly, this

long-lived dark state could be trapped in a protein crystal and visualized by X-ray crystallography.

8. Environmentally stable proteins

As shown in our second article (Duan et al., 2014), the photoswitching behavior and the photostability of IrisFP and the M159A mutant differ a lot in different environments. Unlike the huge improvement that we found in solution, in some particular conditions, such as in PVA gel or live cells, the mutant showed less enhancement, possibly due to the complex external environment. To maintain the enhancement that we obtain within the isolated mutant, additional efforts are necessary.

The importance of the super-resolution techniques that can serve as very powerful tools to investigate subtle cellular architectures or real life processes on the nanometer-scale was recently recognized. The Nobel Prize in Chemistry 2014 was awarded jointly to Eric Betzig, Stefan W. Hell and William E. Moerner for the development of super-resolved fluorescence microscopy **(Fig.17)**.

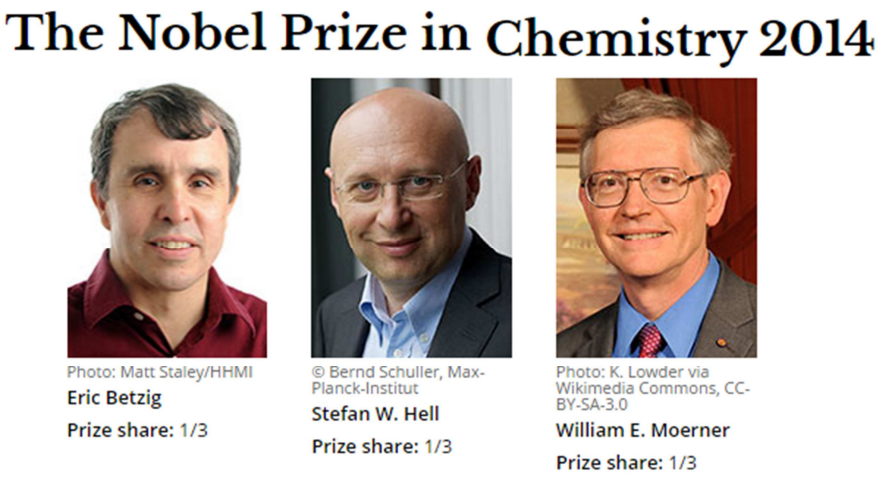

Fig17. *The Nobel Prize in Chemistry 2014: Eric Betzig, Stefan W. Hell and William E. Moerner (image from internet)*

In order to achieve a better spatial resolution of super-resolved fluorescence microscopy, the biological community demands new FPs particularly in the near-infrared range with better brightness and photoresistance. Our studies step forward to meet this demand.

Bibliography

Adam, V., Carpentier, P., Violot, S., Lelimousin, M., Darnault, C., Nienhaus, G.U., Bourgeois, D., 2009. Structural basis of X-ray-induced transient photobleaching in a photoactivatable green fluorescent protein. J Am Chem Soc 131, 18063-18065.

Adam, V., Lelimousin, M., Boehme, S., Desfonds, G., Nienhaus, K., Field, M.J., Wiedenmann, J., McSweeney, S., Nienhaus, G.U., Bourgeois, D., 2008. Structural characterization of IrisFP, an optical highlighter undergoing multiple photo-induced transformations. Proc Natl Acad Sci U S A 105, 18343-18348.

Adam, V., Moeyaert, B., David, C.C., Mizuno, H., Lelimousin, M., Dedecker, P., Ando, R., Miyawaki, A., Michiels, J., Engelborghs, Y., Hofkens, J., 2011. Rational design of photoconvertible and biphotochromic fluorescent proteins for advanced microscopy applications. Chem Biol 18, 1241-1251.

Ando, R., Flors, C., Mizuno, H., Hofkens, J., Miyawaki, A., 2007. Highlighted generation of fluorescence signals using simultaneous two-color irradiation on Dronpa mutants. Biophys J 92, L97-99.

Ando, R., Hama, H., Yamamoto-Hino, M., Mizuno, H., Miyawaki, A., 2002. An optical marker based on the UV-induced green-to-red photoconversion of a fluorescent protein. Proc Natl Acad Sci U S A 99, 12651-12656.

Ando, R., Mizuno, H., Miyawaki, A., 2004. Regulated fast nucleocytoplasmic shuttling observed by reversible protein highlighting. Science 306, 1370-1373.

Andresen, M., Stiel, A.C., Folling, J., Wenzel, D., Schonle, A., Egner, A., Eggeling, C., Hell, S.W., Jakobs, S., 2008. Photoswitchable fluorescent proteins enable monochromatic multilabel imaging and dual color fluorescence nanoscopy. Nat Biotechnol 26, 1035-1040.

Bizzarri, R., Serresi, M., Cardarelli, F., Abbruzzetti, S., Campanini, B., Viappiani, C., Beltram, F., 2010. Single amino acid replacement makes Aequorea victoria fluorescent proteins reversibly photoswitchable. J Am Chem Soc 132, 85-95.

Brakemann, T., Stiel, A.C., Weber, G., Andresen, M., Testa, I., Grotjohann, T., Leutenegger, M., Plessmann, U., Urlaub, H., Eggeling, C., Wahl, M.C., Hell, S.W., Jakobs, S., 2011. A reversibly photoswitchable GFP-like protein with fluorescence excitation decoupled from switching. Nat Biotechnol 29, 942-947.

Chalfie, M., Tu, Y., Euskirchen, G., Ward, W., Prasher, D., 1994. Green fluorescent protein as a marker for gene expression. Science 263, 802-805.

Chang, H., Zhang, M., Ji, W., Chen, J., Zhang, Y., Liu, B., Lu, J., Zhang, J., Xu, P., Xu, T., 2012. A unique series of reversibly switchable fluorescent proteins with beneficial properties for various applications. Proc Natl Acad Sci U S A 109, 4455-4460.

Chattoraj, M., King, B.A., Bublitz, G.U., Boxer, S.G., 1996. Ultra-fast excited state dynamics in green fluorescent protein: multiple states and proton transfer. Proc Natl Acad Sci U S A 93, 8362-8367.

Christ, T., Kulzer, F., Bordat, P., Basché, T., 2001. Watching the Photo-Oxidation of a Single Aromatic Hydrocarbon Molecule. Angewandte Chemie International Edition 40, 4192-4195.

Cordes, T., Vogelsang, J., Tinnefeld, P., 2009. On the Mechanism of Trolox as Antiblinking and Antibleaching Reagent. Journal of the American Chemical Society 131, 5018-5019.

Cormack, B.P., Valdivia, R.H., Falkow, S., 1996. FACS-optimized mutants of the green fluorescent protein (GFP). Gene 173, 33-38.

Cubitt, A.B., Heim, R., Adams, S.R., Boyd, A.E., Gross, L.A., Tsien, R.Y., 1995. Understanding, improving and using green fluorescent proteins. Trends in Biochemical Sciences 20, 448-455.

Dedecker, P., Mo, G.C., Dertinger, T., Zhang, J., 2012. Widely accessible method for superresolution fluorescence imaging of living systems. Proc Natl Acad Sci U S A 109, 10909-10914.

Dickson, R.M., Cubitt, A.B., Tsien, R.Y., Moerner, W.E., 1997. On/off blinking and switching behaviour of single molecules of green fluorescent protein. Nature 388, 355-358.

Duan, C., Adam, V., Byrdin, M., Bourgeois, D., 2014a. Structural basis of photoswitching in fluorescent proteins. Methods Mol Biol 1148, 177-202.

Duan, C., Adam, V., Byrdin, M., Ridard, J., Kieffer-Jaquinod, S., Morlot, C., Arcizet, D., Demachy, I., Bourgeois, D., 2013. Structural evidence for a two-regime photobleaching mechanism in a reversibly switchable fluorescent protein. J Am Chem Soc 135, 15841-15850.

Duan, C., Byrdin, M., El Khatib, M., Henry, X., Adam, V., Bourgeois, D., 2014b. Rational Design of Enhanced Photoresistance in a Photoswitchable Fluorescent Protein. Methods and Applications in Fluorescence, In press.

Giordano, L., Jovin, T.M., Irie, M., Jares-Erijman, E.A., 2002. Diheteroarylethenes as thermally stable photoswitchable acceptors in photochromic fluorescence resonance energy transfer (pcFRET). J Am Chem Soc 124, 7481-7489.

Gollnick, K., Franken, T., Fouda, M.F.R., Paur, H.R., Held, S., 1992. Merbromin (mercurochrome) and other xanthene dyes: Quantum yields of triplet sensitizer generation and singlet oxygen formation in alcoholic solutions. Journal of Photochemistry and Photobiology B: Biology 12, 57-81.

Grotjohann, T., Testa, I., Leutenegger, M., Bock, H., Urban, N.T., Lavoie-Cardinal, F., Willig, K.I., Eggeling, C., Jakobs, S., Hell, S.W., 2011. Diffraction-unlimited all-optical imaging and writing with a photochromic GFP. Nature 478, 204-208.

Grotjohann, T., Testa, I., Reuss, M., Brakemann, T., Eggeling, C., Hell, S.W., Jakobs, S., 2012. rsEGFP2 enables fast RESOLFT nanoscopy of living cells. eLife 1, e00248.

Groulx, N., McGuire, H., Laprade, R., Schwartz, J.-L., Blunck, R., 2011. Single Molecule Fluorescence Study of the Bacillus thuringiensis Toxin Cry1Aa Reveals Tetramerization. Journal of Biological Chemistry 286, 42274-42282.

Gurskaya, N.G., Verkhusha, V.V., Shcheglov, A.S., Staroverov, D.B., Chepurnykh, T.V., Fradkov, A.F., Lukyanov, S., Lukyanov, K.A., 2006. Engineering of a monomeric green-to-red photoactivatable fluorescent protein induced by blue light. Nat Biotechnol 24, 461-465.

Gustafsson, M.G., 2005. Nonlinear structured-illumination microscopy: wide-field fluorescence imaging with theoretically unlimited resolution. Proc Natl Acad Sci U S A 102, 13081-13086.

Heim, R., Cubitt, A.B., Tsien, R.Y., 1995. Improved green fluorescence. Nature 373, 663-664.

Henderson, J.N., Gepshtein, R., Heenan, J.R., Kallio, K., Huppert, D., Remington, S.J., 2009. Structure and mechanism of the photoactivatable green fluorescent protein. J Am Chem Soc 131, 4176-4177.

Hofmann, M., Eggeling, C., Jakobs, S., Hell, S.W., 2005. Breaking the diffraction barrier in fluorescence microscopy at low light intensities by using reversibly photoswitchable proteins. Proc Natl Acad Sci U S A 102, 17565-17569.

Hoogenboom, J.P., van Dijk, E.M., Hernando, J., van Hulst, N.F., García-Parajó, M.F., 2005. Power-law-distributed dark states are the main pathway for photobleaching of single organic molecules. Phys Rev Lett 95, 097401.097401-097401.097404.

Jablonski, A.E., Vegh, R.B., Hsiang, J.C., Bommarius, B., Chen, Y.C., Solntsev, K.M., Bommarius, A.S., Tolbert, L.M., Dickson, R.M., 2013. Optically modulatable blue fluorescent proteins. J Am Chem Soc 135, 16410-16417.

Jimenez-Banzo, A., Nonell, S., Hofkens, J., Flors, C., 2008. Singlet oxygen photosensitization by EGFP and its chromophore HBDI. Biophys J 94, 168-172.

Luo, D., Smith, S.W., Anderson, B.D., 2005. Kinetics and mechanism of the reaction of cysteine and hydrogen peroxide in aqueous solution. Journal of Pharmaceutical Sciences 94, 304-316.

Malkani, N., Schmid, J.A., 2011. Some secrets of fluorescent proteins: distinct bleaching in various mounting fluids and photoactivation of cyan fluorescent proteins at YFP-excitation. PLoS One 6, e18586.

McKinney, S.A., Murphy, C.S., Hazelwood, K.L., Davidson, M.W., Looger, L.L., 2009. A bright and photostable photoconvertible fluorescent protein. Nat Methods 6, 131-133.

Mizuno, H., Mal, T.K., Tong, K.I., Ando, R., Furuta, T., Ikura, M., Miyawaki, A., 2003. Photo-induced peptide cleavage in the green-to-red conversion of a fluorescent protein. Mol Cell 12, 1051-1058.

Mizuno, H., Mal, T.K., Walchli, M., Kikuchi, A., Fukano, T., Ando, R., Jeyakanthan, J., Taka, J., Shiro, Y., Ikura, M., Miyawaki, A., 2008. Light-dependent regulation of structural flexibility in a photochromic fluorescent protein. Proc Natl Acad Sci U S A 105, 9227-9232.

Moeyaert, B., 2010. Structural insight into fluorescent protein properties by rational design and characterization of photoconvertible, photoswitchable and phototoxic fluorescent proteins. PhD thesis. Katholieke Universiteit LEUVEN,

Moeyaert, B., Nguyen Bich, N., De Zitter, E., Rocha, S., Clays, K., Mizuno, H., van Meervelt, L., Hofkens, J., Dedecker, P., 2014. Green-to-red photoconvertible Dronpa mutant for multimodal super-resolution fluorescence microscopy. ACS Nano 8, 1664-1673.

Ormö, M., Cubitt, A.B., Kallio, K., Gross, L.A., Tsien, R.Y., Remington, S.J., 1996. Crystal structure of the Aequorea victoria green fluorescent protein. Science 273, 1392-1395.

Patterson, G.H., Lippincott-Schwartz, J., 2002. A photoactivatable GFP for selective photolabeling of proteins and cells. Science 297, 1873-1877.

Pattison, D.I., Rahmanto, A.S., Davies, M.J., 2012. Photo-oxidation of proteins. Photochem Photobiol Sci 11, 38-53.

Penttilä, A., Boyle, C.R., Salin, M.L., 1996. Active Oxygen Intermediates and Chlorophyllin Bleaching. Biochemical and Biophysical Research Communications 226, 135-139.

Prasher, D.C., Eckenrode, V.K., Ward, W.W., Prendergast, F.G., Cormier, M.J., 1992. Primary structure of the Aequorea victoria green-fluorescent protein. Gene 111, 229-233.

Rasnik, I., McKinney, S.A., Ha, T., 2006. Nonblinking and long-lasting single-molecule fluorescence imaging. Nat Methods 3, 891-893.

Rego, E.H., Shao, L., Macklin, J.J., Winoto, L., Johansson, G.A., Kamps-Hughes, N., Davidson, M.W., Gustafsson, M.G., 2012. Nonlinear structured-illumination microscopy with a photoswitchable protein reveals cellular structures at 50-nm resolution. Proc Natl Acad Sci U S A 109, E135-143.

Shimomura, O., Johnson, F.H., Saiga, Y., 1962. Extraction, Purification and Properties of Aequorin, a Bioluminescent Protein from the Luminous Hydromedusan, Aequorea. Journal of Cellular and Comparative Physiology 59, 223-239.

Shroff, H., Galbraith, C.G., Galbraith, J.A., White, H., Gillette, J., Olenych, S., Davidson, M.W., Betzig, E., 2007. Dual-color superresolution imaging of genetically expressed probes within individual adhesion complexes. Proc Natl Acad Sci U S A 104, 20308-20313.

Sniegowski, J.A., Lappe, J.W., Patel, H.N., Huffman, H.A., Wachter, R.M., 2005. Base catalysis of chromophore formation in Arg96 and Glu222 variants of green fluorescent protein. J Biol Chem 280, 26248-26255.

Song, L., Hennink, E.J., Young, I.T., Tanke, H.J., 1995. Photobleaching kinetics of fluorescein in quantitative fluorescence microscopy. Biophysical Journal 68, 2588-2600.

Song, L., Varma, C.A., Verhoeven, J.W., Tanke, H.J., 1996. Influence of the triplet excited state on the photobleaching kinetics of fluorescein in microscopy. Biophysical Journal 70, 2959-2968.

Stiel, A.C., Trowitzsch, S., Weber, G., Andresen, M., Eggeling, C., Hell, S.W., Jakobs, S., Wahl, M.C., 2007. 1.8 A bright-state structure of the reversibly switchable fluorescent protein Dronpa guides the generation of fast switching variants. Biochem J 402, 35-42.

Subach, F.V., Patterson, G.H., Renz, M., Lippincott-Schwartz, J., Verkhusha, V.V., 2010a. Bright monomeric photoactivatable red fluorescent protein for two-color super-resolution sptPALM of live cells. J Am Chem Soc 132, 6481-6491.

Subach, O.M., Malashkevich, V.N., Zencheck, W.D., Morozova, K.S., Piatkevich, K.D., Almo, S.C., Verkhusha, V.V., 2010b. Structural Characterization of Acylimine-Containing Blue and Red Chromophores in mTagBFP and TagRFP Fluorescent Proteins. Chemistry & Biology 17, 333-341.

Tsien, R.Y., 1998. The green fluorescent protein. Annu Rev Biochem 67, 509-544.

Vegh, R.B., Bravaya, K.B., Bloch, D.A., Bommarius, A.S., Tolbert, L.M., Verkhovsky, M., Krylov, A.I., Solntsev, K.M., 2014. Chromophore Photoreduction in Red Fluorescent Proteins Is Responsible for Bleaching and Phototoxicity. The Journal of Physical Chemistry B 118, 4527-4534.

White, J., Stelzer, E., 1999. Photobleaching GFP reveals protein dynamics inside live cells. Trends Cell Biol 9, 61-65.

Wiedenmann, J., Ivanchenko, S., Oswald, F., Schmitt, F., Rocker, C., Salih, A., Spindler, K.D., Nienhaus, G.U., 2004. EosFP, a fluorescent marker protein with UV-inducible green-to-red fluorescence conversion. Proc Natl Acad Sci U S A 101, 15905-15910.

Wustner, D., Solanko, L., Lund, F., Sage, D., Schroll, H., Lomholt, M., 2012. Quantitative fluorescence loss in photobleaching for analysis of protein transport and aggregation. BMC Bioinformatics 13, 296.

Yang, F., Moss, L.G., Phillips, G.N., Jr., 1996. The molecular structure of green fluorescent protein. Nat Biotechnol 14, 1246-1251.

York, A.G., Ghitani, A., Vaziri, A., Davidson, M.W., Shroff, H., 2011. Confined activation and subdiffractive localization enables whole-cell PALM with genetically expressed probes. Nat Methods 8, 327-333.

Zhang, L., Patel, H.N., Lappe, J.W., Wachter, R.M., 2006. Reaction progress of chromophore biogenesis in green fluorescent protein. J Am Chem Soc 128, 4766-4772.

Zheng, Q., Juette, M.F., Jockusch, S., Wasserman, M.R., Zhou, Z., Altman, R.B., Blanchard, S.C., 2014. Ultra-stable organic fluorophores for single-molecule research. Chemical Society Reviews 43, 1044-1056.

Zijlstra, N., Blum, C., Segers-Nolten, I.M.J., Claessens, M.M.A.E., Subramaniam, V., 2012. Molecular Composition of Sub-stoichiometrically Labeled α-Synuclein Oligomers Determined by Single-Molecule Photobleaching. Angewandte Chemie 124, 8951-8954.

Zondervan, R., Kulzer, F., Kol'chenk, M.A., Orrit, M., 2004. Photobleaching of Rhodamine 6G in Poly(vinyl alcohol) at the Ensemble and Single-Molecule Levels. The Journal of Physical Chemistry A 108, 1657-1665.

Résumé

Etude structurale des mécanismes de photoblanchiment des protéines fluorescentes photocommutables

La découverte des Protéines Fluorescentes Phototransformables (PTFPs) issues d'espèces anthozoaires a ouvert, grâce à leurs propriétés photophysiques particulières, un vaste champ d'investigation pour l'imagerie biologique de fluorescence. L'un des sous-groupes des PTFPs est formé des protéines fluorescentes réversiblement photocommutables (RSFPs), qui peuvent être commutées réversiblement entre des états non-fluorescent et fluorescent. Le photoblanchiment est la perte définitive d'émission de fluorescence sous excitation et est un phénomène commun à toutes les molécules fluorescentes. Le photoblanchiment a un impact important sur la qualité des images de microscopie, notamment en imagerie de super-résolution. Les RSFPs ont tendance à perdre de leur performance à chaque cycle de commutation, un processus dénommé "photofatigue". Notre intérêt est centré sur l'étude des mécanismes de photofatigue des RSFPs.

Nous avons rapporté les structures cristallographiques d'IrisFP photoblanchie par une forte et une basse intensité d'illumination à température ambiante ainsi que les modifications spectroscopiques associées. Nos résultats démontrent que différentes intensités d'excitation peuvent donner lieu à différentes voies de photoblanchiment. Sous faible intensité d'excitation, une voie de photoblanchiment dépendante de l'oxygène a été mise en évidence. Les modifications structurales induites par la production d'oxygène singulet à l'intérieur de la poche du chromophore ont révélé l'oxydation de deux résidus soufrés, Met159 et Cys171, piégeant le chromophore dans un état protoné non-fluorescent. Sous haute intensité d'excitation, une voie de photoblanchiment oxygène-indépendante totalement différente a été trouvée. Le Glu212, strictement conservé, subit une décarboxylation associée à un important réarrangement du réseau de liaisons hydrogènes autour du chromophore, et un changement d'hybridation sp^2 vers sp^3 du carbone reliant les cycles du chromophore est observé. En tant que résidu clé impliqué dans le photoblanchiment induit par faible intensité d'excitation, nous avons muté Met159 en alanine afin d'éviter une sulfoxydation. Nous avons trouvé que le mutant IrisFP-M159A démontre une photostabilité améliorée en solution, en gel PVA et dans des cellules *E. coli*.

Mots-clés : *protéines fluorescentes, photoblanchiment, cristallographie, spectroscopie, ingénierie rationnelle*

Abstract

Structural insight into photobleaching mechanisms of reversible photoswitchable fluorescent proteins

The discovery of phototransformable FPs (PTFPs) from Anthozoa species, thanks to their photophysical properties, has opened a large field in biological fluorescence imaging. One of the PTFPs' sub-groups consists of Reversible Photoswitchable Fluorescent Proteins (RSFPs), which can be reversibly switched between nonfluorescent and fluorescent states. Photobleaching is the permanent loss of the fluorescence-emitting capacity under excitation, which is a common phenomenon among all the fluorescent molecules. Photobleaching has a large impact on the microscopy image quality, notably on super-resolution imaging. Photoswitchable fluorescent proteins have a tendency to lose performance within every switching cycle, a process referred to as "photofatigue". Our interest of study is focused on the photobleaching mechanisms of RSFPs.

We have reported the crystallographic structure of photobleached IrisFP under high and low illumination intensity at room temperature as well as its spectroscopic modifications. We found that different illumination intensities can result in different photobleaching pathways. Under low illumination intensity, an oxygen-dependent photobleaching pathway was evidenced. Structural modifications induced by singlet-oxygen production within the chromophore pocket revealed the oxidation of two sulfur-containing residues, Met159 and Cys171, locking the chromophore in a nonfluorescent protonated state. Under high illumination intensity, a completely different, oxygen-independent photobleaching pathway was found. The conserved Glu212 underwent decarboxylation concomitantly with an extensive rearrangement of the H-bond network around the chromophore, and an sp^2-to-sp^3 hybridization change of the carbon atom bridging the chromophore cyclic moieties was observed. As Met159 is the key residue involved in low-intensity illumination photobleaching, we have then mutated Met159 into Alanine in order to avoid sulfoxidation. We found that the IrisFP-M159A mutant display an enhanced photostability in solution, in PVA gel and in *E.coli cells*.

Keywords: *fluorescent proteins, RSFPs, photobleaching, crystallography, spectroscopy rational design*